Radiation dose optimization of CT acquisitions in PET/CT examinations

Mattias Verhelst

Supervisors: Prof. dr. ir. Klaus Bacher, Prof. ir. Yves D'Asseler
Counsellor: Ir. Caro Franck

Master's dissertation submitted in order to obtain the academic degree of
Master of Science in Biomedical Engineering

Vakgroep Medische Basiswetenschappen
Chairman: Prof. dr. Katharina D'Herde

Vakgroep Radiologie en Nucleaire Geneeskunde
Chairman: Prof. dr. Ingeborg Goethals

Faculty of Engineering and Architecture
Academic year 2014-2015

UNIVERSITEIT GENT

Radiation dose optimization of CT acquisitions in PET/CT examinations

Mattias Verhelst

Supervisors: Prof. dr. ir. Klaus Bacher, Prof. ir. Yves D'Asseler
Counsellor: Ir. Caro Franck

Master's dissertation submitted in order to obtain the academic degree of
Master of Science in Biomedical Engineering

Vakgroep Medische Basiswetenschappen
Chairman: Prof. dr. Katharina D'Herde

Vakgroep Radiologie en Nucleaire Geneeskunde
Chairman: Prof. dr. Ingeborg Goethals

Faculty of Engineering and Architecture
Academic year 2014-2015

UNIVERSITEIT GENT

Foreword

Deze masterproef werd gerealiseerd met de hulp en medewerking van verschillende personen, die ik allen wil bedanken voor hun bereidwillige hulp.

Een speciaal woord van dank aan mijn promotor Prof. Ir. Klaus Bacher, voor de professionele begeleiding die ik reeds voor de tweede maal mocht ondervinden bij het realiseren van een masterproef en het afwerken van mijn voorbereidingsprogramma en tweede master. Anderzijds wil ik ook Prof. Ir. Yves d'Asseler bedanken voor de samenwerking bij de vele experimenten met de PET-CT. Beide professoren stelden , met hun deskundig advies, mij in de mogelijkheid mijn kennis te verruimen in de stralingstechnologie en om deze masterproef succesvol af te ronden.

Tevens wil ik ook Ir. Caro Franck bedanken voor de vele tips en nuttige informatie tijdens dit traject. Ik wens haar dan ook heel veel succes bij het beëindigen van haar doctoraat.

Daarnaast wens ik ook het UZ Gent, en heel specifiek de dienst radiologie en nucleaire geneeskunde, te bedanken voor het gebruik van de fantomen en de PET-CT scanner.

Dank aan mijn ouders voor de kansen die ze mij gaven om mijn studies te voltooien en voor hun steun bij elke beslissing die ik maakte gedurende mijn studiekeuze.

Aan mijn klasgenoten Celine, Denise, Gerlinde, Henri en William; dank voor alle plezante momenten die we deelden gedurende de laatste twee jaar.

Tot slot een woordje van dank aan mijn vriendin Emmily, voor haar steun en geduld die ik kreeg gedurende deze drukke periode.

Mattias Verhelst

4 juni 2015

Admission to loan

Mattias Verhelst

4 juni 2015

Radiation dose optimization of CT acquisitions in PET/CT examinations

MattiasVerhelst

Master dissertation submitted in order to obtain the academic degree of

Master of Science in Biomedical engineering

Academic year 2014-2015

Supervisors: Prof. Ir. Klaus Bacher, Prof. Ir. Yves D'Asseler

Counsellor: Ir. Caro Franck

Vakgroep Medische Basiswetenschappen

Chairman: Prof. dr. Katharina D'Herde

Vakgroep Radiologie en Nucleaire Geneeskunde

Chairman: Prof. dr. Ingeborg Goethals

Faculty of Engineering and Architecture

Summary

The combination of PET/CT has been proven to be a great success by co-registering anatomical and functional information into one single acquisition. The CT component delivers important diagnostic value and anatomical localization while the PET component gives crucial molecular information. An extra advantage of combining PET with CT, is that the CT data can be used as low-noise attenuation correction of PET images to improve its quantitative accuracy.

The most crucial disadvantage of this modality is the CT radiation dose contribution to the patient, which can range from two to four times the dose delivered by the PET component.

In this article different protocols are proposed to decrease the delivered CT dose, by optimizing CT settings while maintaining the image quality and quantitative accuracy of the PET image. Four major experiments were performed, namely the CT acceptance test, automatic tube current modulation analysis, low dose CT protocols and an attenuation correction analysis.

From the results of this study three main conclusions can be drawn. First of all, from the automatic tube current modulation analysis, it is seen that a shift of the tube current profile is achieved while changing the CT scan direction from cranio-caudal to caudo-cranial. Also the table height has a high influence on the estimated tube current for the same patient. Therefore great care in isocentering the patient should been taken by the medical staff. Secondly from the low dose protocol experiment, a protocol is suggested based on lowering the tube voltage. Third, from the attenuation correction analysis, it can be concluded that the dose has no effect on the recovery coefficients of the corrected PET images.

A major difference should be implemented between diagnosis and follow-up scans of the patient suffering from cancer. Based on these results for a diagnosis scan, a low dose CT protocol is suggested (100 kV instead of 120 kV) that reduces the dose with 30% compared to the standard protocol. While for a follow-up scan, very low dose protocols should be used, as only attenuation correction is needed. Combining, this can result in a dose reduction of up to 60% (one diagnosis + four follow-up scans).

Keywords: PET-CT, dose reduction, attenuation correction, tube voltage reduction, automatic tube current modulation

Extended abstract

Radiation dose optimization of CT acquisitions in PET/CT examinations

Mattias Verhelst

Supervisor(s): Prof. Ir. Klaus Bacher and Prof. Ir Yves D'Asseler

Abstract **PET-CT has proven to be a great success in diagnosis and follow-up of tumors. The disadvantage of this method is the rather high dose delivered to the patient. The goal of this article is to optimize CT settings of a PET-CT scanner to lower the CT dose delivered while maintaining the image quality and quantitative accuracy of the PET image.**

Keywords **PET-CT, dose reduction, attenuation correction, tube voltage reduction, tube current modulation**

I. Introduction

Cancer is currently the leading cause of death worldwide, accounting for 8.2 million deaths in 2012 and the number of new cases is expected to rise above 70% over the next 20 years [1]. It has been shown that diagnosing cancer in an early stage, increases the chances for survival of the patient. A successful technique in diagnosis of cancer is positron emission tomography (PET) co-registered with computed tomography (CT). By combining the structural information delivered by the CT component with the metabolic information of the PET, delivers a high added value to the diagnosis by the physician. The advantages of combining PET and CT is threefold. First of all structural information is giving by the CT, but also anatomical localization is provided. Third the CT images can be used to correct for the attenuation in PET, which is very important for the PET quantitative accuracy.

An important disadvantage of using PET-CT is the radiation exposure delivered to the patient by both modalities. The highest radiation exposure is delivered by the CT component compared to the PET component. The CT-dose can range up to four times the dose of the PET-dose. (18.6 mSv versus 6.23 mSv [2]). The goal of this project is to optimize the CT settings to lower the CT dose delivered to the patient while maintaining the image quality and quantitative accuracy of the PET image. This is investigated by performing four experiment.

- Acceptance test
- Automatic exposure control analysis
- Low dose protocol testing
- Attenuation correction analysis

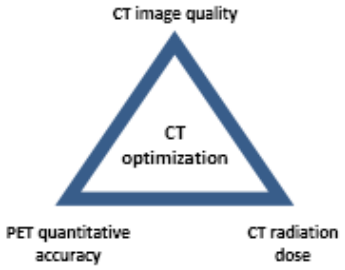

II. Materials and Methods

A. PET-CT scanner and phantoms

All experiments in this project were performed on the Biograph mCT flow PET-CT scanner (Siemens, Germany). This is the first sequential PET-CT scanner with a flow PET system, which means that the PET scan is taking in a continuous way and not via bed positions.

Four different phantoms are used. The body CT phantom that is used in the acceptance test. Next the RANDO phantom for the tube current modulation experiment. For image quality and dose analysis the Catphan 404 phantom is used and at last to evaluate the attenuation correction the NEMA PET phantom was used.

B. Dosimetry and image quality parameters

For every experiment the CT dose index (CTDI) is used as a parameter for the dose delivered to the patient per exam. By using CTDI, direct X-rays and scatters are accounted for and this predicts the dose for one rotation in a CT-scan. This CTDI can be multiplied by the scan length, to result in the dose-length product (DLP). From this DLP it is possible to calculate a pseudo-effective dose by using a conversion factor proposed by the European Working Group for Guidelines on Quality Criteria in CT, which is equal to 0.017 mSv/mGycm. In PET it is also possible to calculate a pseudo-effective dose delivered by the radiotracer by multiplying the activity of injected FDG with a conversion factor (0.019 mSv/MBq). The summation of these two effective doses represents the total dose delivered by PET-CT.

E-mail: Mattias.Verhelst@UGent.be

Three parameters in CT are used to analyze the image quality of CT images. These parameters, noise, spatial resolution and low contrast detail, can all be measured in the Catphan 404 phantom. Extra mentioning is the low-contrast detail which is quantified by using the inverse image quality number. Where Ci is the corresponding contrast level and Di the smallest diameter still distinguishable from the background in the image.

$$IQFinv = \frac{100}{\sum Ci * Di}$$

The stability of CT numbers is also investigated using the Catphan 404 phantom. To evaluate the attenuation correction of the CT images on the PET image the recovery coefficient is used. This recovery coefficient is the relative ratio of the observed activity to the true activity. The higher this ratio, the better the quantitative accuracy of the PET scanner is.

III. Results

A. *Acceptance test*

From the results of the acceptance test, it can be stated that the Biograph mCT flow at the university hospital of Ghent is approved for acceptance.

B. *Tube current modulation analysis*

In a study of Franck[3], it has been shown that some inconsistencies were reported on the tube current modulation system of a stand-alone CT system. Therefore in this project, this behavior is investigated on the CT component of the Biograph mCT flow scanner. In a first experiment the influence of the scan direction is investigated by scanning the RANDO phantom in a cranio-caudal direction and a caudo-cranial direction, based on the same topogram. While all parameters are the same the DLP of both protocols is also approximately the same but in figure 1, it can be seen that locally the tube current varies intensely, especially in the neck region. The variation is highest at 33 mm, with a tube current difference of 120 mA.

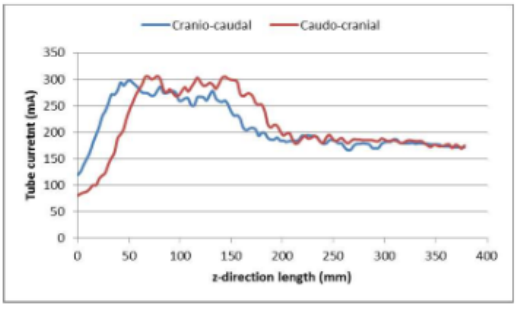

Fig 1: Tube current per slice as function of z-direction length for cranio-caudal and caudo-cranial scanning.

Not only the scan direction, but also the influence of the topogram is investigated. Therefore a lateral topogram is performed and a CT scan based on this topogram.

Compared to the standard PA topogram, this leads to an overall tube current reduction of 35%.

At last the influence of the table height on the tube current modulation is analyzed. By using three different table heights (99, 150 and 256 cm) a comparison can be made and is shown in figure 2. Out of these results it is seen that how further the patient is from the detector, the higher the tube current will be, hence increasing the dose to the patient significantly.

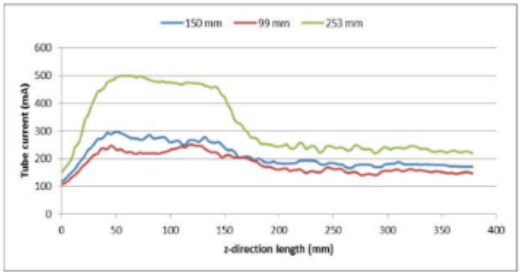

Fig 2: Tube current per slice as function of z-direction length for three different table heights

C. *Low dose protocol CT*

As a patient who suffers from cancer will undergo multiple PET-CT scans, the accumulated dose can reach high levels. Therefore it should be advised to keep the dose per CT-acquisition as low as possible (ALARA). In this experiment, low dose protocols are analyzed, based on lower tube voltage and/or lower tube currents, compared to the standard CT-acquisition which is used in the clinical practice. In a first comparison the dose versus noise is analyzed.

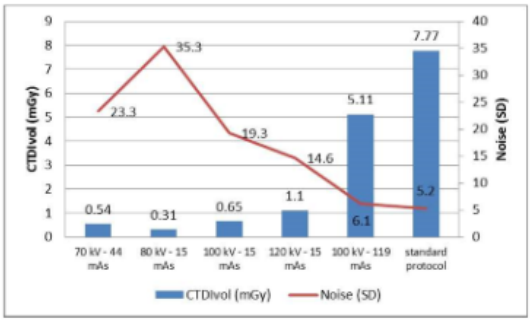

Fig 3: CTDIvol and noise for the different low dose protocols

From figure 3 it can be stated that dose and noise are strongly related. The lower the dose in CT, the higher the noise levels will be in the image. Specifically for the Biograph mCT flow the relationship between noise and dose can be expressed as:

$$Noise = 14.95 * CTDI^{-0.54}$$

Next the spatial resolution and low contrast detail are investigated for the different protocols. There is no difference seen in spatial resolution between the protocols. For the contrast, there is no significant correlation.

At last, the difference of CT numbers in function of tube voltage is investigated, since CT numbers are converted from the CT image to create the attenuation map to correct the PET images. The linearity of the standard protocol of 120 kV is perfect compared to the theoretical calculation. For different tube voltages, the variation is the highest for material with a density around 1 g/cm³ and for high density material (> 2 g/cm³).

D. Attenuation correction analysis

As there is a low variability in CT-numbers between the different tube voltages, the influence of this is investigated on the PET images reconstructed by the low dose protocols. The comparison is performed by the recovery coefficient. By using a correction based on the standard CT protocol an increase of 45% is achieved compared to non-corrected PET image. Next the influence of the sphere size inside the PET phantom on the recovery coefficient is analyzed and concluded from figure 4 a very high recovery coefficient of almost 1 over a range from 22 to 37 mm. The recovery coefficient decreases from this point on, up to a value of 0.71. It is also seen that there is a difference between the slow and fast scan for these small spheres, resulting in a higher recovery coefficient for the slow scan.

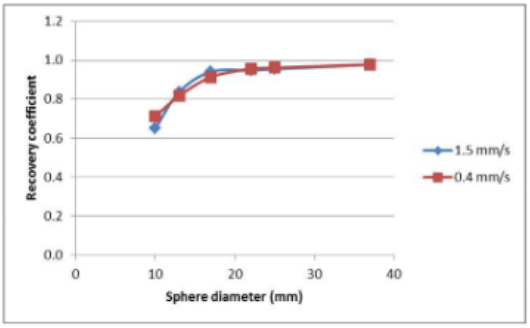

Fig 4: Recovery coefficient as a function of sphere diameter for the fast and slow scan

For the low dose protocols, there was no difference in recovery coefficients for each sphere diameter, compared to the standard protocol correction. Therefore the recovery coefficient is independent on the dose delivered to the patient from the CT image.

IV. Discussion

As CT delivers a rather high dose compared to other X-ray modalities, a lot of effort has been done in the past to lower the dose delivered to the patient. In this project, an optimization of the CT dose is performed by changing the parameters. One successful example of dose reduction is the use of the automatic exposure control. It has been shown that the scan direction doesn't have an influence on the pseudo effective dose, but locally the difference can be rather high, especially in the neck region. This can have an influence on the organ dose, for example the thyroids. The same results have been shown on a stand-alone CT scanner. Currently an explanation of this shifting is being investigated by Franck C. The results of that research can be extrapolated to these results.

From the AEC experiments, it can be concluded that a lateral topogram will result in a dose reduction of 35% compared to the standard CT scan based on a PA topogram. Also the table height has a very important influence on the tube current modulation. As the magnification is largest when the patient is farthest to the detector, this leads to an overestimation of the tube current needed for this patient. A possible solution is to rescale the measurements. But for PET, isocentering the patient is very important due to the parallax error. Therefore in PET-CT a lot of attention should be taken by the medical staff to position the patient exactly at the isocenter.

From the experiments of the low dose protocols, it can be concluded that it is possible to reduce the dose by changing the parameters while maintaining the image quality. By reducing the tube voltage from 120 kV to 100 kV and increasing the tube current from 106 mAs to 119 mAs, this results in a dose reduction of 33% while noise only increases by 6%. Other image quality parameters are shown in table 1.

Table 1 Dose and IQ parameters for standard protocol and dose reduction protocol

	120 kV	100 kV	Difference %
Dose	7.7	5.11	-33.6
Noise	7.4	7.9	6.8
IQFinv	11.49	12.2	6.2
Resolution	7.1	7.1	0

In the last experiment, the recovery coefficients are measured and compared. A very important conclusion that can be made by this experiment is that the dose has no influence on the recovery coefficients. Therefore quantitative PET analysis is not influenced by the CT-scan used for attenuation correction.

V. Conclusion

The conclusion of this project is twofold. First for a diagnostic scan, it should be advised to lower the tube voltage to 100 kV for a normal sized patient. This will reduce the dose delivered to the patient drastically while maintaining the image quality needed for diagnostic purposes and maintaining quantitative analysis of the corrected PET image. Secondly a difference should be made between diagnosis and follow-up scans. In follow-up scans, anatomical localization and diagnostic information is not needed, hence very low dose protocols should be used.

An example of a fictional patient who needs one diagnostic scan and four follow-up scans can lead to a dose reduction of approximately 60% by implementing the strategy proposed in this project.

References

[1] Who.com
[2] Huang B, Law M, Khong P (2009) Whole body PET/CT scanning: estimation of radiation dose and cancer risk. Radiology;251:166-174.
[3] Franck C. (2011) Evaluatie van dosis reductivetechnieken op een dual source CT. Master's thesis. University Gent

Content table

List of figures

List of tables

List of abbreviations

68Ge/68Ga	Gallium-68 generator
AEC	*Automatic exposure control*
ATP	Adenosin Tri Phosphate
Bq	Becquerel
CNR	Contrast to noise ratio
Cs	Cesium
CT	Computed tomography
CTDI	CT dose index
DLP	Dose length product
DNA	Desoxyrubinucleineacid
ED	Effective dose
FBP	Filtered back projection
FDG	18F-fluorodeoxyglucose
FOV	Field of view
FWHM	Full width half maximum
GLUT	Glucose transport proteins
Gy	Gray
HU	Hounsfield units
IQFinv	Inverse image quality
IR	Iterative reconstruction
Kcps	Kilocounts per second
kV	Kilovolts
LAT	Lateral
LDPE	Low density polyethylene
LOR	Line of respons
LSO	Cerium-doped lutetium oxyorthosilicate
mA	Milliampere
MTF	Modulation transfer function
NEMA	National Electrical Manufacturers association
PA/AP	Posterior-anterior/anterior-posterior
PET	Positron emission tomography
PMP	Polymethylpenthene
PMT	Photomultiplier tube
RMSE	Root mean square error
ROI	Region of interest
SAFIRE	Sinogram Affirmed Iterative Reconstruction
SD	Standard deviation
SNR	Signal to noise ratio
SPECT	Single Photon Emission Computed Tomography
TOF	Time of flight
Z	Atom number
μ	Linear attenuation coefficient

1. Introduction

1.1.Nuclear medicine

Every medical process can be represented by three F's, namely Find, Fight and Follow-up. With Find, the diagnosis is meant of a certain disease. If a patient gets sick it is important that the disease is detected as soon as possible and that this diagnosis is correct as it will have a great influence on the treatment and recovery of the patient. Often the earlier a disease is detected ,the higher the chances for survival, hence early and accurate detection is very important in medical healthcare. With Fight, it is meant that once the disease has been diagnosed, the right treatment, in the right amount of doses, at the right time, etc will be given, hence an optimal recovery can be assured to the patient. The last F is Follow-up. Here it means the follow-up of the development of the disease and the evaluation of the therapy that is used to cure/treat the disease. The three F's are equally important in the medical field and should all three be optimized as much as possible. This optimization process is important to improve the comfort and recovery of the patient. In most cases, a process is focused on one F, but certain systems can cover multiple domains. An important example of coverage of the three F'sis nuclear medicine[1].

In nuclear medicine a radioactive tracer is introduced in the body and by radioactive decay, this particle will emit photons that can be visualized by a PET or SPECT camera. As these radiotracers can be very specific, it can be used as a diagnosis and follow up in cardiology, oncology, etc. By using the same agents but different radiotracers, it can be used as a treatment method. For example I-123 can be used as diagnostic tool for thyroid pathologies, but I-131is used in thyroid cancer treatment. In Europe, every year over 6 million patients benefit from a nuclear medicine procedure, so it can be stated that nuclear medicine is a frequently used imaging method in a wide range of fields[1].

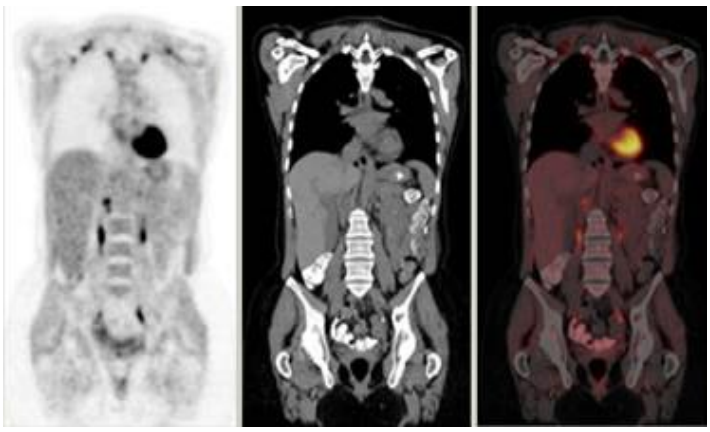

Figure 1-1PET-image (left), CT-image (middle) and PET-CT image (right) of a cardio-patient[2]

The main application of Positron Emission Tomography (PET)situates in the oncology field. According to statistics of the World Health Organization (WHO), cancer is the leading cause of death worldwide, accounting for 8.2 million deaths in 2012 and a morbidity of approximately 14 million new cases. The number of new cases is expected to rise above 70% over the next 20 years[3].

Cancer arises from one single cell, which transforms from a normal cell to a tumor cell due to mutations in the DNA. Risk factors for these mutations can range from external factors (ionizing radiation, food contaminants, infections,…) to spontaneous events (ageing,...). Typically a progression from a pre-cancerous lesion to a malignant tumor goes through a multistage process, which can take numerous of years. The success of a treatment of cancer is highly dependent on the early detection of the tumor and on the type of cancer (breast cancer, cervical cancer,…).Early diagnosis is particularly relevant when there are no effective screening methods available. In absence of any early detection or screening, patients are diagnosed at late stages when curative treatment is no longer an option[3,4].

A way of achieving an early detection of cancer is the use of PET. By introducing a radioactive tracer, specifically for tumor cells, it is possible to diagnose cancer at an early stage, increasing the chances for survival and cure of the patient. Combining the metabolic information of the PET scan with the structural information of a computed tomography (CT) scan can deliver an immense added value for the diagnosis by the physician.

1.2.Computed tomography

1.2.1. Production of X-rays

Computed tomography is only possible by the use of X-rays. X-rays are a form of electro-magnetic radiation with a wavelength ranging from 0.01 to 10 nanometers, which corresponds to an energy ranging from 100 eV to 100 keV. In diagnostic applications, X-rays are generated by the use of an X-ray tube. A schematic of an X-ray tube is depicted in figure 2.

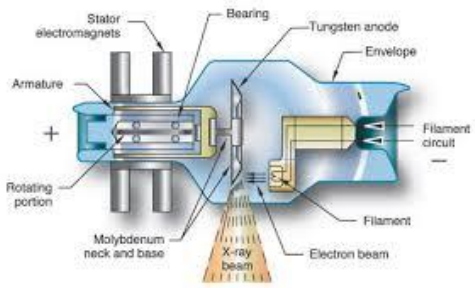

Figure 1-2: components of a X-ray tube[5]

The main components of an X-ray tube are a tungsten anode, a cathode and a vacuum envelope. In the cathode a filament is present, where electric current will pass through. Whenever there is an electric current going through the filament, this filament will heat up and will emit electrons. These electrons will be accelerated by a high electrical field present between the anode and cathode. The accelerated electrons will collide with the anode and will produce X-rays mainly by the brehmstrahlung principle[6]. The main problem in producing X-rays is the low yield, which is less than 1 percent in the range of 30 to 140 kV, as the rest of the energy will be converted into ionization of the cathode atoms, which results in heat. Hence a rotating tungsten anode is used to achieve the highest heat dissipation. At last, the tube envelope should be vacuum, so electrons in the beam will not interact with air particles and be lost in the process.

Three ways of interacting of the colliding electrons with the cathode are possible. As already mentioned, the first and main way of creating X-rays is by the Brehmstrahlung effect. This means that the electrons will be decelerated by the nuclei of the anode, which will create a continuous X-ray spectrum (1/E spectrum). The higher the deviation of the electron will be, the higher the energy of the created photon[7]. The path of the electron (straight line) and created photon due to Brehmstrahlung is depicted in figure 3.

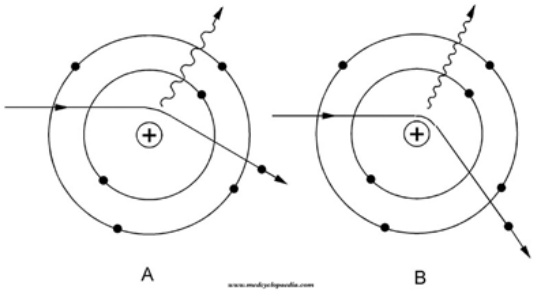

Figure 1-3 Creation of X-rays due to Bremstrahlung[8]

A second way of interacting is by the creation of characteristicsX-rays. By colliding with the orbital electrons of the anode, atoms will be exited. During their relaxation, specific X-rays will be emitted with discrete energy levels, equal to the energy differences of the orbits[7].

These are plotted on the continuous X-ray spectrum which is visualized in figure 4. A third phenomenon happening in this interaction is the creation of an Auger electron, which has a negligible influence on the created X-ray spectrum[6].

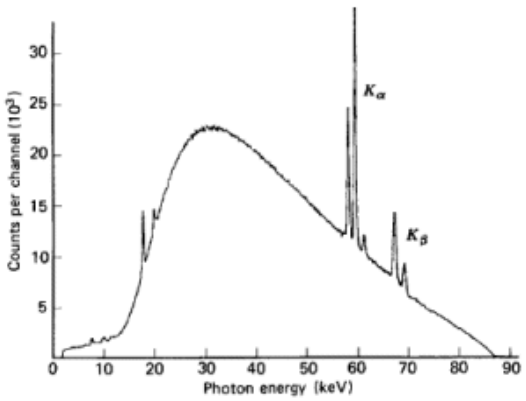

Figure 1-4*: Typical X-ray spectrum of tungsten anode*[6]

Two important parameters in CT, which have an influence on the spectrum, are the tube current and the tube voltage. The tube voltage is expressed in kilo volt (kV) and is the size of the electric field applied to accelerate the electrons. The tube current is expressed in milli-ampere (mA) and represents the current of electrons inside the electron beam. The higher the tube voltage is, the higher the maximum energy and mean energy of the photons will be. If the tube current is increased, the energies of the photons stay the same, but the counts per channel will increase in the spectrum.

1.2.2. Computed Tomography principle

Computed tomography (CT) is one of the most used image modalities for structural information. By using external ionizing radiation, an image of the internal structure of a patient is created. The advantage of CT over conventional radiography is that trans-axial images are taken, which eliminates the problem of superposition. Also due to the reduction of scatter radiation, the low contrast resolution will greatly increase. Contrast differences up to 0.3% can be detected by a CT scanner[9].

Typically a spiral CT scan is taken, which means that a X-ray tube rotates around the patient while the table moves in the axial direction (z-direction) at a constant speed. In this way the patient body is scanned in a helical way. An important parameter for this acquisition is the pitch. The pitch is defined as the distance the table has traveled in one 360° gantry rotation divided by the beam collimation.

$$Pitch = \frac{table\ feed}{nominal\ beam\ width} \tag{1-1}$$

In figure 5, a pitch of one means that the table will move the same distance in one rotation of the tube as the beam width, hence slices will connect to each other. A pitch of two means that the table feed will be twice the nominal beam width, which can lead to data loss.

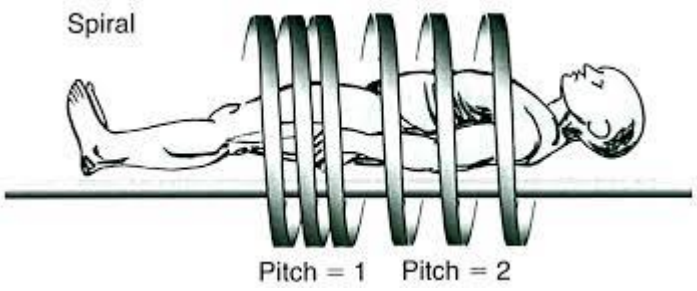

Figure 1-5: Spiral CT scanning with different pitch[6]

Alternatively to spiral scanning, sequential scanning is possible. Sequential scanning means that the X-ray tube rotates around a stationary table. After this rotation, the table is moved in the axial direction and again the X-ray tube rotates around the body. This acquisition technique is also known as the step-and-shoot mode.

1.2.3. CT acquisition

In CT, the X-rays are created by a X-ray source and a detector which both rotate around the patient. As already mentioned the most important parameters of the X-ray beam are the tube current and tube voltage parameters, which units are respectively kilovolt (kV) and milliampere-seconde (mAs). The quality and intensity of the X-ray beam is therefore dependent on the tube current, tube voltage, filtration, etc. These X-rays will enter the human body and will be attenuated by it.

The created X-rays are attenuated by the patients tissue due to a combination of the photo-electric effect and Compton scatter. The attenuation of these X-rays is highly dependent on the density of the tissue (bone versus soft tissue) and the thickness. Logically the denser and thicker the tissue is, the more X-rays will be attenuated and the less X-rays will enter the detector.

The transmission of photons through matter can be characterized by the linear attenuation coefficient, which can be defined as the probability per unit path length that the photon will interact with matter. A large attenuation coefficient means that the X-ray beam will be quickly attenuated while it passes through the tissue [10]. For an ideal monochromatic beam of photons, the relative reduction of the beam intensity –dI/I through matter, which has a linear attenuation coefficient μ is proportional to the material thickness dt which results in the following formula:

$$I(t) = I_0 \exp\left(-\int_0^t \mu \, dt\right) \qquad \textbf{1-2}$$

Where I_0 is the incident beam intensity and t is the thickness of the material. If the material is homogenous, formula 1-2 simplifies to the well-known Lambert-Beer law.

$$I(t) = I0 \exp(-\mu\, t) \qquad \textbf{1-3}$$

The linear attenuation coefficient is expressed in inverse centimeters (cm^{-1}) and is proportional to the density of the matter. Hence the total attenuation coefficient for an interaction is the total sum of possible photon interactions which are the photoelectric effect and the Compton scattering. It is known that the attenuation coefficient is strongly dependent on both photon energy and the material it travels through, according to the following equation[10].

$$\mu \;\alpha\; \frac{Z^{4.5}}{E^3} \qquad \textbf{1-4}$$

The total linear attenuation coefficient for bone and muscle is shown in figure 6 in the range of 10 to 1000 keV. In this figure the attenuation is split up in the photoelectric component and the Compton scatter component. Below 30 keV, the linear attenuation coefficient is dominated by the photoelectric effect for materials with high Z (bony tissue).

For higher photon energies, in the range of 200 to 1000 keV Compton scattering becomes more important for all densities and the slopes are less steep.

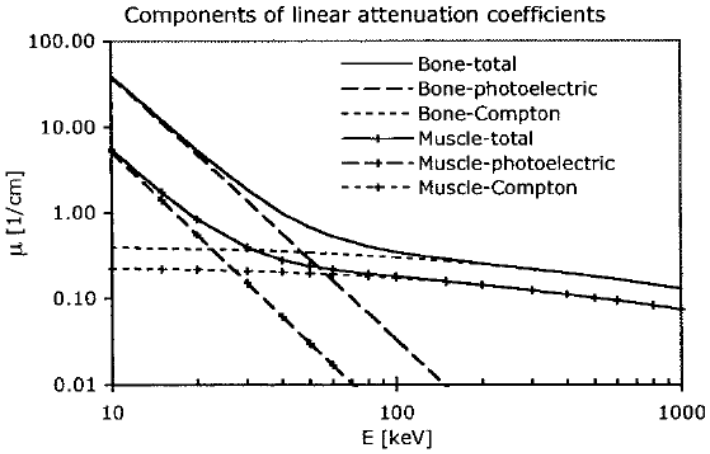

Figure 1-6: Total linear attenuation coefficients for muscle and bone[9]

In a following figure (figure 1-7) the total attenuation coefficient is depicted for different materials in function of photon energy. Here it can be clearly seen that the linear attenuation coefficient for bone or contrast agent is higher than for example fat or muscle in the whole energy range, due to its higher density.

Important to note is the k-edge for certain materials (Iodium and BaSO4), which elevates the attenuation even more. This increase of attenuation is due to the photoelectric absorption of the photons of the inner electron shells. The energy at which the photon is absorbed corresponds to the binding energy of the K-shell electron of an atom. A photon having an energy just above the binding energy is therefore more likely to be absorbed than a photon having an energy just below this binding energy[10]. This explains the important increase of attenuation of contrast agents used in imaging.

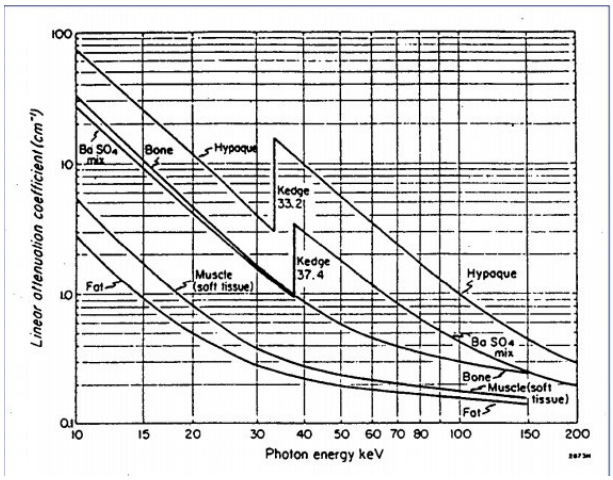

Figure 1-7: Linear attenuation coefficient for different materials in function of photon energy[6]

The differences between the curves in figure1-7 are the basisof contrast in CT. The larger the difference between the curves is, the better the contrast of the image will be. For example, in mammography a tube voltage of 30 kV is chosen as the difference between muscle and fat is high enough to achieve good contrast. But 30 kV will not be possible for a thorax CT-scan as most X-rays will be attenuated by the rib cage and thickness of the patient, whereas the amount of X-rays reaching on the detector will be too low. Therefore typically higher tube voltages are chosen [10].

Another very important conclusion that can be made out of this graph (fig 7) is that the attenuation for different modalities can be completely different based on the photon energy used.

This is of essential importance in comparing X-ray images to PET images. Typically radiographic imaging occurs in the range from 30 to 140 keV and is determined by both photoelectric effect and Compton scatter, whereas PET images use511 keV photons, where the attenuation coefficient is solely governed by Compton scatter and will be much lower for the same material. This is particularly important for attenuation correction of PET images, which will be explained in part 1.4.

After attenuation by the tissue of the patient, the X-rays will be absorbed by the detectors and converted to an electric signal. In the fourth generation of CT-scanners (which are used mostly) these detectors also rotate around the patient, opposed to the X-ray tube, in a fan beam set up. The data collected by the detectors is then stored and images of the patient are created by using reconstruction algorithms. Typically a 512*512 pixel image is created, where the intensity is defined by the attenuation coefficient in that pixel.

In CT, traditionally a 120 kV energy photon bundle is used to scan a patient. The reasons for this are three-fold:

- reduce the dependence of attenuation coefficients on photon energy
- to reduce contrast of bone relative to soft tissue
- to produce a high radiation flux at the detector

These reasons are important to achieve a good detector response and therefore secure the image quality, but known in CT there is always a tradeoff between image quality and dose[11].

1.2.4. CT number

As already mentioned, contrast in a CT image is achieved due to the differences in linear attenuation coefficients of different tissues. In a CT-image, per pixel these attenuation coefficients are converted in CT numbers using following equation:

$$CT\ number = \frac{\mu_t - \mu_w}{\mu_w} * K \qquad \textbf{1-5}$$

In equation 1-5, μ_t is the attenuation coefficient of the measured tissue, μ_w is the attenuation coefficient of water at standard temperature and pressure, and K is a constant. Conventionally the K value is set at 1000, which results in a better contrast scale and is expressed in Hounsfield units (HU)[11].

CT numbers are established on a relative basis with the attenuation of water as a reference, thus the CT number for water will for every CT system be 0, whereas for bone and air these are respectively 1000 and -1000 HU. CT numbers may vary because of their energy dependence. It is therefore essential that CT systems ensure the accuracy and reliability of these numbers. The system incorporates a number of correction schemes to maintain the precision of these CT numbers[11]. The advantage of using CT numbers is that they exist on a relative basis with water as a reference. But a great disadvantage is that these CT numbers can be influenced by CT-parameters for example tube voltage, filtering, etc.

1.2.5. Dose reduction techniques

A CT –scan can deliver high dose, up to 18 millisievert (mSv) to the patient, hence it is important to find strategies to reduce this dose delivered to the patient. In the past, several dose reduction strategies have been invented and implemented.

The most important technologies are automatic tube current modulation, adjusting tube voltage and iterative reconstruction, which will be explained in the following paragraphs in detail.

- **Automatic exposure control**

Automatic exposure control (AEC), also known as automatic tube current modulation, is a technique that modulates the tube current automatically in the x-y plane (angular modulation), along the scanning direction (longitudinal modulation) or both (combination modulation). Angular modulation means that the tube current is modulated during each gantry rotation, according to the size, shape and attenuation of body region being scanned. Longitudinal modulation means that the tube current is adjusted along the scanning direction of the patient.

The modulation is based on the topogram scan where the tube current is estimated according to the patient size, shape and attenuation correction of body parts being scanned. Today, practically all CT systems are delivered with AEC systems operating with tube current modulation in three dimensions (3D). If the AEC system is optimized, it can reduce the radiation dose delivered to the patient by 20-40% while still producing images of sufficient quality for diagnosis[11].

The Siemens CT-systems uses a combined tube current modulation system called CARE Dose 4D. This system adapts the radiation dose to the size and shape of the patient automatically, achieving optimal current modulation in two ways. First, tube current is varied according to the topogram, by comparing the patient to a standard-sized patient. For larger patients this means that the tube current will increase and will be decreased for small patients. Secondly, real-time angular dose modulation measures the actual attenuation in the patient during the scan and adjusts the tube current accordingly. This is important in reducing dose in the shoulder and pelvic region, where the lateral attenuation is higher than the anterior-posterior attenuation[14].The reference for image quality in the Siemens system is the quality reference mAs, which makes sure that the same image quality is achieved as the reference tube current for a standardized patient.

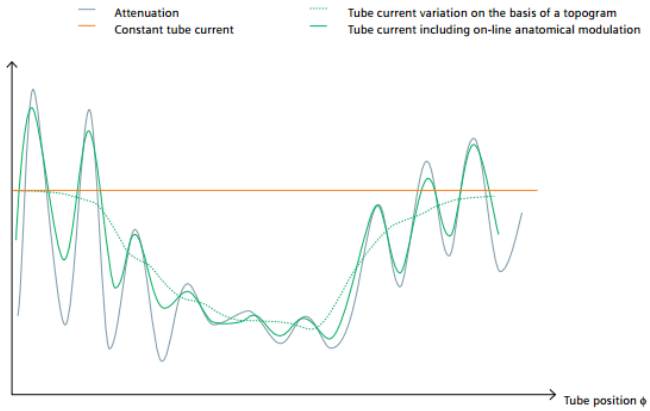

Figure 1-8: attenuation (light green) and tube current in function of axial position[14]

- **Automatic tube voltage selection**

Lowering the tube voltage has been proven to be a great strategy for dose reduction. Low tube voltage protocols take advantage of higher attenuation levels for iodinated contrast medium at lower x-ray tube voltages as a result of a greater photoelectric effect and decreased Compton scattering. The closer the tube voltage approaches the K-edge of iodine (33.2 keV), the greater the attenuation of the contrast medium will be, improving the contrast. However, low tube voltage comes at the cost of greater image noise, and the tube current needs to be increased correspondingly to maintain image quality. Despite promising publications, radiologists have been hesitant to apply low tube voltages in CT mainly due to the challenging interaction of the tube voltage with the image contrast and noise and the time consuming adjustment of the tube current-time product [14].

However the recent invention of an automatic tube voltage selection technique holds the potential to overcome these problems. In a study performed by Schindera et al[15] the radiation dose decreased with 39% when the tube voltage was lowered from 120 kV to 100 kV by the use of automatic tube voltage selection.

The tool in the Siemens system for automatic tube voltage selection is named CAREkV. CAREkV uses information from the topogram to optimize kV and mAs to achieve adequate image quality and lowest dose. The key image quality parameter here is the contrast to noise ratio (CNR). For a constant CNR in CT, the radiation dose can be significantly reduced by choosing 80 kV or 100 kV instead of the classical 120 kV. According to Siemens Healthcare a reduction of 20% in CTDI can be achieved by reducing the voltage from 120 kV to 100 kV [14].

But for larger patients who have higher X-ray attenuation, the output current at lower kV settings may not be sufficient to produce the required CNR. For these patients, higher X-ray tube voltages will be necessary.

- **Iterative reconstruction**

The most used algorithm for the reconstruction of CT image is the filtered back-projection. In filtered back-projection, the projections from several angels, obtained by the detector, are projected back through the image to obtain an approximation of the original. As the projections are projected back over the whole image in a straight line, this will created a high amount of blurring (star-like artifacts) that will occur in the other parts of the reconstructed image. To eliminate the blurring effect a high-pass filter is used. Hence filtered back projection is the combination of back projection and ramp filtering[9,16]. The advantage of the FBP technique is that it is a fast, straightforward process which doesn't need expensive calculation.

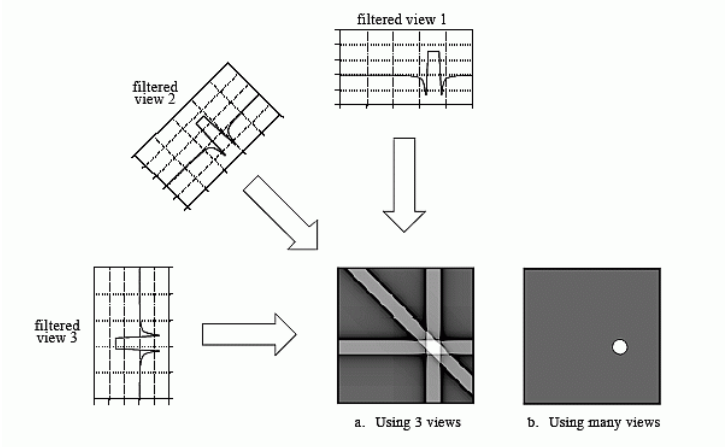

Figure 1-9: Filtered backprojection principle[9]

Alternatively, a second reconstruction algorithm for CT exists, which is the iterative reconstruction. Iterative reconstruction results in less noisy images but is a computationally more expensive method, compared to the filtered back projection method[9]. Iterative reconstruction uses a correction loop. After the image is reconstructed from the measure projections, the re-projection starts.

In this re-projection a simulation of the CT-scan is performed with the reconstructed image as measuring object. Next these simulated projections are compared to the real measured data and corrections are calculated. This loop is repeated until the difference between the measured and estimated projections is smaller than a certain threshold.

In every iteration, non-linear image reconstruction algorithms are needed to improve the spatial resolution in high contrast zones and reduce noise in lower contrast regions. This step is essential for noise reduction in iterative reconstruction. Hence IR starts with an initial estimation of the object, which will then be improved in every iteration step by comparing the measured projections with the estimated projections[17]. The highest disadvantage of this technique is that this takes a lot of time, as it needs a lot of transformations and iterations. It takes approximately 100 to 1000 times more than FBP.

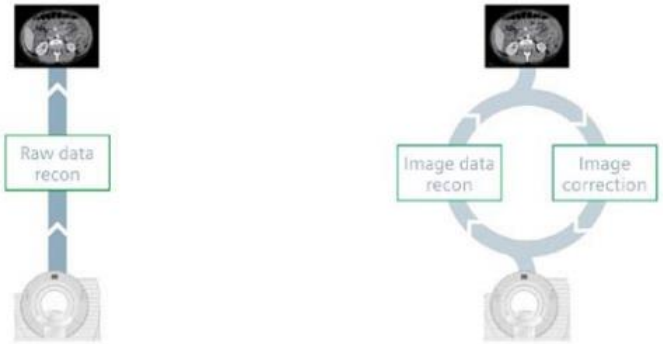

Figure 1-10 Standard filtered backprojection (left) and iterative reconstruction (right)[18]

IR is already been used for a long time in PET and SPECT imaging, but due to the faster processors and bigger memories of current computer system, IR can be implemented in the CT world. A new approach to IR is the use of SAFIRE, by Siemens. SAFIRE stands for Sinogram Affirmed Iterative Reconstruction and is a IR technique that utilizes both projection space data and image space data, with the number of iterations in each space dependent on the needs of a specific scan. Since normal IR is very time-consuming, the use of SAFIRE, reduces this a lot. It can reconstruct up to 20 images per second and provide up to 60% reduction in dose.

SAFIRE performs an initial reconstruction using a weighted FPB, following two different correction loops in the reconstruction process (figure 1-11). The first loop (where the data is re-projected in the raw data space (sinogram space) is utilized to correct for imperfections in the original reconstruction and remove any artifacts from the data. The detected deviations are again reconstructed using the weighted FBP, yielding an updated image.

This loop is repeated several times depending on the exam type. In each iteration, a dynamic raw-data based noise model is applied reducing the image noise without decreasing the sharpness of the image. The second correction loop occurs in the image space, where noise is removed from the image through a statistical optimization process. The corrected image is compared to the original and is repeated a number of times, again depending on the exam type[18].

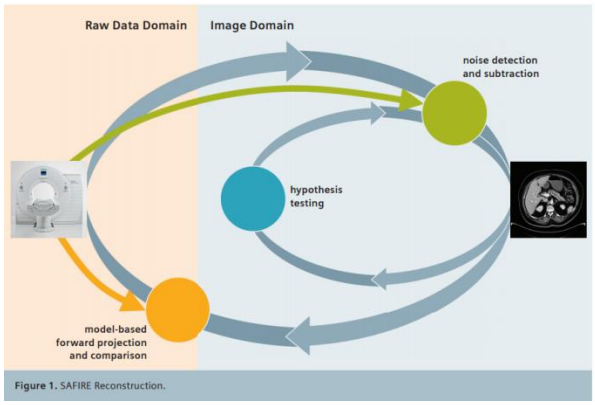

Figure 1-11*: Schematic of SAFIRE reconstruction*[18]

In a study at the Mayo Clinic[19] the difference in image quality between SAFIRE reconstructed images at half the routine dose where compared to full dose FBP images. This resulted that the image quality in both reconstructions were the same, showing that by implementing SAFIRE in CT systems, a dose reduction of 50% can be achieved.

1.3.Positron emission tomography

A CT image of a patient can provide exquisite anatomical detail that is often invaluable for diagnosis. On the other hand, positron emission tomography (PET) provides functional information regarding the patient and disease[1]. Especially in the field of tumor detection and cardiology imaging, PET gives a great advantage in diagnosis and follow up in comparison to CT. As functional changes occur before anatomical changes in time, it is important for an early diagnosis to image functional processes, which can be done by using molecular imaging, such as PET. Hence by using functional imaging it is possible to detect a disease earlier, starting a treatment earlier, thus increasing the survival chances of the patient. This is schematized in figure 1-12, where the symptoms of a disease are shown as a function of time.

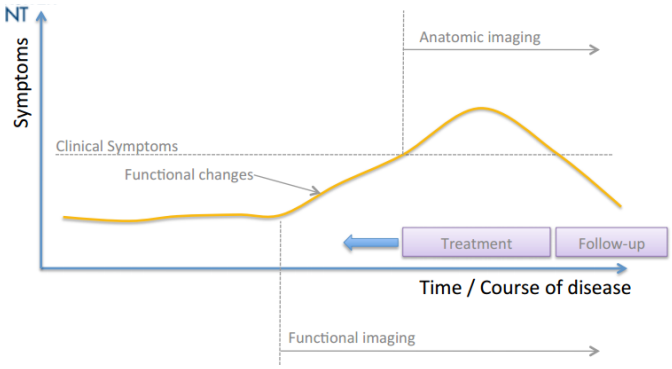

Figure 1-12: Symptoms in function of time where functional changes occur before anatomical changes[1]

1.3.1. Radioactive decay

In PET, imaging is done by the tracer principle which means that a radiotracer is introduced in the body and will be distributed over the body, according to its specificity. A radiotracer consists of two parts, the agent and the label. The agent will define the specificity of the radiotracer by binding to a biological component, while the label will make it possible to detect the radiotracer in PET by means of radioactive decay.

Radioactive decay means that the label consists of radioactive nuclei. The atomic nucleus contains a number of protons and neutrons. In some cases, there may be too many of one or the other or they may be configured in such a way to make the nucleus unstable. In these cases, the nucleus may seek to become more stable by undergoing a nuclear transformation with the emission of a particle such as a gamma ray, an alpha particle or beta particle. If the nucleus contains too many protons, the nucleus may transform itself by emitting a positive beta particle, also known as a positron, or by capturing an orbital electron. A positron has the same mass as an electron but a positive charge.

The formula for positron decay is shown in equation 1-6. Radioactive nucleus X will decay to nucleus Y by emitting a positron and a neutrino[20].

$$ {}^{A}_{Z}X \rightarrow {}^{A}_{Z-1}Y + {}^{0}_{+1}e^{+} + \nu_e \qquad \textbf{1-6} $$

After emission of the particle by the nucleus, the positron will travel several millimeters in the tissue until it loses most of its kinetic energy due to ionisations, at which point it will combine with an orbital electron to form a 'positronium'. This positronium only exists for a very short time (10^{-10}s) and will annihilate, meaning that it will convert its mass into two photons that are emitted in opposite direction (180°) to preserve equilibrium of momentum. The energy of the two photons is determined by Einstein's equation, therefore the two photons each have an energy of 511 kilo-electronvolt (keV), equal to the rest mass of an electron[11].This process is shown in figure 1-13.

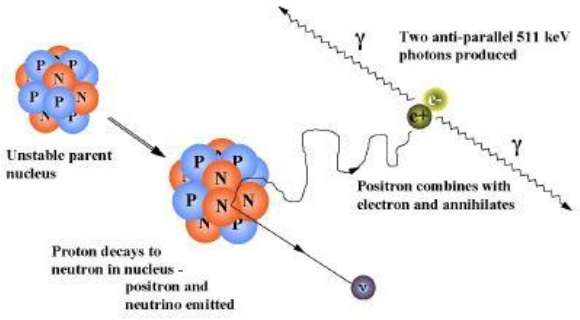

Figure 1-13: positron emission and annihilation process[21]

The amount of disintegrating nuclei per second is expressed as activity with Becquerel (Bq) as its unit. One Bq is the same as one disintegrating nucleus per second, hence this is a very small unit. Mostly this activity is expressed in megabecquerel (MBq).A second important quantity in radioactive decay is the half-life $T_{1/2}$. The half-life is the time it takes for the activity of a given amount of radioactive substance to decay to half its initial value and can be calculated as followed:

$$ T\frac{1}{2} = \frac{\ln(2)}{\lambda} \qquad \textbf{1-7} $$

,where $\lambda$is the decay constant, which is the inverse of the mean lifetime of a radioactive particle[20]. For example, fluor-18, which is the most used radioactive element for PET applications, has a lambda of 0.00632 min^{-1}, which results in a half-life of 109.7 min.

Due to the decay of the nuclei, the activity decreases exponentially over time according to the formula. This formula is important in PET to calculate the activity of injected FDG after measuring the initial activity.

$$A(t) = A0 * \exp(-\lambda * t) \quad \text{1-8}$$

In order to have a good bio-distribution of the radioactive element, the tracer should be coupled to an agent. In oncology, fluor-18 is coupled to a glucose molecule, which then is named 18F-fluorodeoxyglucose, or shorter FDG. FDG is a glucose analog where the hydroxyl group in the C2 position is replaced by 18-fluorine. As FDG has approximately the same structure as glucose, it will behave biologically almost the same[22]. The structure of FDG is shown in figure 1-14.

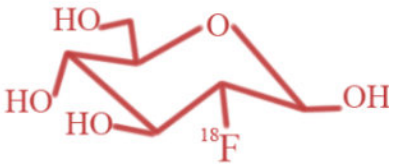

Figure 1-14: chemical structure of 18F-fluorodeoxyglucose[23]

Just as glucose, FDG is transported in the cell actively by a group of structurally related glucose transport proteins (GLUT). Once intracellular, glucose and FDG are both phosphorylated by hexokinase as a first step in the glycolysis. Normally phosphorylated glucose continues the glycolytic pathway to transform to ATP for energy production [22]. FDG however cannot enter the glycolysis pathway and becomes trapped inside the cell. It cannot leave the cell, hence the higher the metabolism of a cell is, the more FDG will be trapped in the cell.

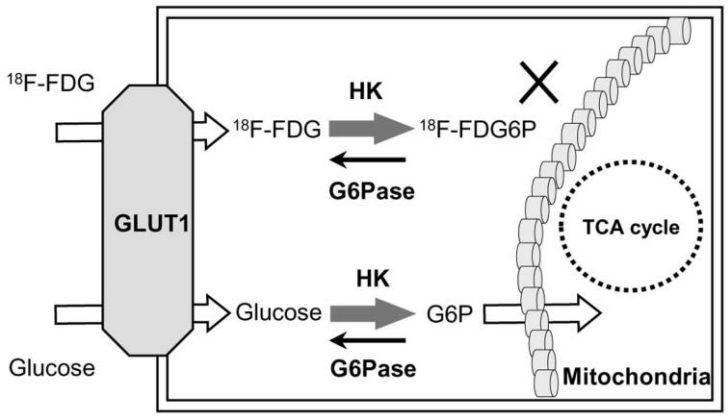

Figure 1-15: Molecular pathway of glucose and FDG[24]

It has been shown[25] in human studies that tumor cells show increased glucose transport by increased and deregulated expression of GLUT1 and GLUT3. These high levels of GLUT1 expression in tumors have been associated with poor survival in cancer patients. Tumor cells are highly metabolically active and favor the anaerobic pathway adding to the glucose demands. This combination of mechanisms allows the tumor cells to uptake and retain higher levels of FDG, compared to normal tissue[22].

It has been reported that the degree of FDG uptake in tumor cells is correlated with the degree of malignancy of the tumor, hence diagnosis and staging is possible by assessing FDG uptake[26].Diagnosis of tumors by the use of FDG-PET is possible due to this principle of a higher metabolism of tumor cells, but FDG is not cancer specific in regions where high levels of metabolism and glycolysis is present. For example in the brain there is always a high uptake of glucose, but also in sites of hyperactivity (muscular, nervous system), inflammation (infection) or bowel activity[26,27]. To overcome this problem of specificity, other radioactive agents can be used for diagnosis in oncology, cardiology…

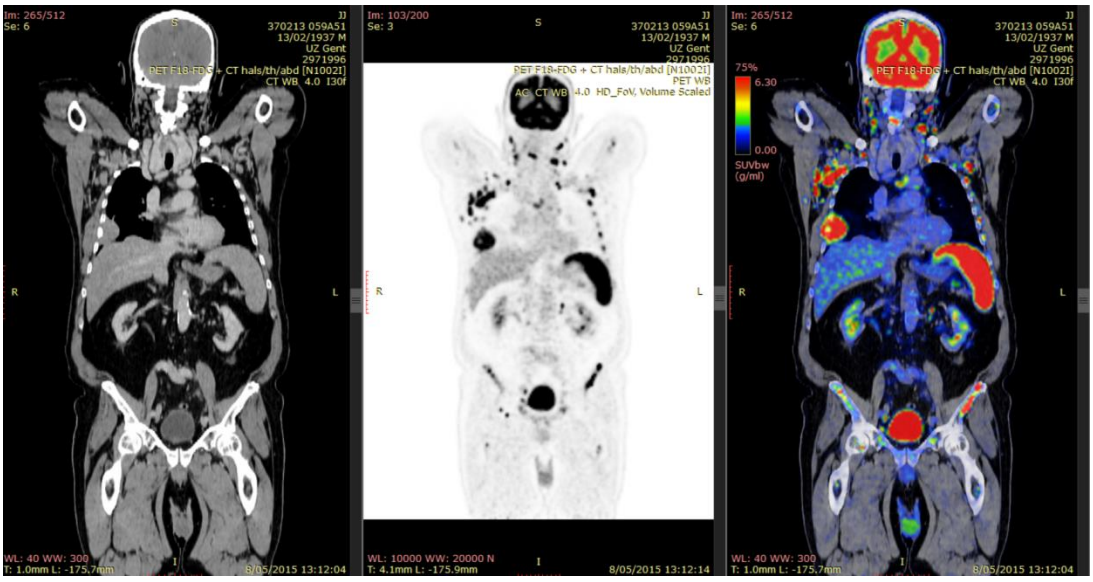

Figure 1-16: cancer patient undergoing a PET-CT examination. CT-scan (left), PET-scan (middle) and combined scan (right)

An example of diagnosis of tumors by the use of PET-CT is shown in figure 16.The CT and corrected PET image are depicted respectively left and in the middle. On the right the combined PET-CT is shown. It can be clearly seen that there is a high FDG tumor uptake in bone and lymph nodes. Clearly a tumor is visualized inside the lungs. Important to note is the unspecific uptake in the brain and bladder.

1.3.2. PET principle

As hidden in the name, PET is based on the detection of positron emission. As it is not possible to detect the positron itself, decay products can be measured. In this case, both created photons are used to localize the position of positron emission. If each of these photons interact with detectors on opposite sides of the PET scanner and are detected within a short time window (5-15 ns), a 'coincidence' detection occurs, and the annihilation event can be assumed to have occurred along the line that connects the two detectors, referred as the line of respons (LOR).

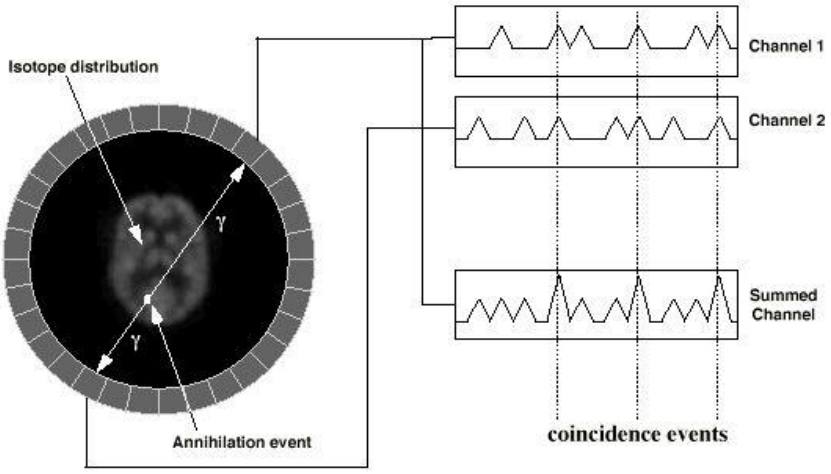

Figure 1-17: basic principle of coincidence detection in PET[28]

To a first approximation, the spatial resolution of a PET scanner is determined by the size of the detectors used in the PET scanner. Modern clinical PET scanners use detectors between 4 and 7 mm in size. On the other hand, even if the annihilation event could be localized exactly, this is really not the locus of interest. One really wants to know from where the positron was emitted, in other words the location of the radioactive nucleus. Because the positron traveled several mm before annihilation (positron range), the distribution cannot be localized exactly. In addition, the two photons may not be emitted at exactly 180 degrees to each other. If the positron-electron pair was not completely at rest when annihilation occurred, conservation of momentum would state that the photons would be emitted at an angle slightly different than 180 degrees.

These two factors (positron range and non colinearity) lead to the best possible spatial resolution of 3 mm for a whole-body PET scanner[9].

Two small detectors on either side of the patient would not collect many photons, therefore the placement of a large number of detectors around the patient is necessary to acquire high-resolution PET data in a reasonable amount of time. To acquire data simultaneously from a number of imaging planes, several detector rings can be placed next to each other. Thus, a single detector module becomes a rectangular mosaic of small detectors [11].

Not all coincidence detection events are true detections. When both annihilation photons exit the patient without undergoing any interaction and are detected in coincidence, this is called a true coincidence. However, it is possible that one or both of the photons will scatter due to Compton interaction before exiting the patient. In this case the LOR linked with this coincidence detection may not pass through the actual annihilation and therefore does not localize this event. This effect is known as a scatter event.

Last, at higher count rates it is possible that two independent events occur simultaneously and that two photons are randomly detected in one coincidence window. The resulting LOR does not accurately localize an annihilation event, as this is random event. Randoms and scatters will lead to a background activity which reduces the image contrast of an PET image[9].

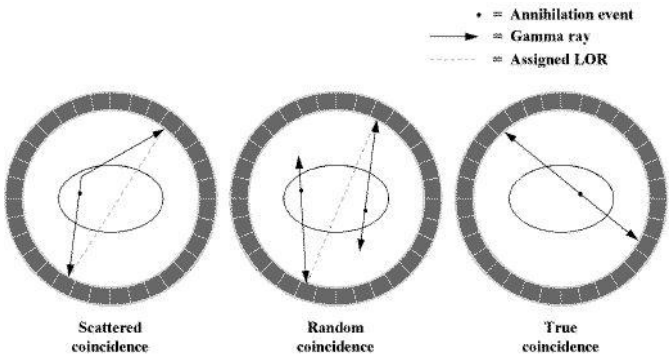

Figure 1-18: schematic of scattered, random and true coincidences [28]

One approach to reduce scatter coincidences is to introduce absorbing septa between the detector rings. These septa act similarly to the anti-scatter grids used in radiography and thereby reduce inter-planar scatter within the scanner. With the septa in place, detectors are allowed to be in coincidence with either detectors in the same ring or adjacent rings and thus the data can be reconstructed as a series of two-dimensional transverse plane, which is called 2D PET. Removal of the septa will lead to a 3D PET acquisition. The difference in 2D and 3D imaging is shown in figure 1-19.3D PET leads to a high increase of sensitivity, particularly in the center of the axial FOV. The disadvantage of 3D mode is the higher scatter fraction (35-50% for 3D vs 10-20% for 2D)[9,29].

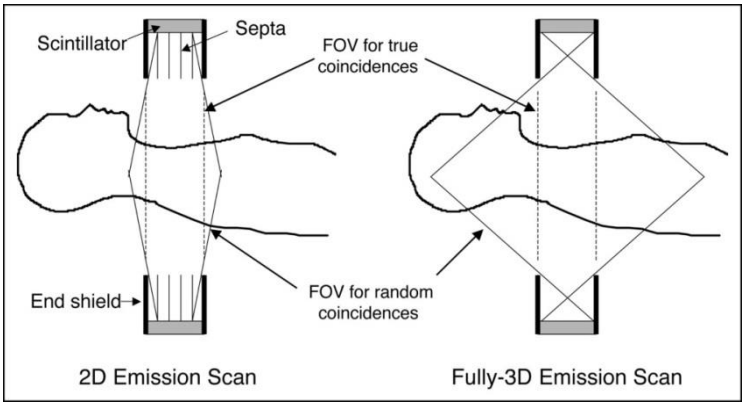

Figure 1-19: 3D versus 2D PET[29]

1.3.3. Time of flight PET

As already mentioned the signal for PET imaging is produced by the annihilation process of an emitted positron, where two photons are emitted back-to-back with an energy of 511 keV. These two photons need to be detected in a certain coincidence time window by the detector ring to generate a signal to create a LOR. The emission distance (see figure 1-20) along the LOR is determined by

$$d = c * \frac{t1 - t1}{2} \quad \textbf{1-9}$$

,where c is the light speed and t1 and t2 are the arrival times of the two photons. In conventional PET, the difference in arrival time cannot be measured precisely enough to localize the emission point along the LOR. All the LORs are collected and assuming uniform probability that the emission points lie along the LOR, reconstruction is possible. However by the assumption of uniform probability, noise from different emission events is projected during image reconstruction, leading to an increased noise, resulting in a lower signal to noise ratio.

In time-of-flight PET (TOF-PET), it is possible to measure the arrival times of the photons with high precision, due to new scintillator crystals (LSO) and fast electronics. Due to this precise time measuring it is possible to localize the emission point along the LOR within a small uncertainty. The uncertainty is determined by the system coincidence timing resolution (Δt). The coincidence timing resolution is measured as the full width at half maximum of the histogram of TOF measurements from a point source.

The corresponding spatial resolution related to the timing resolution is given by:

$$\Delta x = c * \frac{\Delta t}{2} \quad \textbf{1-10}$$

If Δx is the same as or smaller than the detector spatial resolution, which is approximately 4-5 mm, then it is possible to create an image without image reconstruction algorithms. Typically, this is not the case asΔx is typically an order of magnitude higher than the detector spatial resolution, hence image reconstruction is currently still needed. However, the noise will be reduced greatly since the noise from different events will now only be forward and backward projected over a limited amount of voxels[30].

Karp et al[31]tried to quantify the difference of TOF PET compared to non-TOF PET and concluded that TOF leads to a better contrast vs noise trade-off than non-TOF both in experimental phantoms and patient studies.

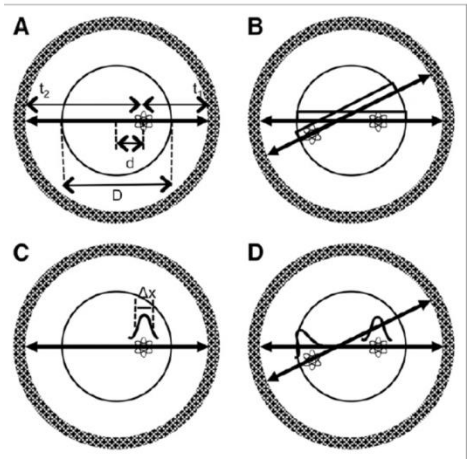

Figure 1-20: Principle of conventional PET (A,B) versus TOF-PET (C,D) [30]

Figure 1-20 clearly summarizes the principle of TOF-PET. In A, the emission point is shown at a distance d from the center of the scanner within an object (D). The two 511 keV photons are detected by the detector ring in coincidence at times t1 and t2. First no correction is done based on TOF (B), where uniform distribution is used to reconstruct the image, leading to an increase of noise. In C, with TOF information, position of the emission point is localized along the LOR with an uncertainty delta x. (D) At last the reconstruction for TOF-PET has a better localization and will lead to a reduced noise correlation of events in image space.

1.3.4. Standardized uptake value

The FDG uptake in tumors is correlated with the degree of malignancy, to differentiate recurrent tumors from scar tissue, for staging and to asses response after therapy. Hence quantification of the amount of FDG uptake is necessary in PET. In assessing glucose uptake in tumors, certain studies have tried to measure the absolute glucose metabolic rate[26, 32]. But the feasibility of this is low due to the variability of the parameters used to calculate metabolic rates[33].

Therefore non-kinetic quantification or tumor uptake is necessary. This can be achieved by normalizing tumor uptake to injected dose per body weight[33]. This is known as the standardized uptake value (SUV). The formula is shown in 1-8. The FDG uptake is divided by the injected activity dose, corrected for the body weight of the patient.

$$SUV = \frac{FDG\ uptake}{\frac{injected\ dose}{(body\ weight)}} \qquad \textbf{1-11}$$

However several studies have shown that by normalization of FDG by body weight and generating the SUV leads to an overestimation of FDG uptake in heavy patients. To solve this problem Kim et al[33] have shown that normalization by using the body surface area of the patient is more accurate than the body weight.

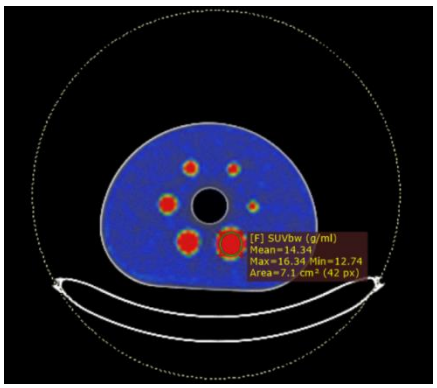

Figure 1-21: PET-CT image of NEMA phantom with SUV measurements (max and mean)

Moreover patient size is not the only source of variability in the usage of SUV. Measurement times are also important. It has been shown that the uptake period (time from tracer injection to PET scanning time) has an extreme effect on the SUV. In a study of Hamburg et al[34], it has been proven that it takes several hours before a plateau phase is reached for FDG uptake in lung tumors.

Scans obtained at usual imaging times for a PET scan (approximately 45-60 min) occur during a rapid uptake phase of FDG, hence resulting in a high variability. If in studies, imaging times are not managed correctly, this will lead to false conclusions, hence delaying scan times for several hours is advised to ensure that SUV measurements are made at plateau values. In many studies, the actual time of imaging is not even described[35].

Another factor that influences the SUV uptake is the plasma glucose levels. These levels have a major effect on the SUV. The blood glucose level has been shown to inversely-linearly affect SUVs. Intra-subject variations of plasma glucose can have highly significant effects on measured SUVs, although most studies indicate that the patients were studied in fasting state, the plasma glucose levels are rarely mentioned or corrected[36].

As this has shown that the SUV can be interpreted as a ‘silly useless value’, it usage as a quantitative index for malignancy should be discouraged. Therefore in this project, no SUV will be measured but a recovery coefficient for phantom studies will be created, which is the ratio of the measured activity and the true activity. This will be explained in chapter 2.

A last factor that influences the SUV is the region of interest effects. The size, shape and placement of the ROIare all important if the average counts within the ROI are used as measurement values. Placing a large ROI around an object and averaging all counts within the region will change the measured value because counts from the edge are reduced and will decrease the value.

1.4.Hybrid imaging PET-CT

PET scans will provide physiological information via the tracer principle, but a drawback of this method is that no accurate structural localization is available as only the tracer is visualized. Therefore combining PET with CT will lead to a combination of metabolic information with structural information. In addition, the CT part of a PET/CT study can be used to measure the attenuation information used for correction of PET images. Hence the advantage of combining PET and CT is threefold: Diagnostic information, anatomical localization and attenuation correction.

There are several physical effects that can influence the tracer uptake in PET images. The most significant of these effects are photon attenuation, scattered and random coincidences, detector time efficiency variations and scanner dead time. Of these effects, the most important one is photon attenuation, which has an effect on both the visual quality and the quantitative accuracy[10]. The difference between a corrected and a non-corrected PET image can clearly been seen in figure 1-22.

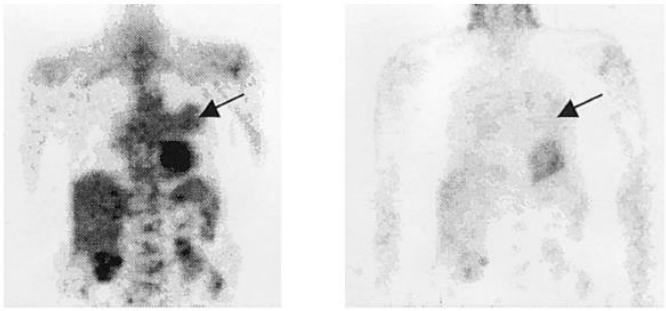

Figure 1-22: Example of FDG uptake with and without attenuation correction, respectively left and right[10]

In PET imaging, two high energy photons are emitted back-to-back and are detected to form a LOR. A problem in PET can be that there is a possibility that one or both photons will be attenuated in the body of the patient, resulting in a lower SNR of the image. The probability of detecting photons from an annihilation event from the center of an object is less than that for an event on the periphery because at least one of the photons is more likely to be absorbed or scattered if it has to travel through more material[10].Thus if there are two features, each with exactly the same amount of activity, the one on the periphery will have a much higher signal than the one at the center. To achieve uniform quantitative accuracy, the spatial variation in attenuation needs correction. The total probability that both photons escape without attenuation does not depend on where along the LOR the event occurs. It only depends on the thickness and attenuation coefficients of the object along the LOR[11].

By using the geometry in figure1- 23, the collected emission projection data can be represented by the formula 1-12, where the exponential term represents the attenuation along the LOR at detector position x' and projection angle ϕ, and where f(x,y) represents the distribution of the positron tracer in the patient[10].

$$p(x',\phi) = (\exp(-\int_{-\infty}^{\infty} \mu(x,y)dy')) \int_{-\infty}^{\infty} f(x,y)dy' \quad \textbf{1-12}$$

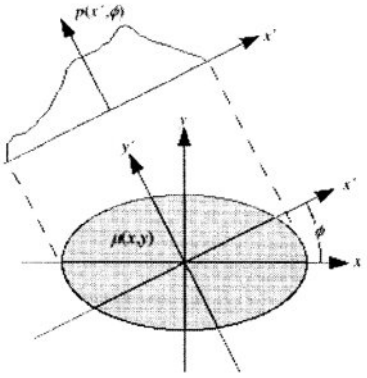

Figure 1-23Geometry used for projections of the attenuation object for eq. 1-12[10]

In PET, the goal is to estimate the distribution of radiotracer by using tomographic reconstruction to calculate the f(x,y)from the projection p(x',ϕ). The form can be simplified by expressing the inverse of the exponential term as an attenuation correction factor a:

$$a(x',\phi) = \exp(\int_{-\infty}^{\infty} \mu(x,y)dy') \quad \textbf{1-13}$$

,which is the inverse of the photon attenuation along the LOR for detector x' and projection angle ϕ. The correction of the projection data for photon attenuation can then be given by formula 1-14:

$$pcorr(x',\phi) = \mathrm{a}(\mathrm{x}',\phi)\mathrm{p}(\mathrm{x}',\theta) = \int_{-\infty}^{\infty} f(x,y)dy' \quad \textbf{1-14}$$

In this formula pcorr is the projected data that has been corrected for attenuation. These projections can be used in reconstruction algorithms such as FBPto create the image, which is the two-dimensional distribution of the radionuclide f(x,y).

In iterative reconstructions, the projection data can be constructed directly by using the attenuation correction factors as proper statistical weighting to the data.

Globally there are two ways of achieving the attenuation correction factors, calculated and measured attenuation. A calculated attenuation map is possible if the object has a simple geometry and is homogenous. Then the attenuation correction factors can be derived of the geometry and the known material density. The advantage of this method is that it is straightforward and doesn't need transmission data, but in practice this is only possible for brain imaging. This approach however is not possible to use in heterogeneous anatomical regions, for example thorax or abdomen. In this case, measured attenuation factors are needed [10].

For measured attenuation coefficients, typically transmission data is used that is measured by using positron sources, gamma-ray sources or x-ray sources. In these cases the attenuation image can then be obtained by reconstructing the transmission data.

A first approach to create a measured attenuation coefficient map is by the use of coincidence-timing mode with a 68Ge/68Ga positron source. In this approach the positron source rotates around the patient and two scans are performed. First a blank scan is made, and a transmission scan of the patient to calculate the attenuation coefficient at 511 keV. The advantage of this approach is that the attenuation coefficients are measured in the correct energy range (511 keV), but the throughput of this approach is very low, as the full procedure takes a long time to make both scans.

A second approach is using gamma-ray sources. A 137Cs source rotates around the patient and a transmission map is created. This approach is particularly useful for PET scanners which only operate in 3D mode where a positron source will give high noise levels for the transmission scan. The disadvantage of this approach is that the attenuation coefficients are not measure at 511 keV, but at the 662 keV photon energy of Cs. Hence, attenuation coefficient transformation is needed. An additional disadvantage is introducing an extra bias by an increase of scattered photons, which cannot be corrected[10].

A third approach to create a measured attenuation coefficient map is the use of CT sources. Four major advantages exists by the use of CT to acquire the attenuation map. First, the CT data will have lower statistical noise. Second, the CT scan can be acquired in a much shorter time than a PET transmission scan. Third is the ability to collect uncontaminated post-injection transmission scans.

CT transmission scans can be acquired any time after the PET tracer is injected because the X-ray photon flux is orders of magnitude higher than the emission PET photons. Fourth, by using CT-data also anatomical information is available for the combination for PET-CT. It can be stated that currently PET-CT is the best available method for attenuation correction, but a disadvantage of this method is the same as with the gamma-ray source.

Attenuation coefficients are measured between 30 and 120 keV and hence need to be converted to attenuation coefficients at 511 keV. The CT values are reconstructed in units of HU and cannot be directly used to correct for the emission data, so a conversion is needed to 511 keV attenuation. There are two different conversion methods available: segmentation and scaling.

A first method is segmentation, where it is possible to divide the CT image into regions corresponding to different tissue types. The CT number for each tissue type is then replaced by the appropriate attenuation coefficient of that tissue type at 511 keV. A problem with segmentation is that some tissue regions don't have a homogenous density, for example in the lung region, the density can vary by 30%[37].

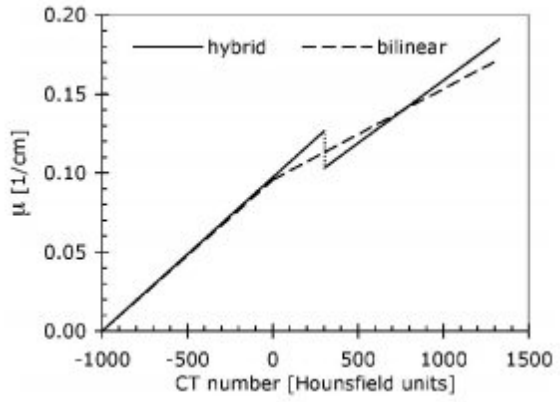

Figure 1-24: Conversion of CT numbers to linear attenuation coefficients at 511 keV[10]

A second method that is used for converting attenuation coefficients is scaling. It is known that the CT values are linearly related to the physical attenuation coefficient of the tissue type. Hence it is possible to calculate the attenuation map at 511 keV by simply multiplying the CT image values by the ratio of attenuation coefficients of water at the energy of CT and PET. But this is not efficient over the whole range of CT numbers from -1000 to 1000 HU.

LaCroix et al [38] has proved that linear scaling leads to proper attenuation coefficients for low-Z material (air, water, soft tissue), but for bone linear scaling resulted in a poor approximation due to the photoelectric contributions domination for lower CT energies. A solution for this problem is working with a bilinear method, where compensation happens for high-Z material. In the range of -1000 to 0 HU, tissue consists of lung and soft tissue, whereas regions with a CT number higher than 0 consist of a combination of bone and soft tissue. An example of a bilinear method is shown in figure 1-24.

An alternative approach is combining segmentation with scaling, the so called hybrid method. First a threshold is used to create the attenuation map at 511 keV to separate out the bone of the CT image. Then separate scaling factors are used to convert the attenuation coefficients of the bone and soft tissue components. This approach can be motivated due to the larger photoelectric fraction caused by the large calcium fraction in the bone (Z=20). The hybrid method is also depicted in figure 1-24 and clearly the threshold can be seen at a CT number of 300 HU. This leads to a discontinuity of scaling at the threshold value. In several studies it has been shown that both the bilinear and the hybrid method give reasonable results for biological materials in practice[39,40,41].

1.5.Problem description

1.5.1. Biological effects

The principal advantages of CT are a rapid acquisition of images, a wealth of clear and specific information and a view of a large portion of the body. No other imaging procedure (MRI, US, SPECT,…) combines these advantages in a single session [42]. But important disadvantages are linked to CT and PET. The biggest disadvantage is the rather high dose delivered to the patient in comparison with radiography, as the use of ionizing radiation causes deterministic and stochastic effects due to its interaction with biologic material [43].

Deterministic effects arise due to damage to a large amount of cells and leads to effects on short term like erythema, sterility and loss of hair. These effects will only appear when the dose threshold of 2 Gray (Gy) is exceeded and become evident days to months after the exposure. Most known are skin injuries and cataract. The severity of the effect is proportional to the dose, until a saturation level (figure 8). As CT-scans will always give a lower skin dose than 2 Gy, which is the threshold value, deterministic effects can be excluded. Only stochastic effects should be accounted for in CT [43].

Stochastic effects are effects which will manifest on long term. Due to the interaction of X-rays with DNA, mutations will be induced which can lead to the development of tumors. It has been noted that no threshold is present for stochastic effects, so every exposure to X-rays will lead to a higher chance for development of cancer. The higher the dose, the higher the chances. The risk is also dependent on the gender of the person and age. For a given radiation exposure, the cancer risk is higher in females than in males, in children than in adults, and in adults than in elderly (figure 1-25) [44].

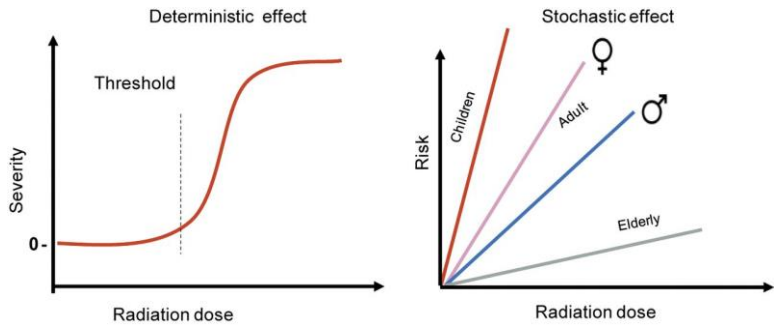

Figure 1-25*: Deterministic and stochastic effects in function of radiation dose* [44]

Therefore optimization and dose reduction in CT is extremely important. A widely used figure is a 5% excess risk of death from cancer for every 1 Sv (1000 mSv) dose[45].

1.5.2. Goal

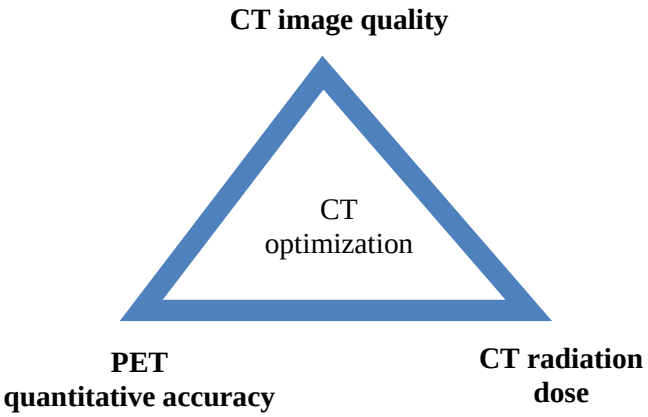

The combination of PET/CT has been proven to be a great success by co-registering anatomical and functional information in a single acquisition. As can be seen from the triangle, the CT component in PET/CT delivers important diagnostic value and anatomical localization, but these data can also be used as low-noise attenuation correction of PET images to improve its quantitative accuracy. As already mentioned, the important disadvantage of this modality is the CT radiation dose contribution to the patient, which can range from two to four times the dose delivered by the PET component (18.6 mSv versus 6.23 mSv)[46].Therefore in this project, the focus will be at the CT component of a PET-CT scanner.

Goal: Optimize CT settings to lower CT dose but maintain the image quality and quantitative accuracy of the PET image.

Practically this means that during this project four experiments will be performed:

1. Acceptance test
2. Automatic mAs modulation analysis
3. Low dose protocols
4. Attenuation correction analysis

2. Materials and methods

2.1.PET/CT scanner

All the experiments performed in this project were done on the Biograph mCT flow (Siemens Healthcare, Germany) at the university hospital of Ghent. The Biograph mCT flow is a sequential PET-CT system, which mean that the PET and CT component are spatially separated.

Figure 2-1: Biograph mCT flow at university hospital Gent

The CT-component consists of a single tube which can vary its tube voltage in discrete levels of 70, 80, 100, 120, 140 kV and its tube current continuously from 20 to 666 mA. Z-sharp Technology has been installed in the Biograph mCT, which means that a flying focal spot is used with a size of 0.7x0.7 mm and 0.9x1.1 mm. The resolution of the CT is 0.24 mm and a minimum rotation time of 0.33 seconds can be achieved. The temporal resolution of the Biograph mCT is down to 83 ms. Important to note is that CareDose and CareKV are installed on the system.

As an overview the most important specifications of the CT-component are listed in table 2-1

CT general specifications	
Aperture	78 cm
Scan field	50 cm
Flying focal spot	Yes
Resolution	0.24 mm
Minimum rotation time	0.33

Max. number of slices/rotation	40 (acquired slices) 120 (reconstructed slices)
Temporal resolution	80 ms
Number of detector rows	32
Number of detector electronic channels	40/64
Number of detector elements	23 552
Number of projections	4 608
Generator maximum power	80 kW
Tube current	20-666 mA
Tube voltage	70,80,100,120,140
Focal spot sizing	0.7x0.7 mm / 0.9x1.1 mm
Reconstructed slice widths	0.6,0.75,1,1.2,1.5,2,2.4,3,3.6,4.8,5,6,7, 7.2,8,9,10,12,14.4,15,20 mm
Pitch factor	0.3-1.5

Tabel2-1: CT specifications of Biograph mCT flow[47]

In this project, six different reconstruction filters will be used to reconstruct the CT image. As mentioned in the introduction, two different reconstruction algorithms are available, namely FBP and iterative reconstruction. Each has two reconstruction filters that will be used. These are i30f and i70f for iterative reconstruction and b30f and b70f for FBP. In clinical practice i30f is used to construct the diagnostic anatomical CT image for the clinician. The higher the number associated to the name of the filter, the sharper the filter is[48]. One extra reconstruction filter is use to create the topogram image, which is the T80f.

For every diagnostic scan in the PET-CT, an extra image is created with another reconstruction filter to be the attenuation map. This is the B19f filter, which is again FBP but makes the data smoother. The reason for this is that there is a substantial difference in the spatial resolution between CT (1.0mm) and PET (6-8 mm). Applying a sharp CT correction to smoother PET data can lead to artifacts at the edge of structures within the object.

To compensate for this, the transformed CT data is smoothed by the B19f filter to a spatial resolution more typical of PET [11]. At last the attenuation correction of the PET data happens by bilinear scaling of the CT-numbers from the CT image. Details about the bilinear scaling of this system are not known.

For the PET component, the most important feature is the detector. In this system a LSO crystal is used. By using LSO detectors it is possible to reduce the injected dose of radiopharmaceutical while maintaining image quality and speed of the examination, due to it high sensitivity[47]. Each detector element has a dimension of 4x4x20 mm. Per block 169 detector elements are present linked to 4 PMT's. The detector ring diameter is 842 mm and the full detector ring consists of 48 blocks. This results in a trans-axial FOV of 700 mm with a spacing of 2 mm.

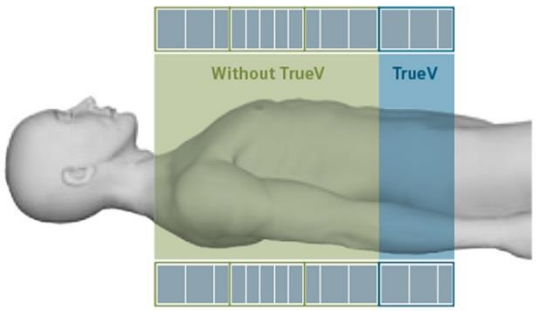

Figure 2-2: increased field of view due to the extra detector blocks of TrueV[47]

In the biograph mCT system, trueV is installed which means that a total of 192 detector blocks are implemented which results in a total of 32.448 detector elements. This increases the system axial FOV from 162 mm(standard) to 216 mm (TrueV HD). The coincidence time window is 4.1 nsec and the energy resolution of the system is less than 12% of FWHM. The time resolution is 540 psec, hence TOF is possible on this system. The true V system has a sensitivity has 905 cps/kBq with a peak NEC rate of 175 kcps at <28kBq/cc.

Extra mentioning is that the Biograph mCT flow is a state-of-the-art PET-CT scanner. It is the first PET-CT scanner where the PET-acquisitions are taken while the bed is continuously moving (flow), instead of using bed positions. By binning the data a PET acquisition can be made. Flow eliminates overlapping bed acquisitions and maintains uniform noise sensitivity across the entire scan range [47].

2.2.Phantoms

2.2.1. Rando phantom

A frequently used method to mimic the standard human body for CT purposes is the use of the RANDO Alderson phantom (RDS Phantoms, USA). The RANDO phantom is an anthropomorphic phantom, existing out of 35 slices with each a thickness of 2.5 cm. These slices are made out of tissue equivalent material.

The RANDO phantom represents a male of 175 cm length and 73.5 kg weight. Soft tissues are mimicked by urethane with an effective atom number (Z = 7.3) and mass density (rho = 0.985g/cm³) approximately the same as muscle tissue with spread fat. The lung material mimics the lung density at medium inhalation and consists of a resinous substitute (Z = 7.3, rho = 0.32 g/cm³) which fits inside the rib cage of the phantom.

The skeleton of the phantom is derived from human bone tissue. Holes were drilled inside the cuts on specific places of a 3 x 3 grid. In these holes it is possible to place thermo-luminescent dosimeters for dosimetry purposes [49].

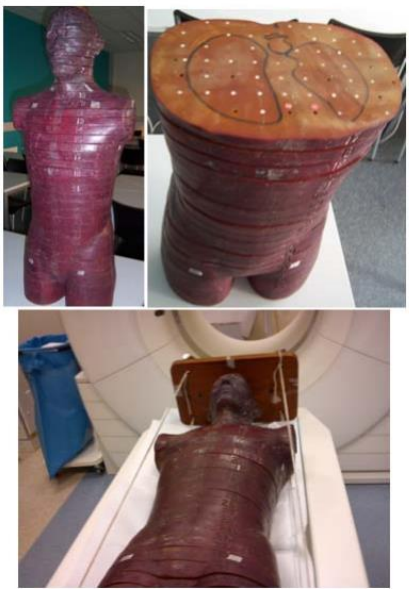

Figure2-3: RANDO Aldersonphantom[17]

2.2.2. Catphan 404

The Catphan 404 phantom is a phantom that is used regularly to analyze CT-scanner performances. It is a cylindrical phantom with a length of 188 mm and has an outer radius of 200 mm. It consist of a shell with 4 modules inside.

These modules are respectively:

- CTP 486 image uniformity module
- CTP528 high resolution module
- CTP401 module with slice width, sensitometry and pixel size
- CTP515 low contrast module

The details of the different modules are described further.

- **CTP 486 image uniformity module**

The image uniformity module is cast from a uniform material, which CT number is chosen to be within 2% of water's density at standard protocols. This module is used for measurements of spatial uniformity, mean CT number and noise value. The noise is measured by placing a region of interest (ROI) inside the slice[50]. A CT scan of the uniformity module is depicted in figure 2-4.

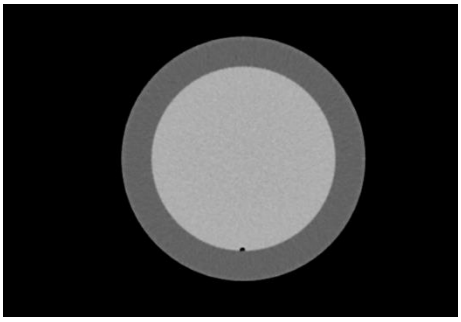

Figure 2-4: Uniformity module of the Catphan phantom

- **CTP 528 high resolution module**

The high resolution module contains 21 line pair per centimeter and two impulse sources which are casted inside the uniform material. The beads inside the slice can be used to measure the point spread function of the CT-scanner or the MTF. Another important application of this module is the calculation of the resolution of the CT system. By using the 21 line pairs, it is possible to determine the spatial resolution. How this is calculated will be explained in the part discussing image quality parameters. A typical example of the high resolution module is shown in figure 25.

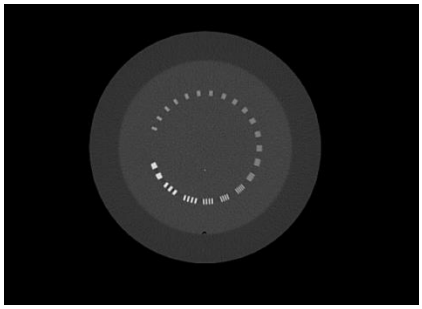

Figure 2-5: high resolution module with 21 line pairs

- **CTP 401 slice width module**

The slice width module can be used for multiple applications. A first application is the patient alignment system check by using the 23° ramps. Also slide width can be measured by using the same ramp. The most important application for this project is the different materials that are present in this module.

Clockwise starting up, these materials are Air, Polystyrene, LDPE, PMP, Teflon, Delrin and Acrylic. The densities of these materials are added in table 2-2[50]. In this way it is possible to measure Hounsfield units for the different materials for different protocols and compare these results with each other.

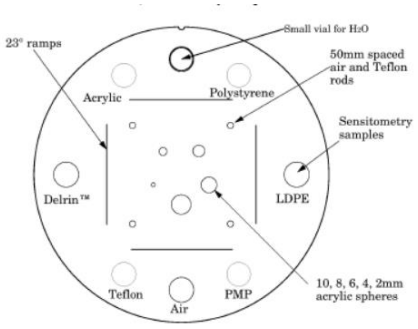

Figure 2-6: schematic of the slice width module with the different materials inside [50]

Material	Density (g/cm³)
Air	0.0012
PMP	0.84
LDPE	0.92
Polystyrene	1
Acrylic	1.18
Delrin	1.42
Teflon	2.2

Tabel2-2: Material and corresponding densities inside the CTP 401 module[50]

- **CTP 515 low contrast module**

The last module inside the Catphan phantom is the low contrast detail module. This module is full of low contrast targets which a range of diameters and contrasts. Diameters ranges from 15.0 mm to 2.0 mm and three contrasts types are present, namely 0.3%, 0.5% and 1%[50]. These are the supra-slice targets, which are depicted schematically in figure 2-7. The sub-slice targets are also present but will not be used in this project. By using these targets it will be possible to calculate the contrast of the image. The detailed way will be explained in the paragraphs on image quality parameters.

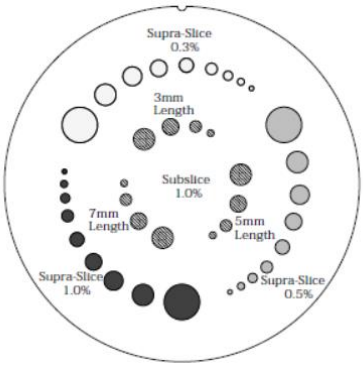

Figure 2-7: supra- and sub-slice targets in the low contrast module [50]

2.2.3. PET phantom

A phantom that is used frequently in PET image quality is the PET phantom – NEMA 2007. The phantom used in this project is depicted in figure 2-8. This phantom complies with the NEMA 2007 Standards and can be used to simulate whole body imaging in PET. In this project the phantom will be used to evaluate the reconstructed image quality in whole body PET.

The phantom has a length of 30.5 cm and a height and width of 24.1 cm. The interior phantom has a length of 180 mm and is made up of polyurethane. Inside the phantom six spheres are present which can be filled with radioactive material. The diameters of these spheres are 10mm, 13 mm, 17 mm, 22 mm, 28 mm and 37 mm[51].

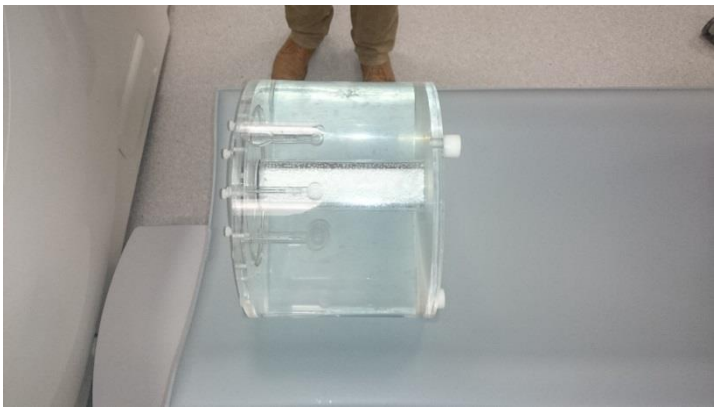

Figure 2-8: PET phantom with fillable spheres

2.3.Dosimetry parameters

2.3.1. CT dose index

In CT dosimetry two physical radiation parameters are used, CT dose index (CTDI) and dose length product (DLP). The CTDI is a parameter for the intensity of the radiation used and quantifies the amount of radiation that was delivered per unit of distance and has a unit of milligray. Per definition the CTDI is equal to the value the dose would be when a slice would be irradiated, if the dose profile would be seen as a simple rectangular with the nominal slice thickness as width:

$$TDI = \frac{1}{(Nh)} \int_{-\infty}^{\infty} D(z)dz \qquad \textbf{2-1}$$

In multi-slice CT, simultaneous N slices are used as nominal slice width.

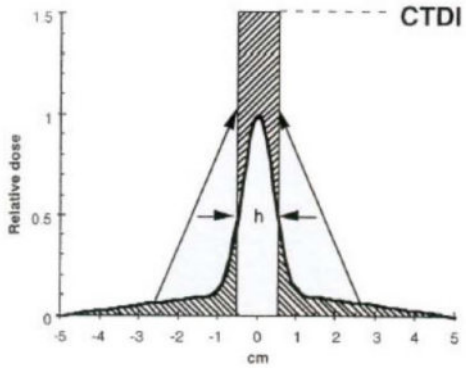

Figure 2-9Dose sensitivity profile and CTDI

Practically, the CTDI is measured in a cylindrical acrylic phantom for one rotation of the source over a length of 10 cm (CTDI100). In this way, direct X-rays and scatter are accounted for. The measured CTDI predicts the dose for one rotation for a CT-scan[52].

Typically two CTDI phantoms are used, a head phantom and a body phantom with a diameter of respectively 16 cm and 32 cm. By the use of a pencil ionization chamber the air kerma over a distance of 100 mm is measured in the center(CTDI100c) and in the periphery (CTDI100p) of the phantom. Finally the weighted CTDI (CTDIw) is calculated according the following equation:

$$CTDIw = \frac{2}{3} CTDIp + \frac{1}{3} CTDIc \qquad \textbf{2-2}$$

For spiral acquisition this weighted CTDI must be corrected to a volume CTDI (CTDIvol). The CTDIvol is defined as the CTDIw divided by the pitch. Once the kV, mAs and pitch are specified, the CTDIvol is fixed and independent of the shape of the patient or the length of the scan.

2.3.2. DLP

The Dose length product was created in dosimetry to take the length of the scan into account. As a longer scan will result in a higher radiation dose to the patient than a shorter scan, this should be taken into account. The DLP is the product of the CTDIvol with the length of the scan, expressed in mGy.cm. This DLP is not a measure for the dose a patient receives (as patient characteristics are not taken into account), but the DLP quantifies the amount of X-rays that were used for certain CT-procedures. Using these DLP's it is therefore possible to compare different procedures[52].

$$DLP = CTDI * length \quad \textbf{2-3}$$

2.3.3. Effective dose CT

Effective dose is not a measure of dose, but rather a concept that reflects the stochastic risk from an exposure to ionizing radiation. The unit for effective dose is Sievert (Sv). The effective dose shows the radiation harm averaged over gender and age over a population, but its use has several limitations. In particular, it uses a mathematical model for a "standard" body and cannot be used as an risk indicator for an individual. The advantage of this unit is that it is possible to perform comparison of biological effects between diagnostic exams of different modalities or protocols[46].

The European Working Group for Guidelines on Quality Criteria in CT has proposed an estimation method to calculate the effective dose in CT. By using a conversion factor (region-specific coefficient), it is possible to convert the DLP from a CT exam to effective dose. In this project all effective doses are calculated this way and are therefore pseudo-effective dose, since it is not calculated by the weighted organ dose, but from a conversion factor. These pseudo-effective doses are only used for comparison reasons. This conversion factor for a chest examination is 0.017 mSv.mGy-1cm-1, this will be also used for whole body examination.

2.3.4. Effective dose PET

Not only the CT component delivers an exposure to the patient, also the PET component delivers a dose. The effective dose associated with the PET exam as a result of the injected FDG activity is calculated based on the reported ICRP values of 0.019 mSv/MBq for a 70 kg adult, 0.025 mSv/MBq for a 57 kg adult and 0.036 mSv/MBq for a 33 kg child[53]. For the same reason as CT effective dose, this will be called the pseudo-PET effective dose.

The effective dose is calculated with the following formula.

$$ED = Injected\ FDG\ (MBq) * Factor\ (\frac{mSv}{MBq}) \quad \textbf{2-4}$$

The total effective dose associated to a PET-CT exam is considered to be the sum of the PET and CT effective dose values.

$$ED\ total = ED\ CT + ED\ PET \quad \textbf{2-5}$$

2.3.5. Recovery coefficient PET

An important parameter in PET is the recovery coefficient. The recovery coefficient is a relative ratio of observed activity contrast to the true activity contrast in a PET image. To measure the recovery coefficient a NEMA phantom is used, which can be filled with activity. First an amount of activity of FDG needs to be prepared in the hot lab in a volume of one liter. Therefore a concentration of FDG is defined (MBq/L). Then this is distributed over the different spheres. For the recovery coefficient, also background compartment of the phantom needs to be measured, which is the activity concentration in the empty phantom in MBq/L. As the volume of the phantom is 9.81 L, the activity injected in the background compartment should be divided by this number.

Figure 2-10: PET phantom with activity inside PET-CT scanner

Next the filled PET phantom is placed in the PET scanner and a PET scan is performed of the phantom (figure 2-10). In this PET image, it is possible to measure the measured activity in ROI's around the different spheres. The diameter of these circular ROI's is based on the CT image of the phantom. On the CT image, the edges of the ROI's are placed just inside of the spheres, to make sure that all activity is accounted for in the whole sphere. These ROI's serve then as a template for the PET images to calculate the concentration of activity of FDG. The CT image with the ROI template is depicted in figure 2-11.

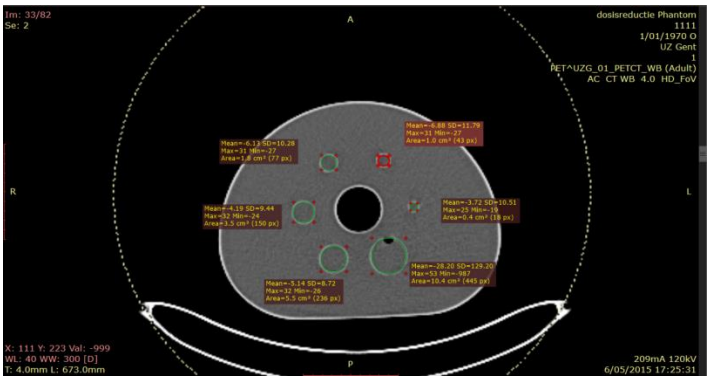

Figure 2-11: CT image of PET phantom with ROI template

At last the measured background should be measured of the PET phantom. For this, the same method as for the measured concentration is used, hence based on the CT image of the phantom, a circular ROI is placed inside the phantom, but should not contain any of the fillable spheres. This is depicted in figure 2-2.

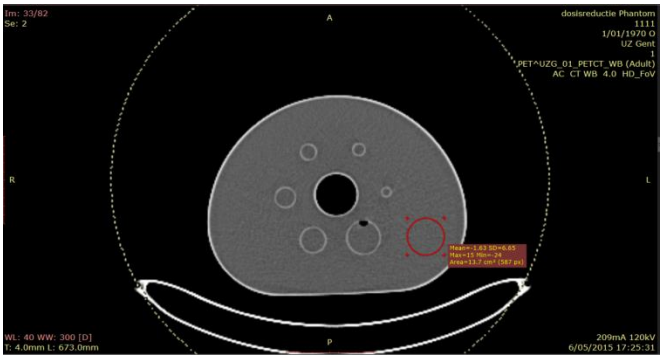

Figure 2-12: CT image of the PET phantom with background ROI template

Out of these four measurements, it is possible to calculate the recovery coefficient by taking the ratio of the measured concentration in the sphere divided by the measured concentration in the background, and the true concentration in the sphere corrected for the true concentration in the background. (Formula 2-6).

$$RC = \frac{\frac{measured\ concentration\ in\ sphere}{measured\ concentration\ background}}{\frac{true\ concentration\ in\ sphere}{true\ concentration\ background}} \qquad \textbf{2-6}$$

2.4.Image quality parameters

2.4.1. Noise

All image quality analysis parameters were evaluated by the use of the RadiAnt program or ImageJ program which are both Dicom viewers. The data was then processed by Excel.

A first image quality parameter is noise. Noise can be defined as an arbitrary variance in a signal. Several causes of noise are physical processes (electron movement in conductors), inaccuracy of detector, discretization, etc. In CT the amount of noise is dependent on the tube current and tube voltage. The more X-rays the detector reach, the higher the signal to noise ratio will be, as this is dependent on sqrt(N), where N is the amount of X-rays detected[6].

Practically, noise is measured by using the CTP 486 image uniformity module of the Catphan phantom. By placing a circular ROI in the center of the module with a radius of 1.5 cm, the minimum, maximum, mean and standard deviation can be measured in that ROI (figure 2-13). The standard deviation can then be used as a measure of the noise in the image.

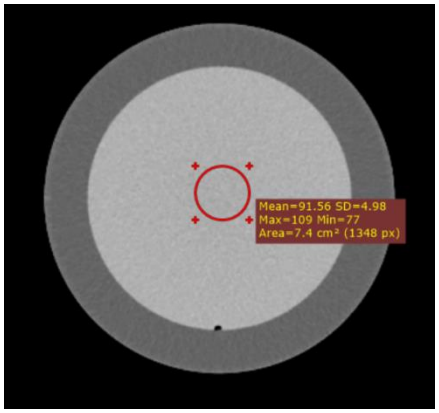

Figure 2-13: Measurement of noise in CT image

2.4.2. Resolution

Spatial resolution can be defined as how closely lines can be resolved in an image. The higher the resolution of an image, the better details can be seen. Practically, spatial resolution for CT can be measured by using the CTP528 high resolution module of the Catphan phantom. By determining which line pair can still be visualized separately, it is possible to assign a quantitative parameter to the spatial resolution, which is the gap size of the line pairs. The corresponding gap size with the line pair is depicted in table 2-3.

Line pair/cm	Gap size	Line pair/cm	Gap size
1	0.500 cm	**11**	0.045 cm
2	0.250 cm	**12**	0.042 cm
3	0.167 cm	**13**	0.038 cm
4	0.125 cm	**14**	0.036 cm
5	0.100 cm	**15**	0.033 cm
6	0.083 cm	**16**	0.031 cm
7	0.071 cm	**17**	0.029 cm
8	0.063 cm	**18**	0.028 cm
9	0.056 cm	**19**	0.026 cm
10	0.050 cm	**20**	0.025 cm
		21	0.024 cm

Tabel2-3 Gap size for the different line pairs

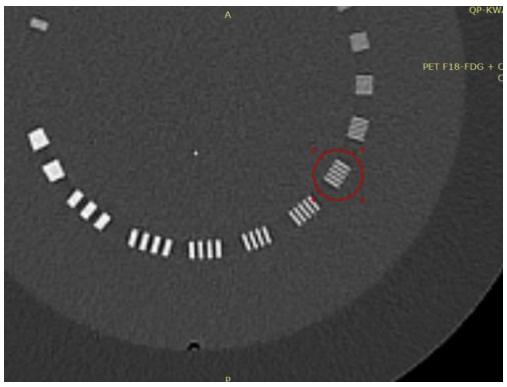

Figure 2-14: example of resolution in CT image

2.4.3. Low-contrast detail

Another important CT image quality parameter is low-contrast detail. The low contrast detail can be obtained in a subjective way by using the CTP515 low contrast module. Three different readers (without knowledge of CT principles) analyzed the low contrast module of the different protocols and counted the spheres of the supra-slice objects that were still distinguishable of the background. This was then represented by the smallest diameter of that sphere, which was performed for the three target contrast levels (1.0%, 0.3% and 0.5%).

From there on the inverse image quality number can be calculated. The formula for this parameter is

$$IQFinv = \frac{100}{\sum Ci * Di} \quad \text{2-7}$$

Where Di is the smallest diameter of the circle that is still distinguishable from the background in the image for each contrast level and Ci is the corresponding contrast level (1.0%, 0.5% and 0.3%). As the results can be dependent on the reader, the mean of this value was calculated for the three readers. It can be stated that the higher the IQFinv, the better the image quality is.

An example of a high IQFinv image, is shown in figure 2-15.

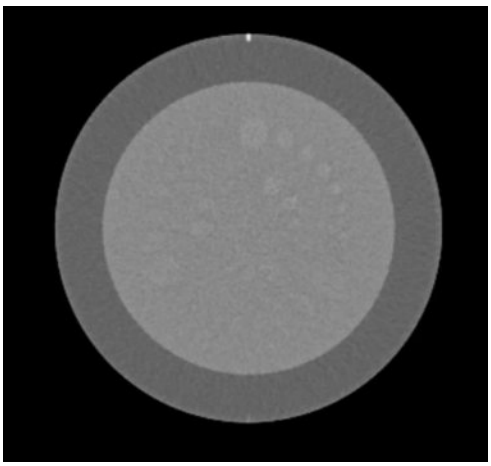

Figure 2-15: low contrast module in CT with a high IQFinv value

3. Results

3.1.Acceptance test

Before a CT-scanner is used in the clinical field, it has to pass the acceptance test. The acceptance test is an extensive testing of the machine performance after the installation by the vendor. This has to be performed by the medical physicist.

It should be noted that in this acceptance test, only the CT-parameters were evaluated. The PET component was already tested extensively to pass its acceptance test. The limits and standards that needed to be fulfilled as acceptance test are present in the decree of the Federal Agency for Nuclear Control (FANC), which is a juridical translation of the protocol which has been proposed by the radiology team of the BHPA ("beroepsvereniging van ziekenhuisfysici"). These norms are based on international references and experience.

The measurement material used for this acceptance test consisted of a dosimeter, phantoms and self-developing film. The dosimeters used were the Unfors Xi R/F & MAM Detector Platinum and Unfors Xi CT detector. As for the phantoms, the body CT-phantom was used. This is a phantom that is made out of solid acrylic that is 15 cm thick and has a diameter of 32 cm. Each part contains 5 probe holes, one in the center and four around the perimeter, each 90 degrees apart and 1 cm from the edge. These holes have a diameter of 1.31 cm. In these holes it is possible to place the pencil dosimeter to measure the CTDI. In the holes are not used, they should be plugged with acrylic rods. To measure the beam collimation, self-developing film was used (Gafchromic XR-CT).

All results have been collected and are added in Appendix A. It can be concluded that the Biograph mCT flow at the university Hospital of Gent is approved for acceptance.

3.2.mAs Modulation

The second part of this paper focuses on the behavior of the tube current modulation system installed on the biography mCT flow. In a study of Franck[17], it has been shown that some inconsistencies were evaluated of the tube current modulation system of a stand-alone CT system. In this part, this behavior is investigated on the PET-CT scanner. As already explained, the tube current modulation system is a system where the tube current varies during one single CT acquisition. The magnitude of the tube current is chosen for each slide, depending on the attenuation of that slice analyzed from the topogram and in real time (CareDose 4D). All experiments in this part of the project are performed with the use of the Alderson RANDO phantom.

The purpose of this experiment is to investigate if the tube current selection would be the same if a different way of topogram scanning would have been used for the same scan of the same phantom. First the influence of the actual scan direction is analyzed (cranial-caudal vs caudal-cranial). In a second part, the influence of the topogram and table height on the tube current modulation is analyzed. A topogram can be made in three ways, an anterior-posterior, a posterior-anterior and a lateral topogram. In anterior-posterior topogram, the tube is fixed at 0°(upside of gantry) and scans the body. Posterior-anterior topogram has the same set-up as anterior-posterior but the tube is fixed at 180° instead of 0° (downside of gantry). In a lateral topogram the tube is fixed at 90° or -90° (left or right side of gantry) and scans the body.

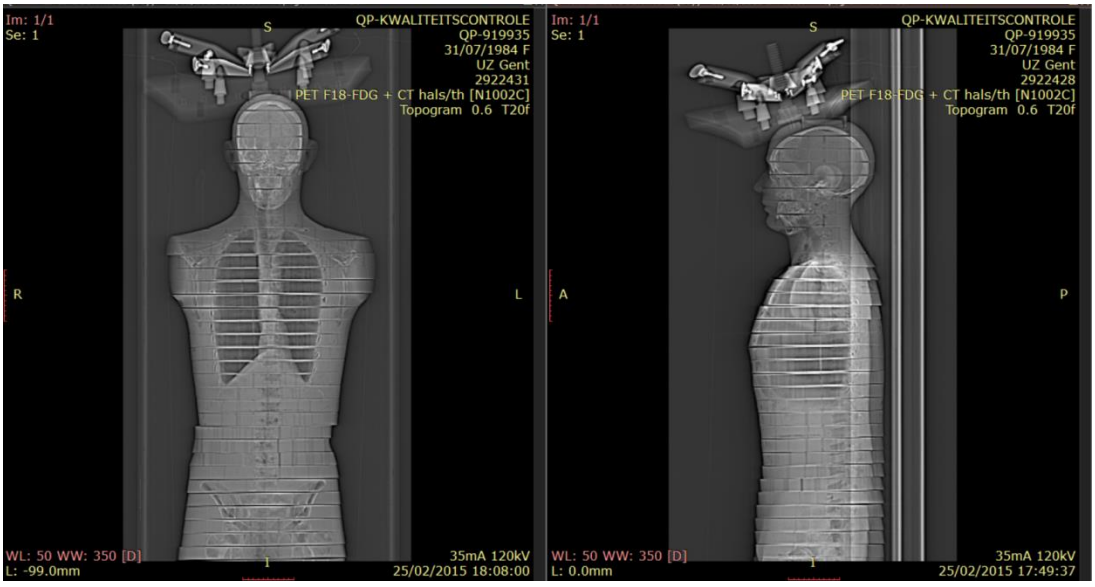

Figure 3-1: posterior-anterior topogram versus lateral topogram

In a last experiment, the influence of the table height on the tube current modulation is analyzed for a posterior-anterior topogram set-up. All numerical data are summarized and added in Appendix B.

3.2.1. Influence of scan direction

First the influence of the scanning direction on the tube current modulation is investigated. For this the RANDO phantom was placed on the PET-CT system and a topogram was made with the following parameters.

Parameters	Topogram
Tube voltage	120 kV
Tube current	35 mA
CTDIvol	0.13mGy
DLP	14mGy*cm
Length	100 cm
Convolution kennel	T20f
Direction*	Posterior-anterior
Table height	150

Tabel 3-1 Parameters topogram

After the topogram, a CT acquisition is made from slice 11 to slice 25 of the RANDO phantom, which represents a whole body scan from the chin to mid thighs of a patient. This has a total length of 376 mm. This CT acquisition is performed two times with the only difference that the first scan direction was cranial-caudal (which means the head was scanned first) and the second direction is caudo-cranial (which means that the legs are scanned first). The parameters for the two scans are identical and are shown in table 3-2.

Parameters	CT-acquisition 1	CT-acquisition 2
Direction	Cranial-caudal	Caudal-cranial
Tube voltage (kV)	120	120
mAs/reference (mAs)	99/110	101/110
CAREdose	YES	YES
CAREkV	NO	NO
CTDIvol	7.27	7.44
DLP	285	292
Slice thickness (mm)	3	3
Table height	150	150

Tabel3-2 Parameters of CT-acquisition 1 and acquisition 2

After the acquisitions, for both CT-data at every slice the tube current per slice is selected and plotted in figure 3-2.

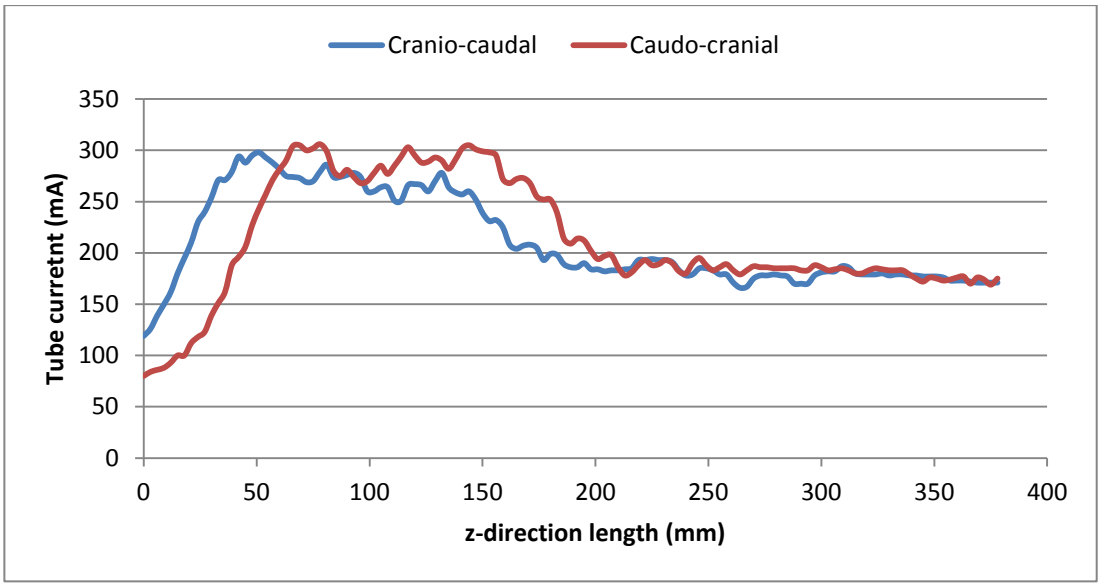

Figure 3-2: Tube current in function of z-direction of cranio-caudal and caudo-cranial scanning

As expected the tube current will be highest at the chest region, as the lateral attenuation will be largest in this region, and will decrease over the abdomen. It can clearly be seen that the modulation is not the same when the direction of the scan is changed (cranial-caudal vs caudal-cranial). The difference can be seen as a shift over approximately20 mm. The biggest difference can be noted at the transition of neck to shoulder. This variation goes up to a maximum of 120 mA at 33 mm (44%).

In a second experiment the direction of the topogram is changed from posterior-anterior to a lateral scout view. Again the influence of the scan direction is investigated on the tube current modulation. The parameters for the topogram and results are added in Appendix C. This result has the same shape as in figure 3-2 with the biggest difference noted again at the transition of neck to shoulder. This goes up to a maximum of 70 mA at 33 mm. (45%)

3.2.2. Influence oftopogram direction – posterior anterior vs lateral

In a next comparison, the influence of the topogram direction is compared. From the results of the data in the previous experiment, it is possible to investigate the behavior of the tube current modulation if the topogram is made in a posterior-anterior way or in a lateral way.

The results of this comparison are shown in the figure 3-3. In this example for both scans the cranial-caudal scan is chosen.

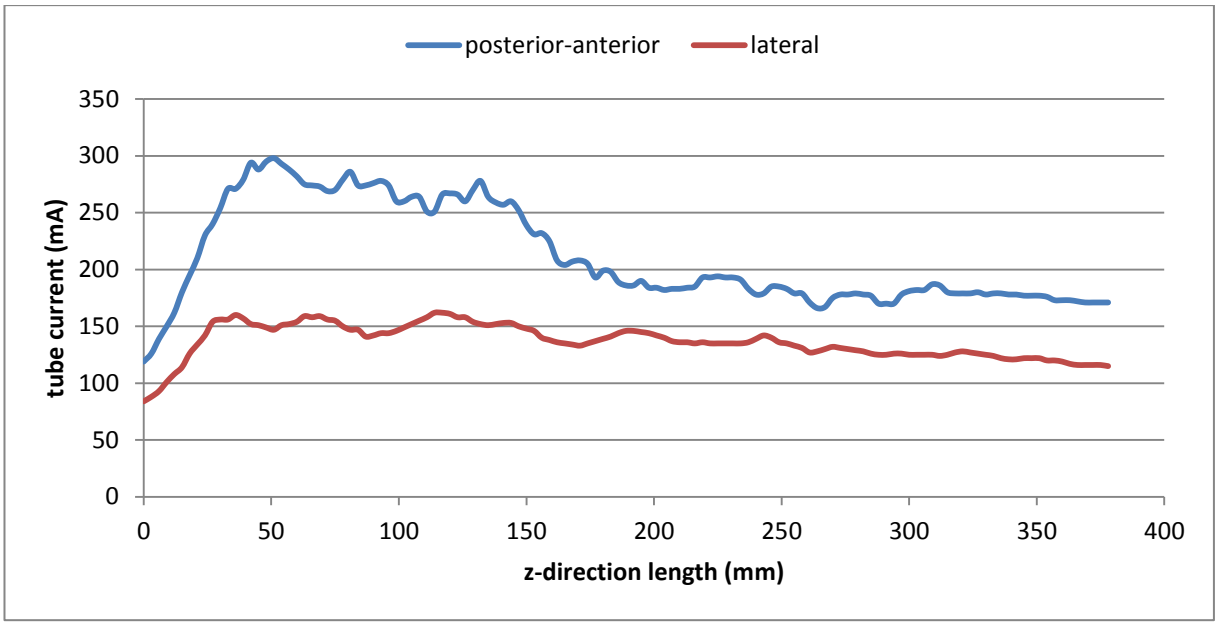

Figure 3-3: Tube current in function of z-direction of posterior-anterior and lateral topogram

The highest tube current is generated for a scan where the topogram direction is posterior-anterior. Approximately a factor of two in the chest region and a factor of 1.4 in the abdomen region is achieved. The difference between the two scans has a maximum around the shoulder region and is 151 mA at 51 mm (50%).

3.2.3. Influence of topogram direction – pa vs ap

Next the influence of the direction of the topogram is investigated on the tube current modulation. As mentioned in the introduction of this chapter, it is possible to perform a topogram posterior-anterior or anterior-posterior. This means where the tube is fixed, 0° vs 180°. In this comparison CT-acquisition 1 is compared to CT-acquisition 5. The parameters for acquisition 5 are depicted in table 3-3.

Parameters	CT-acquisition 5
Scan direction	Cranial-caudal
Topogram direction	Anterior-posterior
Tube voltage (kV)	120
mAs/reference (mAs)	87/110
CAREdose	YES
CAREkV	NO
CTDIvol	6.38
DLP	250
Slice thickness (mm)	3
Table height	150

Tabel3-3 Parameters for CT-acquistion 5

The results of this experiment and comparison are projected in figure 3-4. It can be clearly seen that the shape of the curves is the same but the posterior-anterior topogram will give a higher tube current over the entire scan compared to the anterior-posterior topogram. The maximum difference is located round the neck region and is 106 mA at 48 mm. From this result, it can be suggested that the 150 mm table height, is not perfectly in the iso-center of the CT.

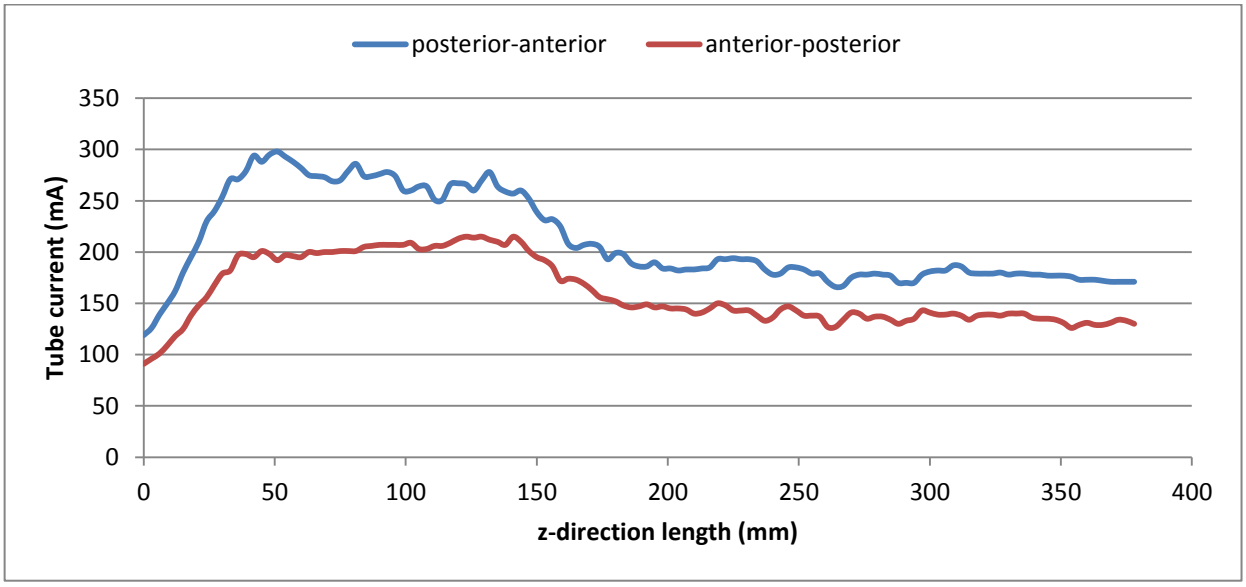

Figure 3-4:Tube current in function of z-direction length for posterior-anterior and anterior-posterior topogram

3.2.4. Influence table height

In a last experiment, the influence of the table height on the tube current modulation is investigated. By taking the same scan each time, but changing the height of the table at 99 cm, 150 cm and 256 cm a comparison at three heights can be made. Each time the same parameters (except for height) are used which are summarized in table 3-4. In this comparison, acquisition 1, 6 and 7 are compared. Important to note is that the topogram direction is posterior-anterior, which means that the tube is fixed on the downside of the gantry. The results are plotted in figure 3-5.

Parameters	CT-acquisition 6	CT-acquisition 7
Direction	Cranial-caudal	Cranial-caudal
Topogram direction	Posterior-anterior	Posterior-anterior
Tube voltage (kV)	120	120
mAs/reference (mAs)	99/110	173/110
CAREdose	YES	YES
CAREkV	NO	NO
CTDIvol	7.27	12.72
DLP	285	499
Slice thickness (mm)	3	3
Table height	99	253

Tabel3-4 Parameters for CT-acquisition 6 and 7

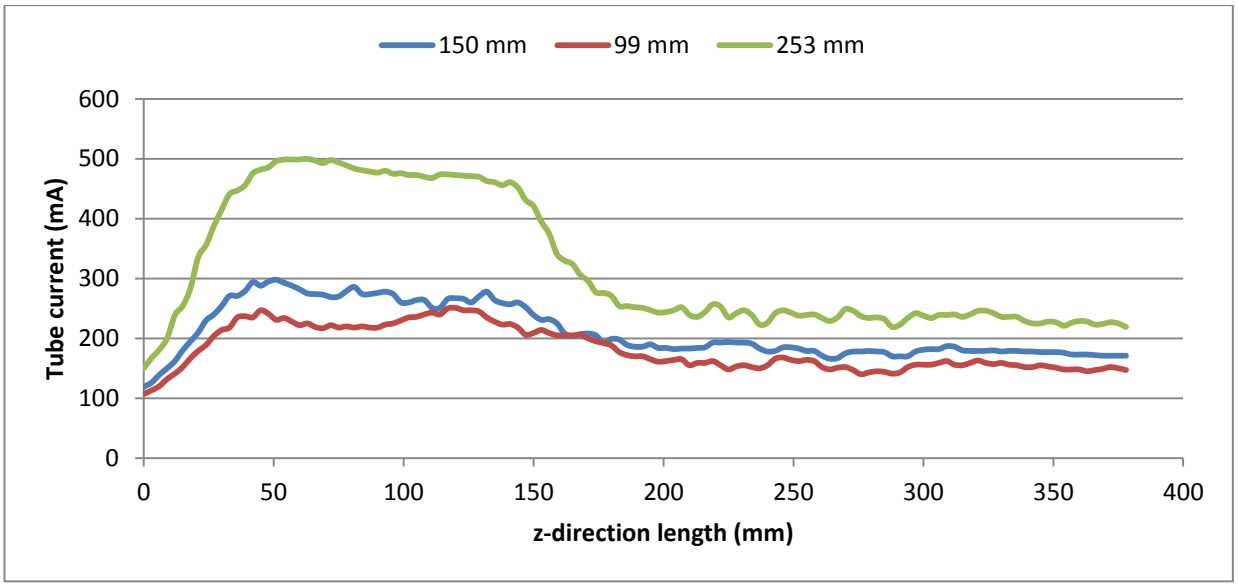

Figure 3-5: Tube current in function of z-direction length for different heights

From figure 3-5, where the tube current is shown over the entire length of the scan for the three different table heights, it can clearly been seen that the tube current will be the highest for the 253 mm height. The tube current is twice as high for the highest protocol compared to the lowest protocol. It can be concluded that the higher the table is placed, the higher the estimated tube current will be for a posterior – anterior topogram. The topogram scan for the three protocols is depicted in figure 3-6, where it can be stated that the higher the table is, the broader the projection of the phantom will be.

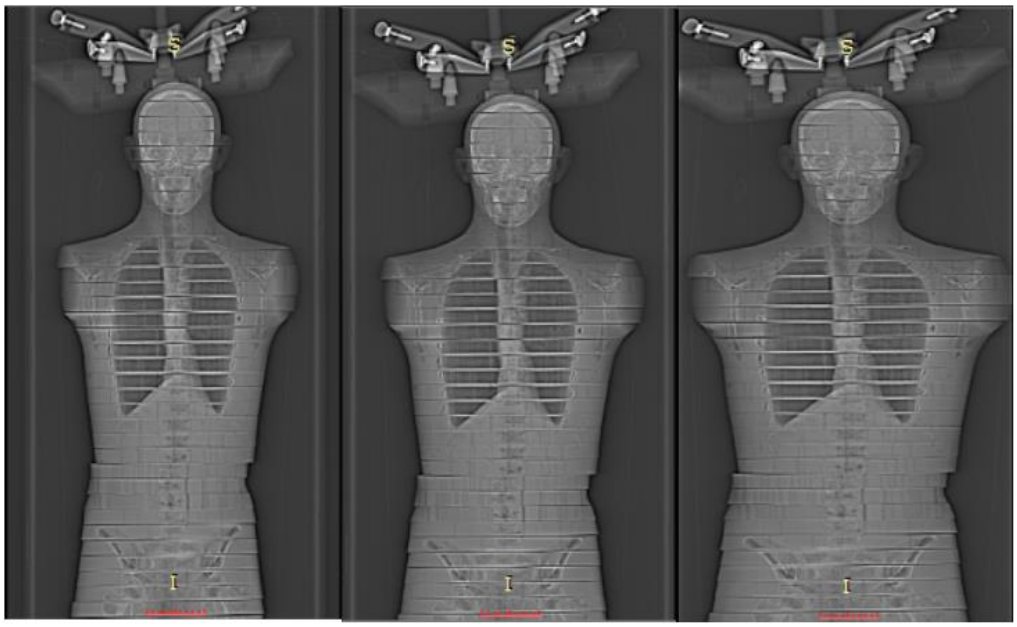

Figure 3-6: Topogram of RANDO phantom with respectively table height of 99 mm, 150 mm and 256 mm

3.3.Low doseCT protocols

The key subject of this project is the dose delivered of a CT scan to the patient during diagnosis and follow-up of a disease for a PET-CT investigation. As a patient who suffers from cancer may undergo multiple PET-CT scans, the accumulated dose can reach high levels. Therefore it should be advised to try to keep the dose per CT acquisition as low as possible. Therefore in this experiment, low dose protocols will be analyzed compared to the standard CT-acquisition that is used in the clinical practice. In this part a dose analysis will be performed and image quality parameters of these different acquisitions will be compared.

3.3.1. Dose analysis

In a first experiment the doses for all different protocols available on the PET/CT compartment are noted and compared to each other. By scanning the Catphan 404 phantom for different parameters (reconstruction filter, varying tube current and tube voltage), the CTDIvol was measured. By keeping the other parameters constant (scan length, rotation time, pitch, etc) the CTDIvol can be compared.

First for each CT-scan a topogram is needed. This was taken from the Catphan phantom with a tube voltage of 120 kV and a tube current of 35 mA. More detailed parameters are summarized in table 3-5.

Parameters	Topogram
Tube voltage	120 kV
Tube current	35 mA
CTDIvol	0.13 mGy
Length	510 mm
Convolution kernel	T80f
Direction	Posterior-anterior

Tabel3-5 Parameters of the standard topogram

Based on this topogram, the length of the CT-scan is defined and different protocols are suggested. First the standard protocol, which is used in the clinical practice as a diagnostic image is performed, which has a tube voltage of 120 kV and an effective tube current of 106 mAs for this phantom. In table 3-6, the details are summarized of this protocol.

Parameters	Standard protocol
Tube voltage	120 kV
Effective tube current time product	106 mAs
CARE dose	Yes
CARE kV	No
Convolution kernel	I30f
CTDI	7.77 mGy
Pitch	0.7
Slice thickness	3 mm

Tabel3-6 Parameters of standard CT-acquisition

After the standard protocol, an analysis of the influence of the tube voltage and tube current is performed. Based on the tube voltage, five categories (70, 80, 100, 120 and 140 kV) are created where in each category the tube current was ranged from the highest to the lowest possible setting. The in between tube currents are chosen in such a way that the CTDI's in the different categories are the same, hence a comparison of dose and image quality is possible based on CTDI. In table 3-7 the different protocols are summarized. The length of each scan is 22 cm and the reconstruction kernel used is the i30, which is used to create the diagnostic CT image. The effective tube current in spiral CT is the tube current divided by the pitch (which is equal to 0.7 in this experiment). In a last column the noise is also added, but this will be analyzed in a following subchapter.

Tube voltage (kV)	Effective tube current (mAs)	CTDIvol (mGy)	DLP (mGy*cm)	Noise (SD)
70	44	0.54	11.88	23.3
70	55	0.69	15.18	19.8
70	87	1.09	23.98	14.9
70	175	2.19	48.18	9.8
80	15	0.31	6.82	35.3
80	34	0.69	15.18	19.1
80	54	1.1	24.2	14.6
80	106	2.19	48.18	9.9
80	179	3.67	80.74	7.8
100	15	0.65	14.3	19.3
100	25	1.08	23.76	13.2
100	51	2.22	48.84	9.6
100	85	3.66	80.52	7.3
100	119	5.11	112.42	6.1
120	15	1.1	24.2	14.6
120	30	2.19	48.18	9.9
120	50	3.65	80.3	7.8
120	70	5.11	112.42	6
120	106*	7.77	170.94	5.2

120	150	10.95	240.9	4.2
140	15	1.65	36.3	13
140	34	3.68	80.96	7.6
140	46	5.1	112.2	6.9
140	71	7.84	172.48	5.3

Tabel3-7 Parameters of the different low dose protocols with noise (standard protocol)*

In the following graph (figure 3-7), the CTDI of the extreme values (highest and lowest tube current) of the different tube voltages are depicted. All other protocols can be placed in between these extreme values. At 120 kV an extra bar is added to show the CTDI of the standard protocol used in the clinical practice with CareDose. In all the other protocols CareDose and CareKv were deselected.

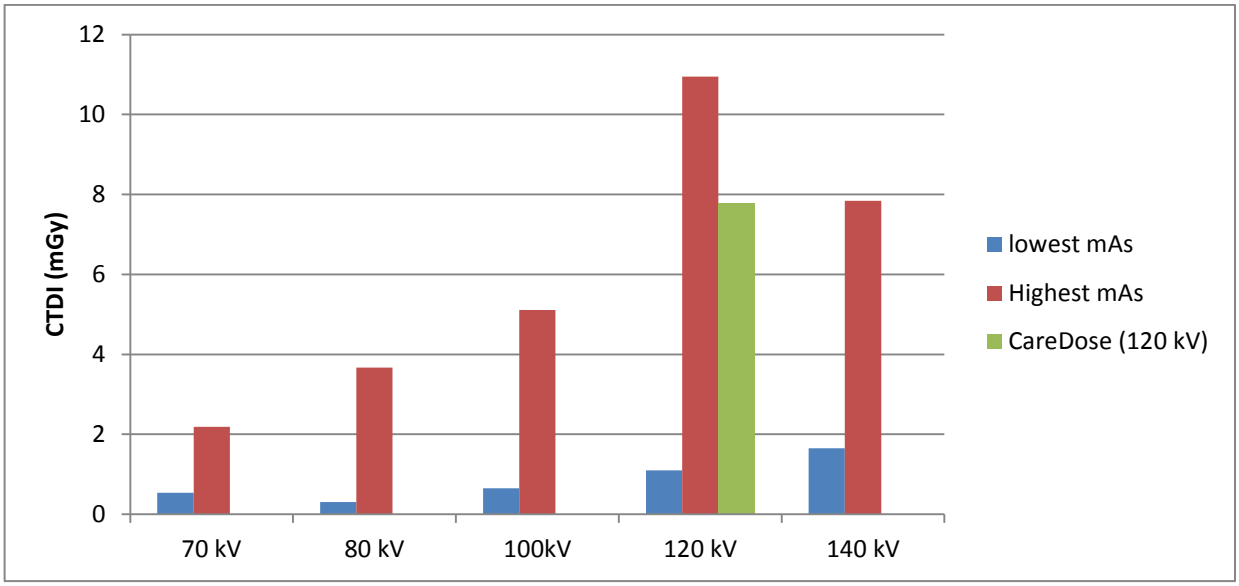

Figure 3-7: CTDIvol for the highest and lowest tube current at different tube voltages.

The protocol most used for a whole body PET is depicted with the green beam and shows a CTDI of 7.77 mGy. It can clearly be seen that by reducing the tube voltage, the CTDI will also be reduced. Remarkable to notice is that the lowest CTDI is achieved at 80 kV and not at 70 kV (0.31 vs 0.54 mGy).This is due to the fact that it is possible at 80 kV to go to an effective tube current of 15 mAs, where the lowest setting for 70 kV is 44 mAs.

In a following comparison, the influence of tube voltage reduction on the dose delivered to the patient is analyzed. The CTDI is plotted as a function of the tube voltage for a constant effective tube current of 50 mAs and 15 mAs, as for these points, the most data is available.

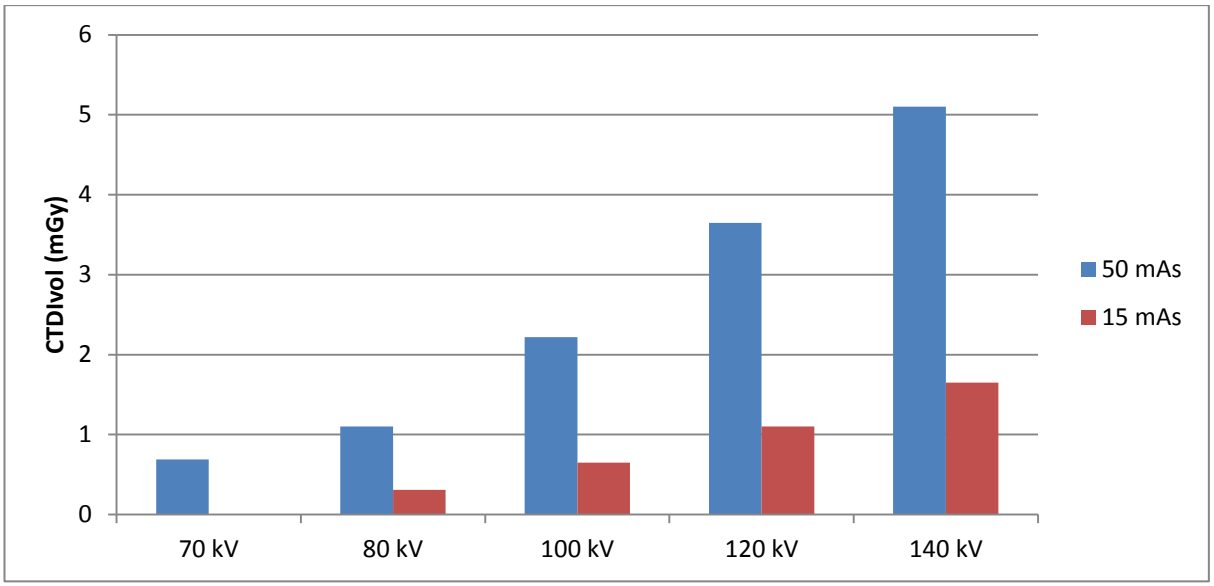

Figure 3-8: CTDIvol for different tube voltages at a constant tube current of 50 mAs and 15 mAs.

In figure 3-8, it can be seen that the dose reduction improves by reducing the tube voltage. For example, reducing the tube current from 120 kV to 100 kV at a steady tube current, leads to a reduction of the CTDI with 40%. By decreasing the tube voltage even more to 80 kV, this leads to a CTDI reduction of almost 70%. Instead of decreasing the tube voltage, voltage can be increased to 140 kV. This results in an increase of CTDI with 40% compared to the 120 kV protocol. These results show that reducing the tube voltage is a possible method to reduce the dose delivered to the patient.

3.3.2. Noise analysis

In the previous analysis, it has been shown that reducing the tube voltage is an effective way of decreasing the patient dose. But as known, in CT there is always a tradeoff between dose and image quality. Technically it is possible to lower the dose to extremely low levels, but image quality should still be sufficient to perform a correct diagnosis by the physician. A first parameter that will be analyzed is the noise in the image.

As mentioned in chapter two, noise is measured by calculating the standard deviations of the Hounsfield units in an ROI, placed in a homogenous field of the phantom. The radius that is used in this case is 1.5 cm. This noise analysis was performed for every protocol and the results are summarized in table 3-7. For every tube voltage, the noise is shown for the highest and lowest tube current in figure 48 and at 120 kV an extra beam is added to show the CTDI of the standard protocol with CareDose 4D.

In all the other protocols CareDose4D and CareKv were selected off. Important to note, is that the convolution kernel used is the I30f filter, as this has an influence on the noise.

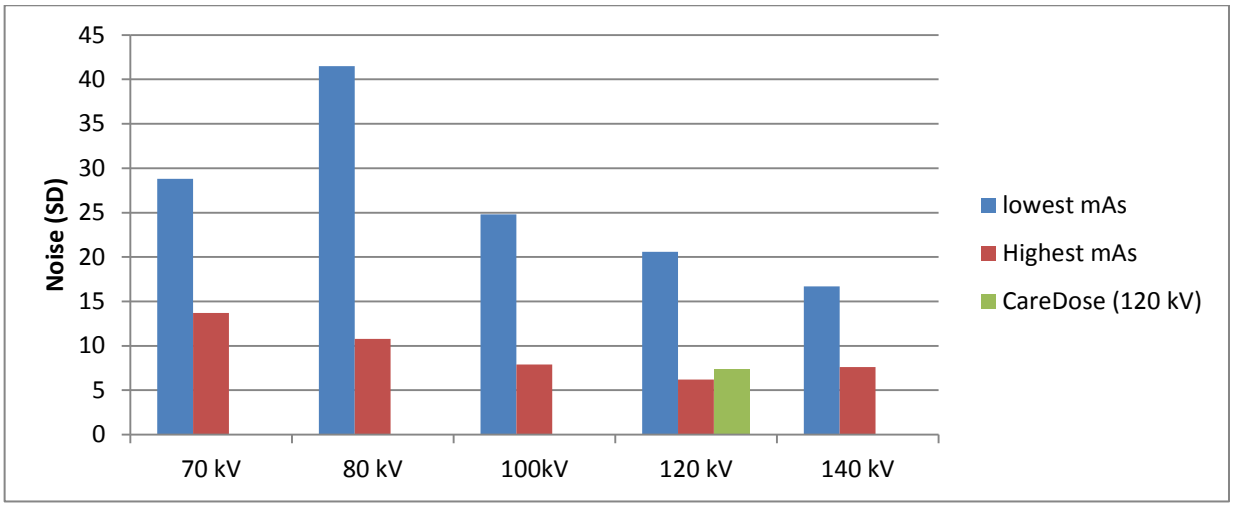

Figure 3-9: Noise in function of tube voltages for the lowest and highest tube current

Out of figure 3-9 it can be stated that the lower the tube voltage, the higher the noise will be. This supports the hypothesis that tube voltage influences the noise. In a following graph (figure 3-10), this hypothesis will be analyzed in more detailed by keeping the tube current constant for every tube voltage and noted how the noise will change. Again the tube current will be fixed at 50 mAs and 15 mAs.

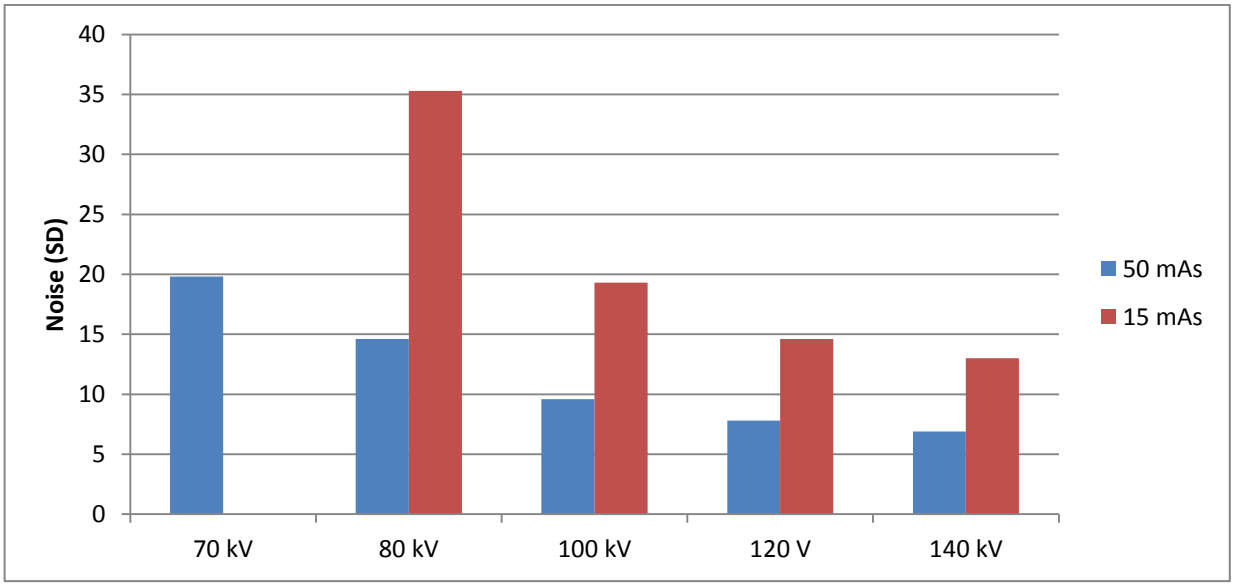

Figure 3-10: Noise for different tube voltages at constant tube current of 50 mAs and 15 mAs

It can be seen that the tube voltage indeed has an important influence on the noise of the CT image. It can be stated that the lower the tube voltage is, the higher the noise in the image will be.

To quantify this noise increase, percentages can be used. Decreasing the tube voltage from 120 kV to 100 kV, leads to a noise increase of 23% for 50 mAs and 32% for 15 mAs.

By reducing the tube voltage even more to 80 kV, this results in a noise increase of 87% for 50 mAs and even to 128% for 15 mAs.

To visualize the influence of the noise on the image quality of a CT image, two images are compared with each other in figure 3-11. On the left the image with the highest noise was selected with a tube voltage of 80 kV and an effective tube current of 15 mAs. The right image is a CT scan with tube voltage of 140 kV and tube current of 71 mAs. It can be clearly seen that the noise on the right image is less present than in the left image.

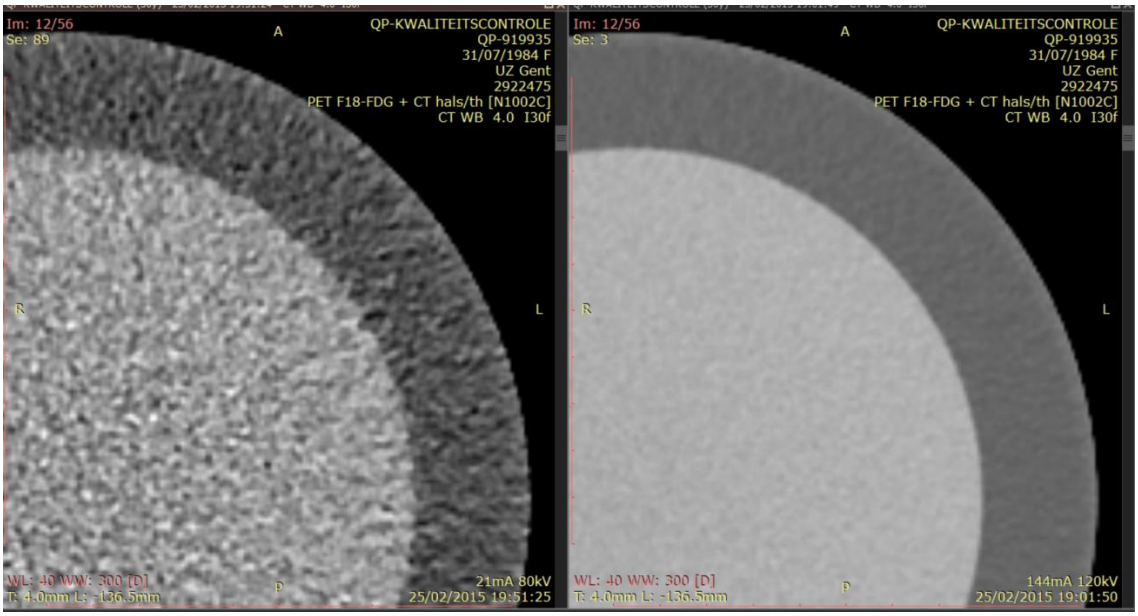

Figure 3-11: Visualization of noise in two CT images. On the left a noisy image of 80 kV and 15 mAs, on the right a noise free image of 140 kV and 71 mAs

As now the data of both the CTDIvol and noise is available for every CT-protocol, it is possible to plot these on each other. In figure 3-12, the noise is plotted as a function of the CTDI for tube voltage of 120 kV and 100 kV. A power curve can be fitted on these points with an approximate formula:

$$Noise = 14.95 * CTDI^{-0.54} \quad \textbf{3-1}$$

This approximation is also plotted in figure 3-12 and follows almost perfectly the curves of 100 kV and 120 kV. This approximation is typical for this CT-scanner.

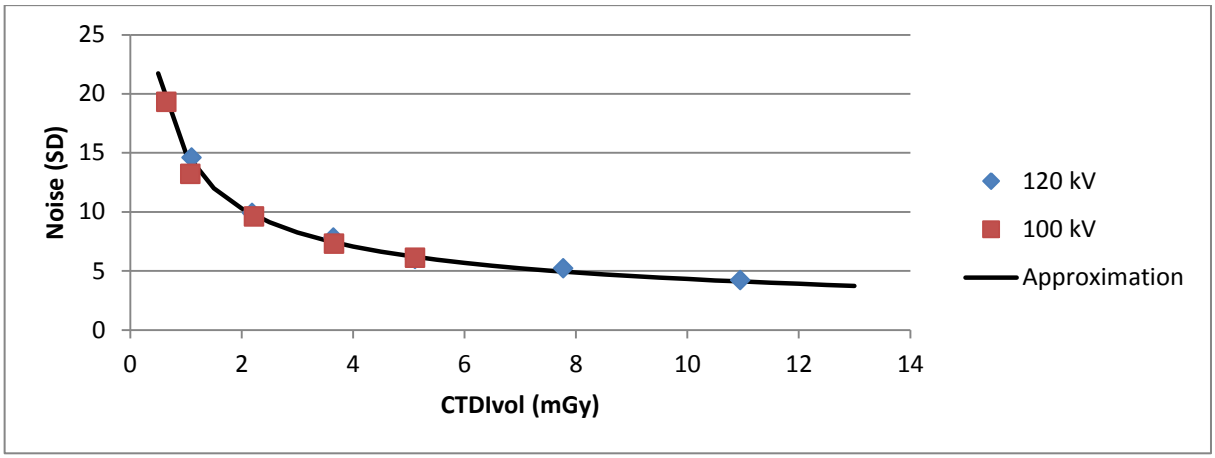

Figure 3-12: Noise plotted in function of CTDIvol for 120 kV and 100 kV, plus the approximation which defines the relationship between noise and CTDIvol for this CT scanner.

To be fully complete the curves of the other tube voltages are plotted on figure 3-12, which results in figure 3-13. It can be seen that there is no big differences in the relationship between CTDIvol and noise. Hence formula 3-1 is a good approximation to define the relationship.

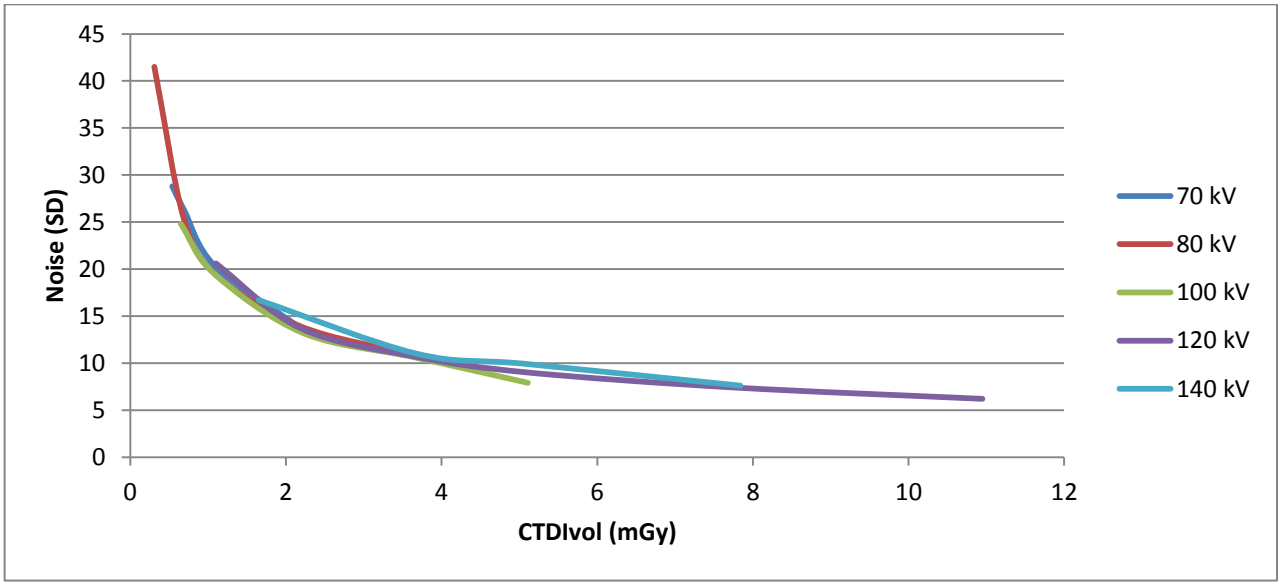

Figure 3-13: Noise plotted in function of CTDIvol for all tube voltages

Another graph is added that shows the same results as figure 52, but where the data is grouped per CTDI (figure 3-14). In this graph it makes it easier to try to find a dose-reduction technique.

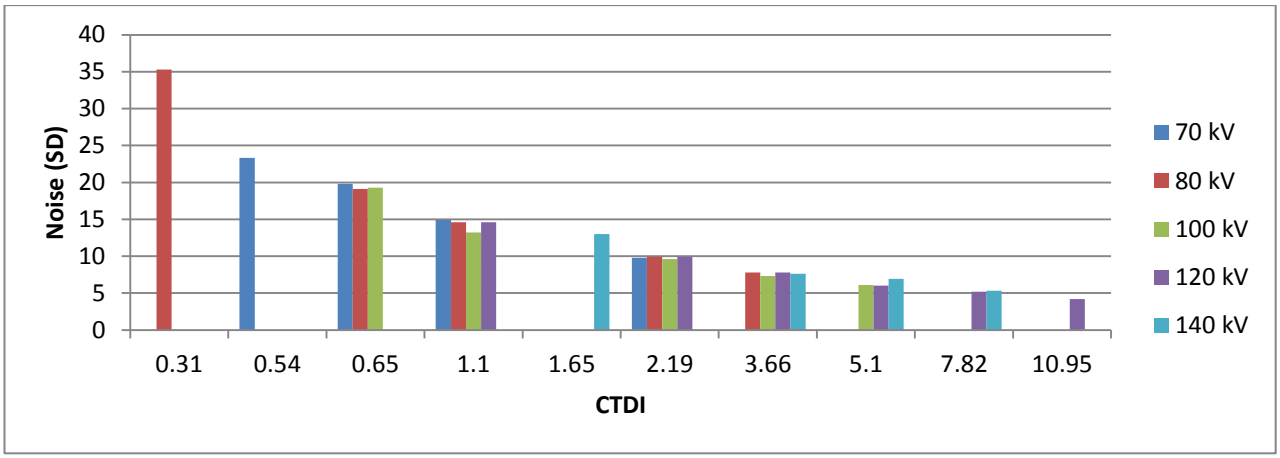

Figure 3-14 : Noise plotted for the different CTDI values

As already mentioned, tube voltage reduction is possible, but now that the data of the noise and CTDIvol is available, a quantitative hypothesis can be made. At a CTDI value of 7.7 mGy for 120 kV (106 mAs), a noise is achieved of 5.2 HU, which is the standard protocol.

If we compare this with a 100 kV protocol (118 mAs) with a CTDI value of 5.11 and a noise value of 7.9 is achieved, a dose reduction can be achieved of 33.6% and only an increase in noise of 6.8%. Further, an example of a decrease of tube voltage to 80 kV, leads to a dose reduction of 52.3% and a noise increase of 45.9%. And in extremis a tube voltage of 70 kV leads to a dose reduction of 71.6% and an increase of 85.1% of noise. These data are summarized in table 3-8.

	120 kv	**100 kV**	**difference**	**%**
CTDI	7.7	5.11	-2.59	-33.6
Noise	7.4	7.9	0.5	6.8
	120 kv	**80 kv**	**Difference**	**%**
CTDI	7.7	3.67	-4.03	-52.3
Noise	7.4	10.8	3.4	45.9
	120 kV	**70 kV**	**Difference**	**%**
CTDI	7.7	2.19	-5.51	-71.6
Noise	7.4	13.7	6.3	85.1

Tabel3-8 CTDI and noise difference for different tube voltages examples

From these results, the hypothesis can be made that reducing the tube current from 120 kV to 100 kV is plausible to be a dose-reducing method. To keep the noise decrease at a minimum, the tube current needs to be increased for this dose-reducing method.

Important to note is that the noise is highly dependent on the used reconstruction filter. To evaluate the influence of the filter on the noise, this is depicted in figure 3-15 for standard protocol 120 kV – 106mAs and the suggested dose-reducing protocol. B stands for filtered back-projection and I for iterative reconstruction.

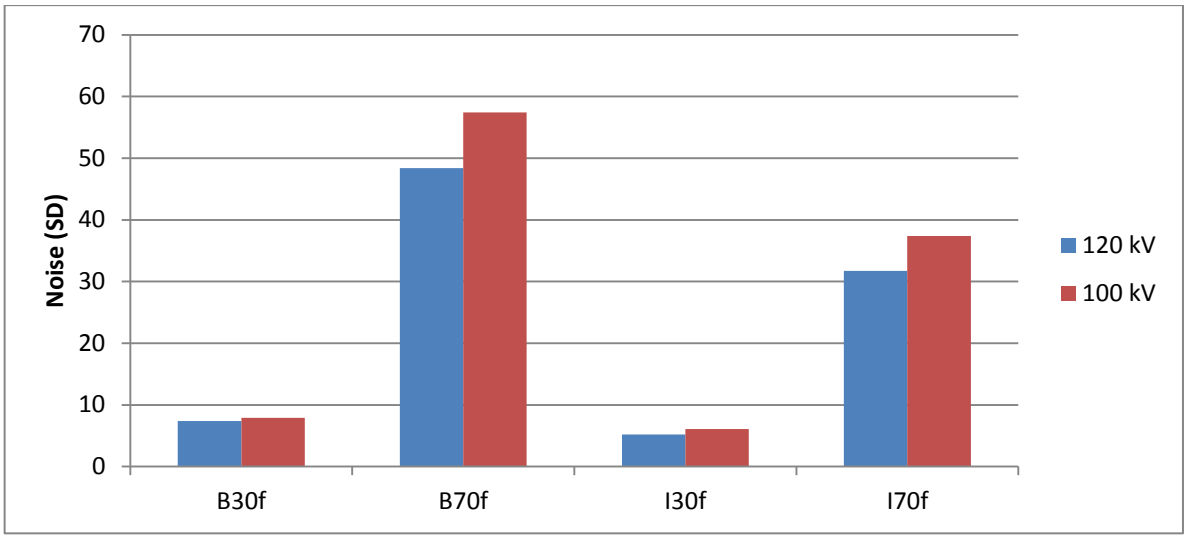

Figure 3-15: Noise in function of the four available reconstruction filters for 120 kV and 100 kV

For every tube voltage, the same pattern is repeated. The lowest noise is achieved with the I30f filter and the highest noise with the B70f. Hence a smooth filter and iterative reconstruction will decrease the noise. Quantitatively this means a decrease of 30% in noise with iterative reconstruction for the smooth filter and 34% for the sharp filter.

Based on noise, the iterative reconstruction with a smooth filter gives the best image quality. But other image qualities should be analyzed, which will be done in the following parts.

3.3.3. Resolution

Another important image quality parameter is the spatial resolution. Hence by using the Catphan at CTP 528 module the resolution is measured for every protocol analyzed in the noise part. This module contains 21 line pairs per cm gauge. Each line pair has a smaller gap size ranging from 5 mm to 2.4 mm. The images of each module were measured for every protocol by looking at the smallest line pair that could still be separated from each other. The gap size at the corresponding line pair is than the spatial resolution. The spatial resolutions for the lowest dose protocols are shown in figure 3-16.

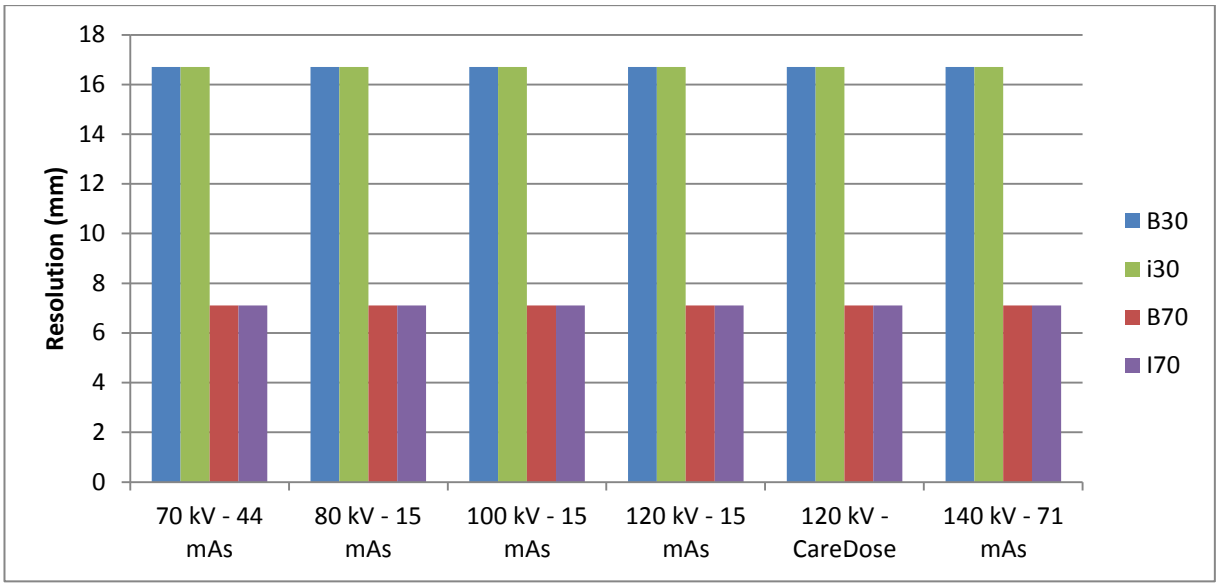

Figure 3-16: Spatial resolution for the low dose protocols and standard protocol (CareDose)for different reconstruction filters

As expected the tube voltage and tube current will not influence the spatial resolution as this is only influenced by the detectors of the CT machine. The only parameter that has an influence on the resolution is the reconstruction filter. Here a sharp reconstruction filter instead of a smooth will improve the resolution from 17.5 mm to 7.1mm. It should be mentioned that these spatial resolutions are not absolute but relative as not the full field of view of the CT scanner was used. This represents a comparison and not absolute data. The resolution of the Biograph mCT can be found in Appendix A.

3.3.4. Contrast

A last important parameter in image quality is the low contrast detail. If an image has no noise and a perfect resolution, low contrast is still needed to distinguish small tumors from normal tissue. As in the part of noise analysis, for all protocols ranging from 70 kV to 140 kV, the IQFinv is calculated and summarized in table 3-9.

Tube voltage (kV)	Effective tube current (mAs)	CTDIvol (mGy)	DLP (mGy*cm)	IQFinv
70	44	0.54	11.88	3.23
70	55	0.69	15.18	5.26
70	87	1.09	23.98	6.67
70	175	2.19	48.18	8.55
80	15	0.31	6.82	2.78
80	34	0.69	15.18	3.51
80	54	1.1	24.2	5.13
80	106	2.19	48.18	9.80
80	179	3.67	80.74	11.90
100	15	0.65	14.3	6.67
100	25	1.08	23.76	4.88
100	51	2.22	48.84	8.70

100	85	3.66	80.52	7.69
100	119	5.11	112.42	12.20
120	15	1.1	24.2	4.88
120	30	2.19	48.18	4.55
120	50	3.65	80.3	7.69
120	70	5.11	112.42	12.35
120	106	7.77	170.94	11.49
120	150	10.95	240.9	20.00
140	15	1.65	36.3	6.90
140	34	3.68	80.96	9.17
140	46	5.1	112.2	9.09
140	71	7.84	172.48	16.67

Tabel3-9 Parameters of the different low dose protocols with IQFinv (standard protocol)*

For every tube voltage, the IQFinv is shown for the highest and lowest tube current in figure 3-17 and at 120 kV an extra beam is added to show the IQFinv of the standard protocol with CareDose. In all the other protocols CareDose and CareKv were deselected. Important to note, is that the convolution kernel used is the I30f filter, as this has an influence on the IQFinv.

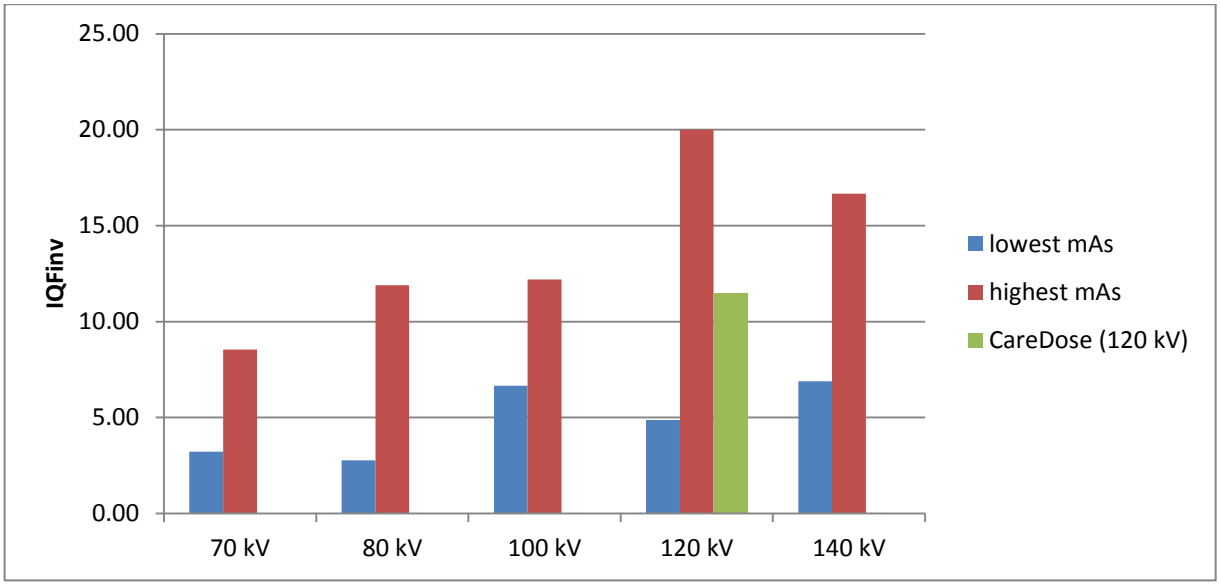

Figure 3-17: IQFinv in function of tube voltages for the lowest and highest tube current plus standard protocol

Out of figure 3-17, it is rather difficult to find a relationship between the IQFinv and the tube voltage used. There is a small trend that the lower the tube voltage, the lower the IQFinv, but this cannot be quantified. Hence the 100 kV and 120 kV are analyzed more in detail in figure 3-18, where the IQFinv is expressed in function of CTDIvol.

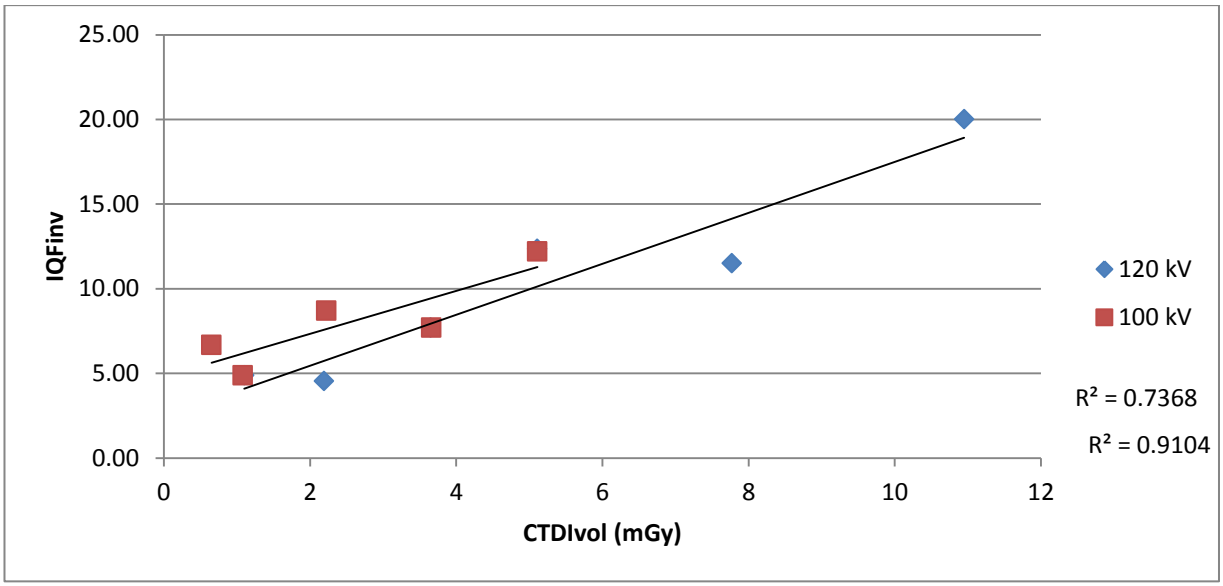

Figure 3-18: IQFinv in function of CTDIvol for 120 kV and 100 kV

In figure 3-18, it is possible to add a trendline but the R^2 is only 0.76 for 100 kV and 0.9104 for 120 kV. Hence these results suggest a linear relationship, but not significant enough to conclude that the IQFinv increases linearly with increasing dose.

Next the IQFinv plotted for every CT protocol is depicted in figure 3-19. Out of this figure it is again possible to make a quantitative analysis of the dose and IQFinv between the suggested dose reduction protocol of 100 kV and 118 mAs. Hence the CTDIvol difference is still a decrease of 33.6%, but an increase of IQFinv is achieved of 6.2% by reducing the tube voltage to 100 kV. For 80 kV and 70 kV, the comparison is summarized in table 3-10.

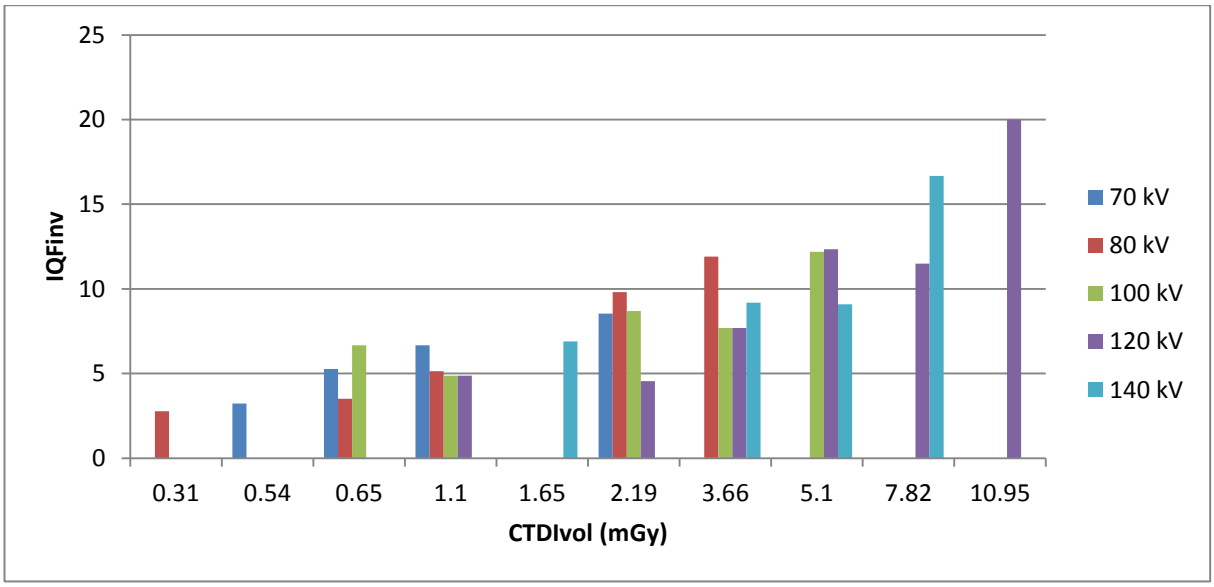

Figure 3-19: IQFinv plotted for the different CTDI values of all protocols

	120 kV	100 kV	Difference	%
Dose	7.7	5.11	-2.59	-33.6
IQFinv	11.49	12.2	0.71	6.2
	120 kV	**80 kV**	**Difference**	**%**
Dose	7.7	3.67	-4.03	-52.3
IQFinv	11.49	11.9	0.41	3.57
	120 kV	**70 kV**	**Difference**	**%**
Dose	7.7	2.19	-5.51	-71.56
IQFinv	11.49	8.55	-2.94	-25.59

Tabel3-10 CTDI and IQFinv difference for different tube voltages examples

To end this part of low-contrast detail, a comparison is made of the four reconstruction filters. The IQFinv was calculated for the standard protocol and the dose-reduction protocol and plotted in figure 3-20. From this figure it can be noted that the iterative reconstruction with a smooth filter delivers a slightly higher IQFinv than FBP with a smooth filter, 4% increase for 120 kV and 10% increase for 100kV. The highest IQFinv is achieved with I30f filter.

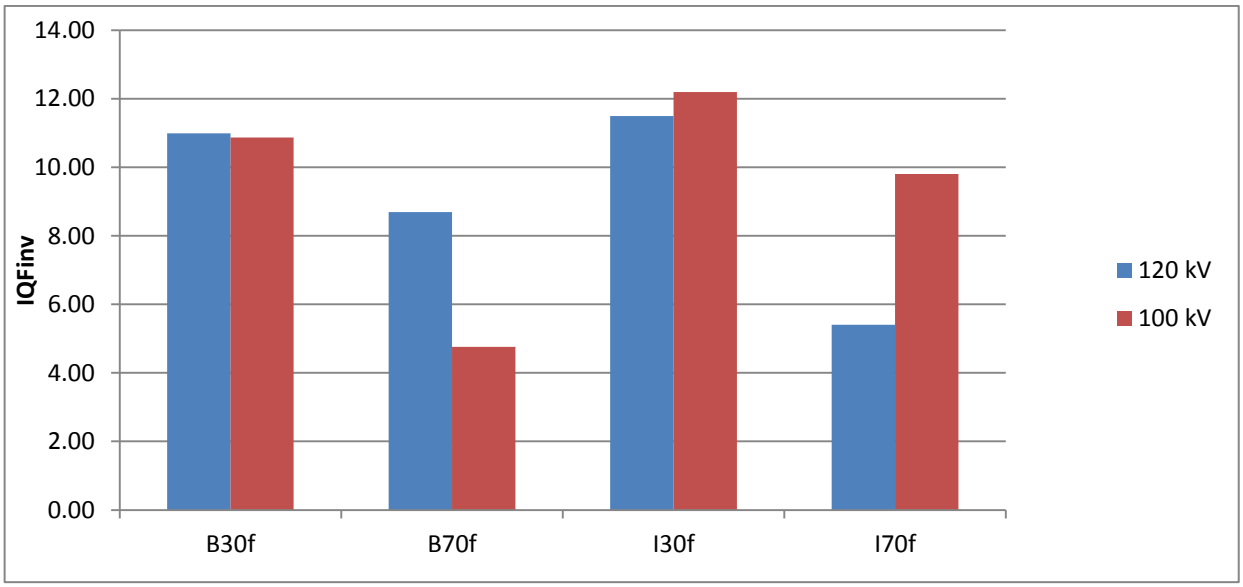

Figure 3-20: IQFinv in function of the four available reconstruction filters for 120 kV and 100 kV

3.3.5. Hounsfield units

A last issue that will be analyzed in this part is the stability of the CT number when parameters of the CT-scanner would change. Ideally, the CT number should be independent of the tube voltage, tube current and reconstruction parameter, as the CT number is relative to the value of water. Hence the CT numbers for every scan parameter should be the same. This is what will be investigated in this analysis.

First the linearity of the CT-numbers is tested of the CT-scanner. This means that a linear relationship should be achieved between the density of the material scanned and the CT-numbers. For this the CTP 515 module is used. By scanning this module with the standard protocol of 120 kV and CareDose on with an effective tube current of 106 mAs, for every material inside this module the mean CT-number is calculated in an ROI. In table, the used materials and their density expressed in g/cm³ are depicted, together with the measured CT-numbers in table 3-11.

Material	Density (g/cm³)	CT number (HU)	Theoretical (HU)
Air	0.0012	-1016	-1000
PMP	0.84	-187	-176.47
LDPE	0.92	-96	-90.90
Polystyrene	1	-37	-16.04
Acrylic	1.18	123	122.99
Delrin	1.42	345	342.24
Teflon	2.2	952	930.48

Tabel3-11 Density, measured CT number and theoretical CT number for the different materials inside the CTP 515 module

To calculate the theoretical CT number, the attenuation coefficient of water needs to be known at 75 keV (mean energy of 120 kVp), which is 0.187 [11]. Next the attenuation coefficients of the different materials need to be known. These can be found in the manual of the catphan phantom and shown in table 3-12.

Material	Density (g/cm³)	Attenuationcoefficient (75 keV)
Air	0.0012	0
PMP	0.84	0.154
LDPE	0.92	0.17
Polystyrene	1	0.184
Acrylic	1.18	0.21
Delrin	1.42	0.251
Teflon	2.2	0.361

Tabel3-12 Density and attenuation coefficient at 75 keV of the different materials inside the CTP 515 module

Next the theoretical Hounsfield units can be calculated according the HU formula 1-5. The results of this calculation are presented in table 3-11. These theoretical and measured CT numbers can be plotted in function of the density (figure 3-21). From this graph it can be seen that the linearity is almost perfect for the measured CT numbers ($R^2 = 0.9956$).

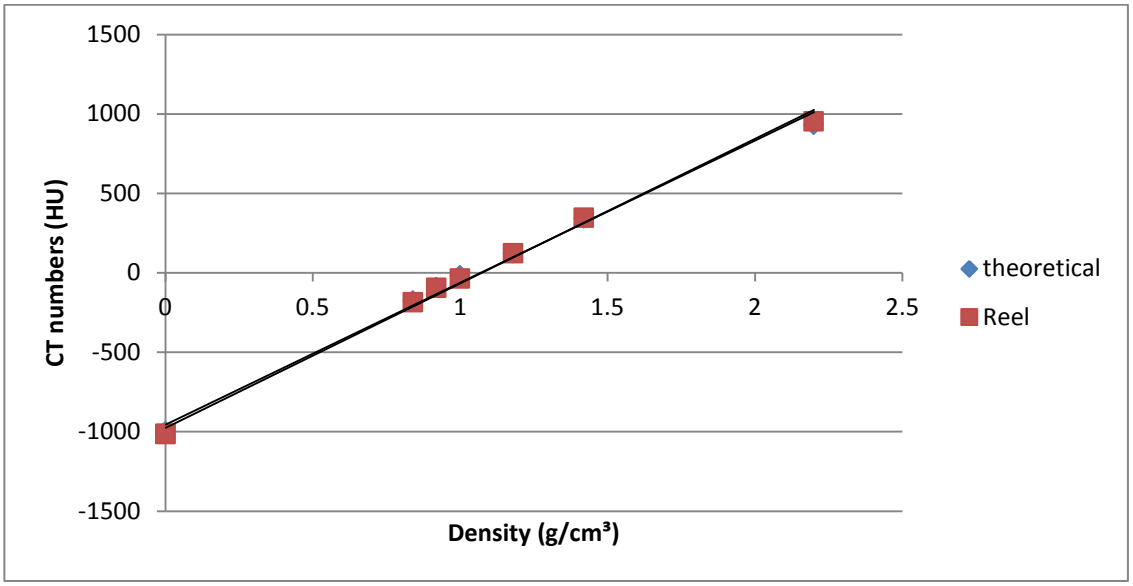

Figure 3-21: Linearity of CT-numbers in function of density theoretically calculated and measured data

Next the CT numbers are calculated for the different tube voltages. For every protocol from table 3-10, the mean CT-number in an ROI is measured. The mean CT number over the different tube currents is used for each tube voltage and plotted in figure 3-22. It should be noted that the i30f filter was used for this.

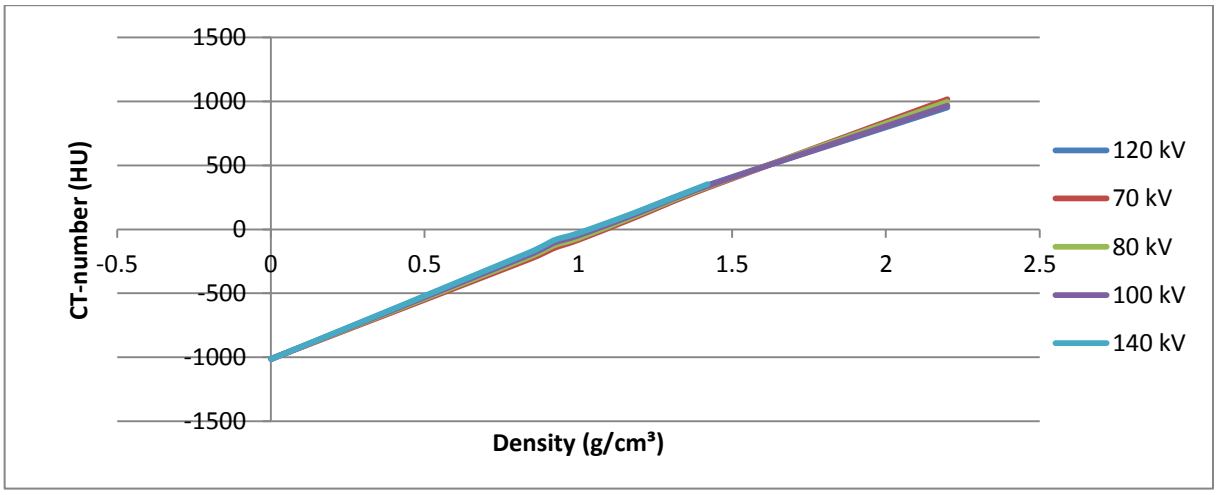

Figure 3-22: CT number for every tube voltage plotted in function of the density

From figure 3-22, it is noted that there is a small variation in CT-numbers due to the tube voltage used, especially around soft tissue of 1g/cm³ and dense materials (2.25 g/cm³). To quantify this, the root mean square error (RMSE) is calculated for every material (table 3-13).

Here it can be seen that the highest variation effectively is present for soft tissue around 1 g/cm³ and dense material (2.25 g/cm³).

Material	RMSE
air	24.0
air	28.0
PMP	75.5
LDPE	69.0
Polystyrene	94.1
acrylic	41.8
delrin	22.5
teflon	116.1

Tabel3-13 RMSE for the different materials

At last the influence of the reconstruction filter on the CT-number is analyzed. After measuring all the mean CT-numbers for every material for each reconstruction filter, these data are then plotted in figure 3-23. The tube voltage for this was 120 kV and the CT-numbers were taken the mean over the tube current. It can be seen that the influence of the reconstruction filter is negligible on the CT-numbers.

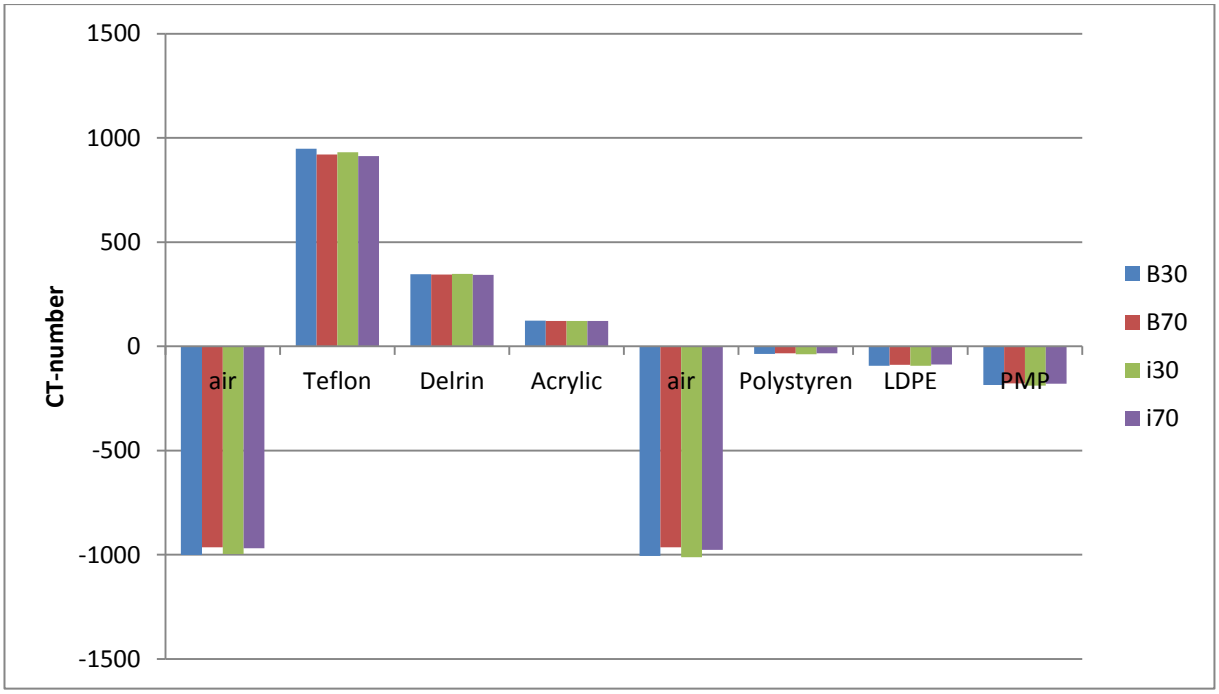

Figure 3-23: CT-numbers for the different reconstruction filters of the different materials

3.4.Attenuation correction analysis

In the previous section, a dose reduction technique was presented based on the positive results on noise, resolution and low contrast detail, by reducing the tube voltage from 120 kV to 100 kV. But in contrast with stand-alone CT, in PET-CT the CT images are used to correct the PET image for attenuation. Hence it needs to be evaluated whether parameters of the CT-scan, has no influence on the correction of the PET image. Mainly this will be analyzed by measuring the recovery coefficient on the reconstructed PET image for the different CT protocols.

In this experiment, the PET-phantom is used and placed inside the PET-CT scanner. First the PET phantom needs to be filled with a certain amount of activity. In the hotlab, FDG is prepared and resolved in a volume of one liter. The activity of FDG is measured at 16:49 and was 91.45 MBq. This results in a concentration of 91.45 MBq/L. Also the background has to be measured, which was done by measuring the activity of the phantom when it was not loaded. This results in a background activity of 96.7 MBq in a volume of 9.89L, resulting in a concentration of 9.78 MBq/L. Hence the ratio of true concentration over background concentration is 9.35. This activity of FDG is then distributed over the spheres of the PET phantom, resulting of a concentration of FDG of 96.7 MBq/L in every sphere.

This filled phantom is placed inside the PET-CT scanner and the scan protocols from the second experiment are performed on this PET phantom. First a topogramis made, to select the scan region and to make automatic current modulation possible. After the topogram, 24 CT scans are performed on the PET-phantom and at the end two PET-scans are performed. First the topogram scan is performed on the PET-phantom with the following parameters (table 3-14).

Parameters	Topogram
Tube voltage	120 kV
Tube current	35 mA
CTDIvol	0.13 mGy
Length	510 mm
Convolution kernel	T80f
Direction	Posterior-anterior

Tabel3-14 Parameters of the CT topogram for the attenuation correction experiment

Based on the topogram scan, the length of the actual CT-scan is selected to be 243 mm. Now the phantom is scanned 25 times with different CT-protocols.

First all parameters arekept the same as a clinical scan would be taken, which means based on the protocol an effective tube current of 170 mAs is used, with a voltage of 120 kV. For the following CT scans, the same parameters as in the third experiment were used (low-dose protocol experiment). To keep an overview, these parameters are again summarized in table 3-15. Again the protocols can be categorized in 5 groups according to their tube voltage (70, 80, 100, 120 and 140kV). *the advised tube current by CT scanner (reference mAs) + CareDose4D.

Tube voltage (kV)	Effective tube current (mAs)	CTDIvol (mGy)
70	44	0.54
70	55	0.69
70	87	1.09
70	175	2.19
80	15	0.31
80	34	0.69
80	54	1.1
80	106	2.19
80	179	3.67
100	15	0.65
100	25	1.08
100	51	2.22
100	85	3.66
100	119	5.11
120	15	1.1
120	30	2.19
120	50	3.65
120	70	5.11
120	106	7.77
120	117*	10.95
120	150	10.95
140	15	1.65
140	34	3.68
140	46	5.1
140	71	7.84

Tabel3-15 Parameters of the 25 CT scans

After the CT-protocols is taken, two PET scans are performed on the PET-phantom. These PET scans are performed caudo-cranial (in difference with the CT scans, which were performed cranio-caudal). The difference between the two PET scanners is the speed at which the acquisition was made. PET scan 1 is performed with a speed of 1.5 mm/s, which is the fast PET scan as it will take approximately 162 seconds (2.7 min).

PET scan 2 is performed at a lower speed of 0.4 mm/s, which results in a scan that lasted for 607.5 s (10.13 min). All the other parameters of the PET scan are the same as performed in a clinical setting.

For every PET scan, 25 PET reconstructions are performed based on the attenuation correction map created for every CT scan taken. Hence in total 50 corrected PET images are achieved (25 for PET 1 and 25 for PET 2). When all images are retrieved, for every corrected PET image the recovery coefficients for the 6 spheres are calculated as explained in chapter 2. The slice is chosen where the diameter of the spheres is highest. Also the accumulation of FDG is visually the highest in this slice. The background concentration is measured inside the phantom, as expressed in chapter 2. The recovery coefficients for every sphere are summarized in table 3-16 and 3-1.

PET scan 1			**RC spheres mean**					
Tube voltage (kV)	Tube current (mAs)	CTDI (mGy)	37 mm	25 mm	22 mm	17 mm	13 mm	10 mm
uncorrected	/	/	0.585	0.546	0.544	0.526	0.415	0.328
70	44	0.54	0.980	0.952	0.946	0.939	0.835	0.647
70	55	0.69	0.980	0.953	0.947	0.939	0.835	0.648
70	87	1.09	0.981	0.953	0.948	0.939	0.835	0.649
70	175	2.19	0.983	0.955	0.949	0.941	0.837	0.650
80	15	0.31	0.982	0.955	0.947	0.940	0.837	0.648
80	34	0.69	0.979	0.951	0.947	0.938	0.835	0.649
80	54	1.1	0.980	0.952	0.946	0.937	0.835	0.647
80	106	2.19	0.982	0.954	0.948	0.940	0.836	0.649
80	179	3.67	0.982	0.954	0.947	0.940	0.836	0.649
100	15	0.65	0.981	0.953	0.948	0.941	0.837	0.648
100	25	1.08	0.980	0.953	0.947	0.940	0.836	0.649
100	51	2.22	0.983	0.954	0.949	0.941	0.837	0.650
100	85	3.66	0.982	0.954	0.094	0.941	0.837	0.650
100	119	5.11	0.982	0.954	0.948	0.941	0.837	0.650
120	15	1.1	0.981	0.954	0.948	0.941	0.836	0.650
120	30	2.19	0.982	0.954	0.948	0.941	0.837	0.065
120	50	3.65	0.978	0.954	0.949	0.941	0.837	0.650
120	70	5.11	0.978	0.954	0.948	0.941	0.837	0.650
120	106	7.77	0.978	0.954	0.948	0.941	0.837	0.649
120	150	10.95	0.977	0.954	0.948	0.941	0.837	0.650
120	170	11.6	0.977	0.954	0.947	0.940	0.837	0.650
140	15	1.65	0.983	0.955	0.949	0.942	0.839	0.652
140	34	3.68	0.983	0.955	0.949	0.942	0.838	0.651
140	46	5.1	0.983	0.955	0.949	0.942	0.838	0.651
140	71	7.84	0.982	0.954	0.948	0.941	0.837	0.650

Tabel3-16 Recovery coefficients of the uncorrected and corrected PET images of the fast scan (1.5 mm/s)

PET scan 2			RC spheres mean					
Tube voltage	**Tube current**	**CTDI**	**37 mm**	25 mm	22 mm	**17 mm**	**13 mm**	**10 mm**
uncorrected			0.579	0.543	0.549	0.512	0.407	0.358
70	44	0.54	0.976	0.960	0.954	0.912	0.815	0.709
70	55	0.69	0.976	0.960	0.954	0.912	0.815	0.710
70	87	1.09	0.977	0.961	0.956	0.913	0.815	0.711
70	175	2.19	0.979	0.962	0.956	0.914	0.817	0.712
80	15	0.31	0.978	0.962	0.955	0.913	0.817	0.710
80	34	0.69	0.975	0.958	0.955	0.911	0.815	0.711
80	54	1.1	0.976	0.960	0.954	0.910	0.815	0.709
80	106	2.19	0.978	0.961	0.955	0.913	0.816	0.071
80	179	3.67	0.978	0.961	0.955	0.913	0.816	0.711
100	15	0.65	0.977	0.961	0.955	0.914	0.817	0.710
100	25	1.08	0.977	0.960	0.955	0.913	0.816	0.712
100	51	2.22	0.979	0.962	0.956	0.914	0.817	0.712
100	85	3.66	0.985	0.968	0.962	0.920	0.822	0.717
100	119	5.11	0.978	0.962	0.956	0.914	0.817	0.712
120	15	1.1	0.977	0.961	0.956	0.913	0.816	0.712
120	30	2.19	0.978	0.962	0.956	0.914	0.817	0.712
120	50	3.65	0.979	0.962	0.956	0.914	0.817	0.712
120	70	5.11	0.979	0.962	0.956	0.914	0.817	0.712
120	106	7.77	0.978	0.961	0.955	0.914	0.817	0.711
120	150	10.95	0.978	0.961	0.955	0.913	0.816	0.712
120	170	11.6	0.974	0.961	0.955	0.914	0.816	0.712
140	15	1.65	0.979	0.962	0.957	0.915	0.819	0.714
140	34	3.68	0.979	0.962	0.957	0.081	0.818	0.713
140	46	5.1	0.979	0.962	0.956	0.915	0.818	0.713
140	71	7.84	0.979	0.962	0.956	0.914	0.817	0.712

Tabel3-17 Recovery coefficients of the uncorrected and corrected PET images of the long scan (0.4 mm/s)

3.4.1. Uncorrected versus corrected PET

Before starting to analyze the different recovery coefficients of the low-dose protocols and standard protocol, first it is analyzed if attenuation correction is actually needed to create a PET image. Therefore for PET scan with a speed of 1.5 mm/s the recovery coefficients of the all spheres are compared of the uncorrected PET image versus the recovery coefficients of the PET image that was corrected by the standard protocol of 120 kV and a tube current of 106 mAs. These two sets of data are expressed in figure 3-24. In this figure it can be seen that the corrected recovery coefficients are significantly higher than the uncorrected. To quantify this, the increase of the recovery coefficients for the standard corrected PET image is shown in table 3-18. On average an increase of 45% is achieved by using a corrected PET image.

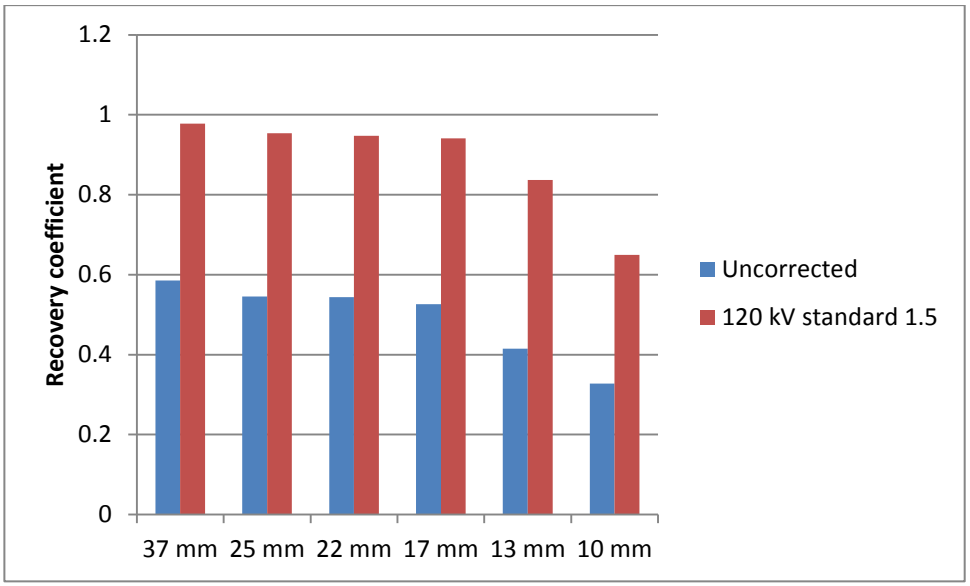

Figure 3-24: Recovery coefficients of the different spheres between the uncorrected PET image and the standard corrected PET image

	37 mm	25 mm	22 mm	17 mm	13 mm	10 mm
Difference %	40,1	42,8	42,6	44,1	50,4	49,5

Tabel3-18 Difference in recovery coefficients between the corrected PET scan and the standard corrected PET scan

3.4.2. Size of sphere influence

Now is it known that corrected PET image result in higher recovery coefficient, it is interesting to investigated the influence of the sphere size on this recovery coefficient. Therefore in figure 3-25, the recovery coefficients are plotted for the different sphere diameters for the fast and slow PET scan (figure 65). The typical exponential curve is created, where a saturation is achieved from a diameter of 22 mm on. For the slow scan, this coefficient ranges from 97.8% to 71.1% and for the fast scan, these range from 97.8% to 64.9%.

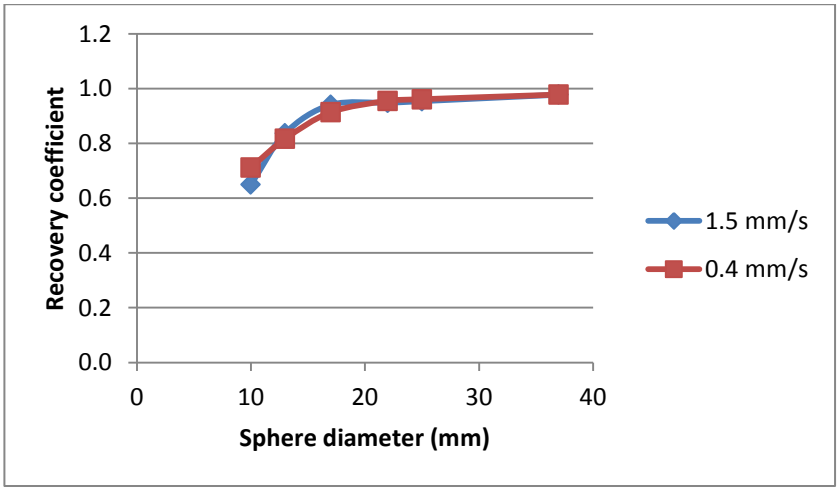

Figure 3-25: Recovery coefficient for the different sphere diameters for the fast and slow scan

3.4.3. Influence PET scan speed

In figure 3-25, it can be seen that there is a small difference in recovery coefficient between the fast and the slow scan. In figure 65, the difference can only be seen for the standard protocol at 120 kV. Hence in table 3-19 the difference (in %) is given between the slow and fast scan for the different spheres. A positive percentage indicates that the slow scan results in a higher coefficient than the fast scan. In all spheres, except for the smallest one, it can be stated that the difference are negligible, as they are lower than 3%. But for the smallest sphere, these differences are rather high, up to 9.34%. Hence the slower scan will give a higher recovery coefficient.

Difference %	37 mm	25 mm	22 mm	17 mm	13 mm	10 mm
70 kV	-0.38	0.79	0.82	-2.93	-2.46	8.75
80 kV	-0.42	0.75	0.78	-2.97	-2.50	8.74
100 kV	0.28	1.44	2.63	-2.25	-1.79	9.34
120 kV	0.08	0.77	0.80	-2.95	-2.48	8.72
140 kV	-0.38	0.79	0.82	-2.94	-2.47	8.74

Tabel3-19 Difference in percentage for the different tube voltage CT protocols for the fast and slow scan

3.4.4. Influence dose on recovery coefficients

To create a link between the low dose protocol experiment and the attenuation correction experiment, it could be interesting to investigate the influence the effect of the dose, represented by CTDIvol, on the recovery coefficients. Independent of the tube voltage or tube current, the reconstructed PET images of a CT image of different CTDIvol's are grouped together and compared to each other. The CTDI'svol chosen to represent this are 0.69, 1.1, 2.19, 3.66 and 5.11 mGy and PET images of the slow scan are used. These recovery coefficients for the CTDI'svol are graphically represented in figure 3-27.

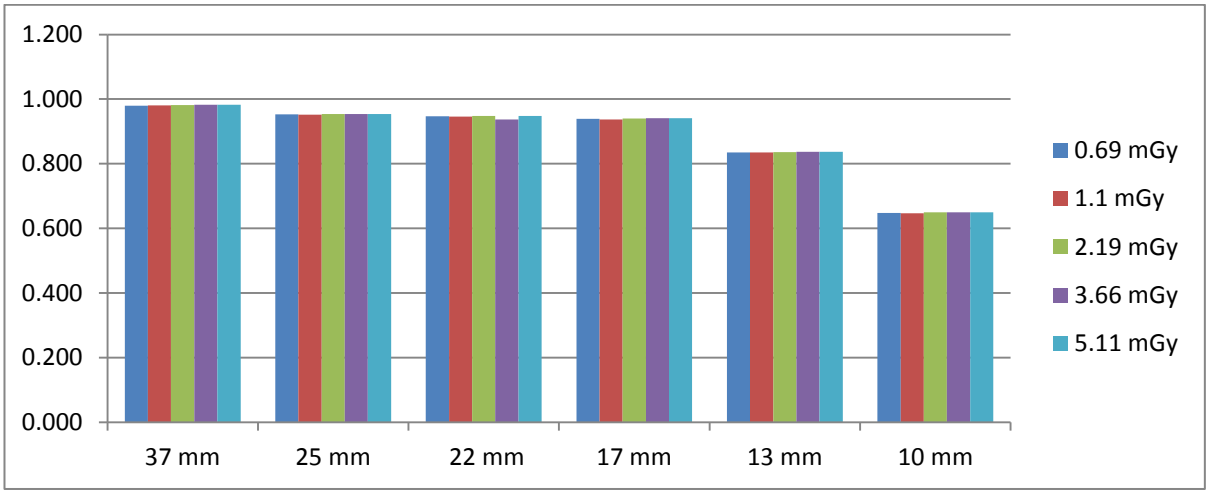

Figure 3-26: Recovery coefficients for the different spheres for different levels of CTDIvol.

An important conclusion that can be seen from this result is that the recovery coefficient is independent on the dose delivered to the patient from the CT image, that is used to correct for attenuation correction.

As extra, the influence of tube current and tube voltage on the recovery coefficients has been examined and added in appendix D. As expected these parameters have no influence on the recovery coefficients.

4. Discussion

4.1.Acceptance test

The first experiment performed in this project was the acceptance test. Out of the results of this test, it can be stated that all parameters of the CT part of the biograph mCT flow at the university hospital at Gent are accepted according to the FANC directives. The only discussion point which may be cited is that the body phantom used for these test, is rather small compared to the normal standard body of a patient. This will not be further discussed, as it is not the focus of this project.

4.2.Tube current modulation experiment

Multi-slice CT scanning has been proven to be a great success for clinical applications due to short acquisition times, thin slices up to 1 mm thick , covering of large organs and high image quality. But as CT utilizes X-rays for images, this means an exposure of radiation to the patient. In Belgium, annually the mean exposure to ionizing radiation is 5.51 mSv per inhabitant in total, which 2.66 mSv originates from medical applications[54]. Approximately 60% of this radiation, originates from CT-scans. In Belgium approximately 2 million CT scans are taken every year, and their dose can range up to 14 mSv[55]. One study suggested that about 0.4% of all current cancers in the United States may be attributable to the radiation from studies based on CT data from 1991-1996, but when organ specific cancer risk was also adjusted in the data, it was shown that 1.5-2% of cancers may be caused by the ionizing radiation used in CT [56]. These data show that the amount of CT-scans taken and the high dosage of CT can have a significant impact on public health, therefore dose-reduction strategies are needed. In PET-CT scans, the CT scan delivers 75% of the total dose to the patient. Approximately the same parameters in PET-CT are used as in stand-alone CT scanners, hence in these cases dose reduction techniques are needed.

As CT delivers a rather high dose in comparison to other X-ray modalities, a lot of efforts has been done in the past to lower the dose delivered to the patient. First of all, the justification and optimization principle should be applied to all X-ray modalities. These guiding principles for radiation protection consist of three points [54]:

- **Justification**: the exam must be medically indicated
- **Optimization**: The exam must be performed using doses that are as low as reasonably achievable (ALARA)

- **Limitation**: As dose levels to occupationally exposed individuals are limited to levels recommended by consensus, limits are not typical for medically-necessary exams or procedures.

The guiding principle for dose management in CT is that the right dose for a CT examination takes into account the specific patient attenuation and the specific diagnostic task. For large patient, this indeed means that a dose increase is consistent with ALARA principles. In this project, the focus of dose reduction will be in optimization of the CT component of PET-CT scans.

One successful example of a dose reducing technology is the automatic exposure control or tube current modulation. In several studies[57, 58, 59] it has been shown that by using this technique, a dose reduction of about 20-40% can be achieved while maintaining the image quality in stand-alone CT scanners. But in another study, performed by C. Franck[17], it has been shown that the topogram and scan direction have a high influence on the behavior of the automatic exposure control unit on the Somatom definition Flash (Siemens). Hence, in this project the question was if this topogram influence is also noted on the Biograph mCT flow.

Indeed out of the results of the automatic exposure control, it can be seen that there is a rather high influence of the scan direction on the automatic exposure control. The hypothesis would be that the curves of the tube current, for a cranio-caudal and caudo-cranial scan, in function of the z-axis length would fit on each other, as the same phantom, positioning , parameters and topogram-information is used. In this experiment, it can be seen that the curves are shifted approximately 2 cm. When the scanning starts at the head, the curve reaches it maximum already in the neck region, which is too early and decreases before the end of the shoulder region, which is also too early. When the scan direction is inverted, the tube current is built up before the shoulder region is reached and it already at is minimum in the neck region. Hence the profile of the tube current is highly dependent on the scan direction, especially in the neck region. For the general dose, this has no consequences, as this will be approximately the same, but for specific organs, for example the thyroid, this means that the dose can be twice as high locally, depending on the scan direction. If the effective dose is calculated for both protocols according to the DLP-effective dose conversion factor, there is no difference between it. Both have an effective dose of 5.61 mSv. It should be investigated in a follow-up study if this shift of tube current has an influence on the thyroid dose by using a RANDO phantom filled with dosimeters (fe TLD's). The probability that indeed there is a difference is small but existing, as the shift is approximately 2 cm and the adult thyroid length is 5 cm. This should be further investigated.

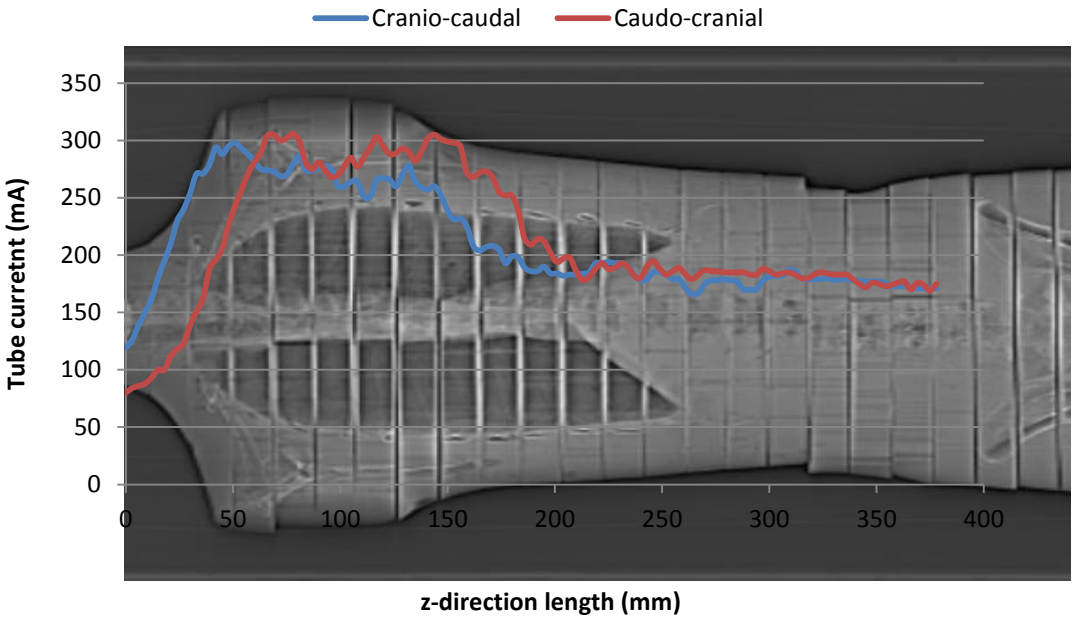

Figure 4-1: Tube current in function of z-direction length plot on the posterior-anterior topogram

In the study of Franck[17]and Kim[60], the same results are achieved for the Somatom CT, but the differences are less pronounced when X-Care and Flash-mode are activated. The reason for this difference in tube current profile are not yet fully understood and are currently investigated in detail by Franck for tube current modulation programs of Siemens and other vendors. The results of her study can then be extrapolated to the results of this study. Based on these results, it can be concluded that for a thorax-scan / PET-CT scan the patient should be scanned in a caudo-cranial way to achieve the lowest dose in the neck region.

In a second comparison the influence of the topogram scan was investigated, by comparing the tube current profile for a CT scan based on a standard PA topogram and a lateral topogram. Out of these results it can clearly been noted that the tube currents will be higher for the PA topogram compared to the lateral one. This is logic, based on the images of the topogram. For a PA topogram the tube current is based on the width of the patient which is always larger than the thickness of a patient. Therefore the tube current modulation will be calculated for a larger object, therefore increasing it tube current. These results are again supported by the results of the study of Franck on the Somatom Flash CT. Since the curves have the same shape, it is possible to use the calculated effective dose to compare the dose delivered to the patient. For a CT scan based on the posterior-anterior topogram this results in a pseudo effective dose of 5.61 mSv, while with a lateral topogram this results in anpseudo effective dose of 3.64 mSv, which is a dose reduction of 35%.

In a last comparison of the automatic exposure control experiment, the influence of the table height on the tube current profile is investigated. This sounds rather useless, but the results of this study

prove the contrary. It is shown that the table height has indeed a high influence on the tube current profile and on the dose delivered to the patient. In this comparison, all topograms were performed with a PA direction but the table was changed from 99 mm to 155 mm to 256 mm. All other parameters stayed the same, and still different tube current profiles were generated. The highest profile was achieved for the highest table height (256 mm). The explanation for this effect can be clearly seen in the figure of the corresponding topograms (figure 3-6) combined with figure4-2. For an posterior-anterior topogram and the lowest table height, the largest magnification is achieved of the patient on the detector. The automatic exposure control will base its tube current on a 'larger object', therefore increasing the dose to the patient.

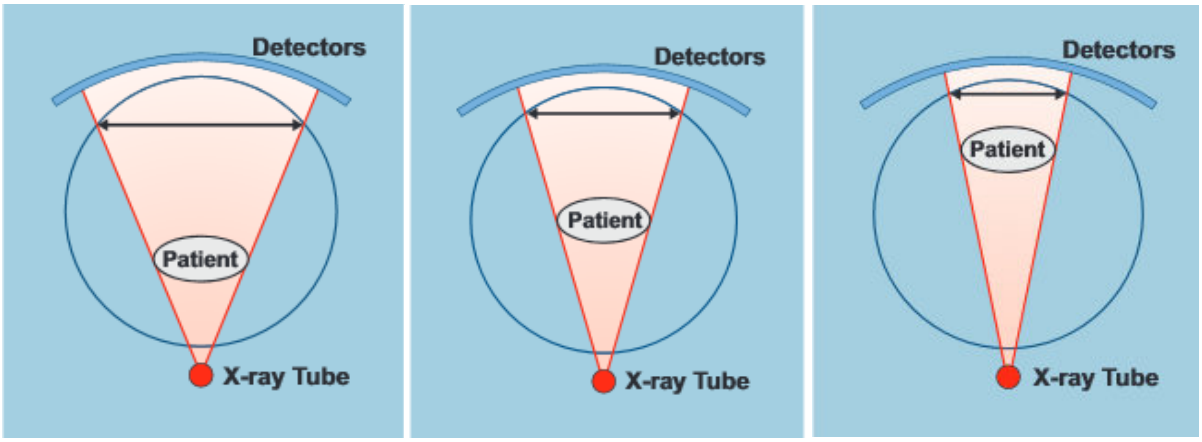

Figure 4-2: Explanation why the projection of the patient on detector is influenced by the table height[61]

A suggestion that can be made in the practical scene, is to account for the table height and rescale the measurements of the topogram to the isocenter for stand-alone CT scanners. This iso-centering of the patient also has an important influence on the spatial resolution of the PET-scan due to the parallax error. If the positron source is located near the edges of the FOV, the resolution will decrease due to the set-up of the PET scanner. The explanation for the parallax error is visualized by figure 4-3.

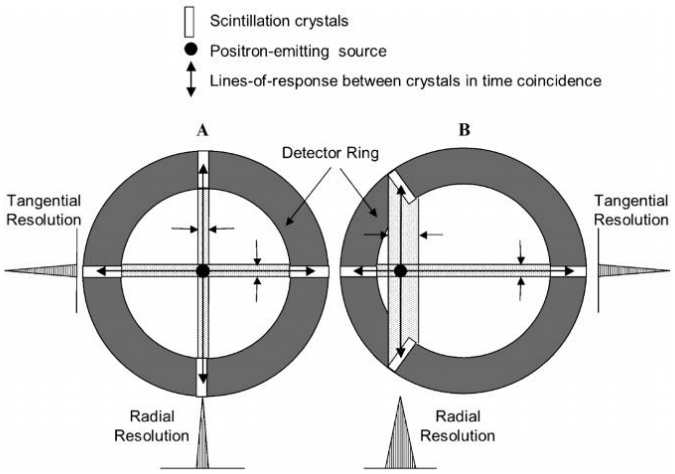

Figure 4-3: Effect on spatial resolution of not centralizing the patient in the center of a PET scanner[62]

The difference between the AP and PA view can also be explained due to concept of isocentering. In a clinical set-up, the patient is centered by aiming the ear on the mid plane. But apparently this is not exactly in the middle, as there is still a difference of tube current profile between the AP and PA view. The tube current values are approximately 30% higher for the PA-topogram, while the phantom is only one cm off-center.

As a summary, the pseudo effective doses are shown in table 4-1. Only these protocols are shown as only in these situations the effective dose can be used as comparison (as the shape of the profiles is the same).

CT-acquisition	1 (pa)	3 (lat)	5	6	7
E Dose topogram (mSv)	0.24	0.24	0.24	0.24	0.24
E Dose CT (mSv)	5.61	3.64	4.25	4.85	8.48
Total effective dose (mSv)	5.85	3.88	4.49	5.08	8.72

Tabel4-1 Effective dose for each CT protocol performed in the first experiment

To conclude, it can be stated that by changing the topogram, scan direction or table height, a maximum dose variation of 56% is possible, purely based on the tube current modulation technique. Important to note is that a dose reduction for the full scan is achieved of 33.7% when the topogram is changed from a posterior-anterior topogram to a lateral topogram, which should be implemented in the clinical set-up. Great attention should be spend to the isocentering of the patient by the staff.

4.3.Low dose protocols

In the third experiment low dose protocols were tested and evaluated. It is known that the dose delivered by a standard CT-scan can go up to 18 mSv, which is rather high, especially if this is compared to the dose delivered by the PET-part or other radiation modalities. Therefore it was the goal of these experiments to optimize the CT-settings and evaluate the dose reduction and image quality.

A known dose reduction technique in stand-alone CT is lowering the tube voltage from 120 kV to 100 kV and even 80 kV[63, 64, 65, 66, 67]. Currently, the tube voltage selected for every patient in PET-CT is always 120 kV, as this will reduce the dependence of the attenuation coefficients on photon energy, reduces the contrast of bone relative to soft tissue which is needed for thorax scans and to produce a high radiation flux at the detector, hence the image quality is high enough. As the Biograph mCT flow has five possible settings for the tube voltage (70, 80, 100, 120, 140 kV). The purpose of this study was two-fold. First to find a way of lowering the dose while maintaining the image quality and secondly to see if it is possible to go to very low dose protocols and push the limits.

In figure 3-8, the CTDIvol is shown as a function of the different tube voltages while fixing the tube current at respectively 50 and 15 mAs. From this graph it can be clearly seen that there is a quadratic relationship between the tube voltage and the CTDIvol. Hence, lowering the tube voltage will decrease the radiation exposure to the patient. Interesting is that for 80 kV program is it possible to go to an effective tube current of 15 mAs but for the 70 kV program it is not possible to go as low. Here the minimum is 44 mAs. Probably the explanation for this difference is due to technical limitations of the CT generator.

Next the correlation between noise and CTDI is shown specifically for the biograph mCT flow. The estimated formula 3-1 expresses the relationship good for all tube voltages. An important conclusion and known statement in CT is the relationship between these two quantities. The lower the dose delivered to the patient, the higher the noise in the image will be. In this project, for different low dose protocols the noise has been noted and it is possible to compare these to each other. In table 3-11, a new protocol is suggested based on this small noise increase. By reducing the tube voltage from 120 kV to 100 kV and increasing the tube current from 106 mAs to 119 mAs, a dose reduction of 33% is achieved, while the noise only increases with 6%. In figure4-4, the images of both protocols are shown where it can be seen that indeed the noise does not increase a lot.

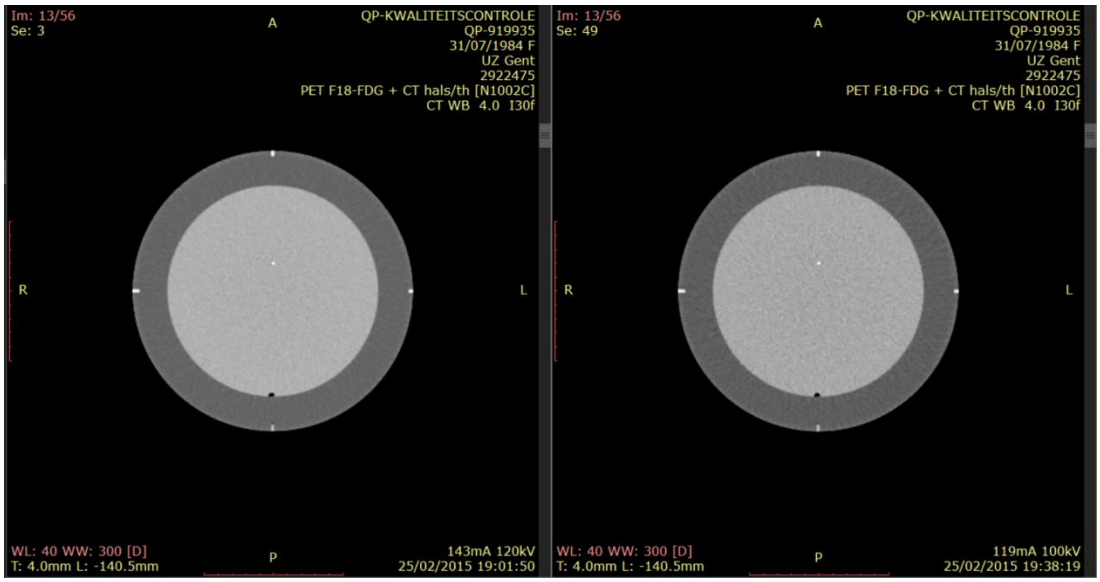

Figure 4-4: Images of the standard protocol (left) and suggested low dose protocol (right)

If the tube voltage is increased even more, the noise levels increase too high, where the danger exists that the diagnostic value of the images gets compromised. In this study an increase of noise of 6% is assumed to be still diagnostically valuable. For normal sized adults, a change of 120 kV to 100 kV should be advised. In a follow-up study, these settings should be implemented in a patient study and analyzed by physicians if the image quality is still valuable enough for diagnostic purposes. In this follow-up study it should also be possible to combine this information, with the knowledge and experience of a physician to determine a threshold for noise. If a threshold could be found, even lower dose level scan be achieved for normal-sized patients. For example, the tube voltage could still be 100 kV, but lowering the dose by changing the tube current to lower values is a possibility.

For the low-contrast detail, the results resemble the results of the noise curve. Generally, the lower the dose delivered to the patient, the lower the IQFinv. For the contrast detail, two important parameters should be accounted for. First, the noise has a high influence on the contrast as it can mask the contrast changes and secondly the tube voltage has an influence on the contrast. In figure 1-7, the attenuation coefficients are depicted as a function of the photon energy for different materials. Here we see that by lowering the tube voltage, increase of contrast is achieved as the difference between the curves are higher. Hence influence of tube voltage and noise is important in contrast. The general statement of lowering dose resulting in lower IQFinv, cannot be stated over the whole line. An important example is the suggestion made in the previous paragraph of lowering the tube voltage from 120 kV to 100 kV. In this decrease of dose, an increase of IQinv of 6% is noted.

In table 4-2, the comparison of all image quality parameters analyzed in this study are shown for the suggested low dose protocol. Indeed by reducing tube voltage, a dose reduction of 30% is achieve while noise, IQFinv and resolution change only little.

	120 kV	100 kV	Difference %
Dose (mGy)	7.7	5.11	-33.6
Noise (SD)	7.4	7.9	6.8
IQFinv	11.49	12.2	6.2
Resolution (mm)	7.1	7.1	0

Tabel4-2: comparison of image quality parameters for the standard and suggested CT protocol

As suggested, reducing the tube voltage would result in a lower radiation exposure to the patient, while maintaining the image quality. In a stand-alone CT scanner, this would be proof enough to implement this protocol, but in this project a PET-CT scanner was used. Which means that not only the image quality for diagnostic purposes should be maintained but also the attenuation correction should not change, or at least not decrease too much in quantification. The scaling from CT-numbers to attenuation coefficients at 511 keV is known to be linearly. Therefore the stability of the CT-numbers should be investigated while varying the tube voltage, hence for example the CT number for 120 kV should be same as for 100 kV.

First the linearity between the density of material investigated and the CT numbers was analyzed for the standard protocol that is always used and this was compared to the theoretical linearity. For this system, the linearity was almost perfect with a very good correlation between measurements and theoretically calculated CT numbers. Hence, the standard protocol is used as reference. The RMSE was calculated for each material for tube voltages ranging from 70 to 140 kV. In these results it can be concluded that the highest RMSE was achieved for dense material. But also in the soft tissue, a higher RMSE was achieved which has not been proven in literature[68]. The difference of the standard protocol to the 100 kV protocol was investigated. This resulted in a small deviation of 10 HU.

Studies from Skrzynski et al [69] and Zurl et al[70] have shown that for thicker anatomical structures and low X-ray energies, the errors will be higher. In general, the deviations are smaller for low-density materials and become larger with increasing density.In a study by Sande et al, the inter-phantom and inter-scanner variations for Hounsfield units were investigated. Results of this study[71] have shown the same results as this project, that the measured HU increased with increasing tube voltage for all materials, except for Teflon (high density).

It is suggested that these changes in HU due to the different tube voltage is corrected by correction schemes in the scaling of the CT numbers to attenuation coefficients at 511 keV. Since there is a high inter-scanner variability of HU [71], it is important to investigate if the attenuation conversion is corrected for or has no influence on the attenuation correction for this specific PET-CT scanner.

Therefore to evaluate if the correction schemes work properly, the following experiment with recovery coefficients is performed.

4.4.Attenuation correction experiment

In the last experiment, the recovery coefficients are used to evaluate if it would be possible to utilize lower tube voltages in CT-scanning for the attenuation correction of the PET images. In the previous chapters, it has been proven that by going from the standard protocol to the proposed protocol will lead to a dose reduction and maintaining image quality. But what is the influence on the attenuation correction. The attenuation correction effect is quantified in this experiment by means of the recovery coefficient. First of all, it was shown that attenuation correction is indeed needed to reconstruct PET images, as this leads to an increase of the recovery coefficient by approximately 40%. To visualize the effect of attenuation correction, figure4-5 contains two PET images, one corrected and one non-corrected. It can clearly been seen that more information is available on the corrected PET image. Clinically this is important, as small uptake of FDG needs to be registered and quantification will be more accurate.

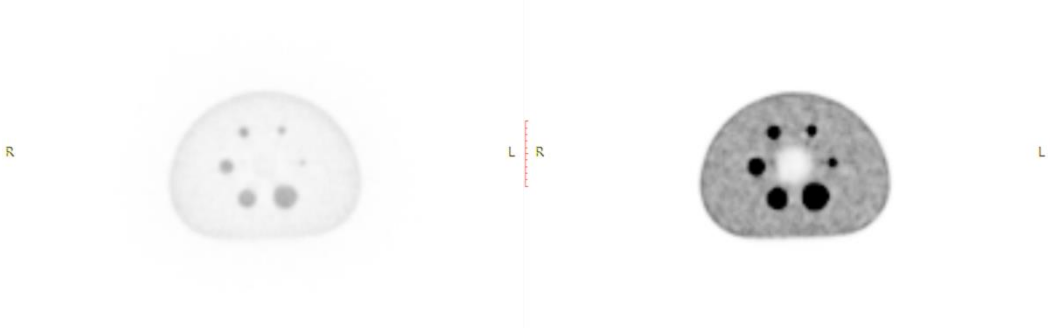

Figure 4-5: Image of the PET phantom with (right) and without (left) attenuation correction

Next the influence of the sphere diameter is investigated on the recovery coefficient. It can be clearly seen from figure 4-6 that there is a saturation present for diameters larger than 20 mm. The decrease of the recovery coefficient for smaller diameters is due to the partial volume effect in PET images. This is an effect caused by blurring due to a combination of the finite spatial resolution of the scanner and image sampling. One can state due to this combination that there is no loss of signal due to PVE but it just displaces the signal in the image. This is a very difficult and important parameter to correct for in PET. More information about partial volume effects in PET imaging can be found in the study of Soret[72].

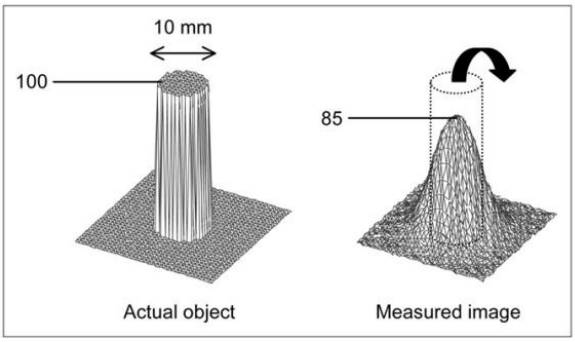

Figure 4-6: Explanation of partial volume effect due to finite spatial resolution[72]

The most important conclusion that can be made from these experiments is that the dose delivered to the patient due to the CT-scan has no influence on the correction as the recovery coefficients stay constant. This is a very important conclusion since it can be stated that by using the low dose protocol suggested in table 4.2 (100 kV, 166 mAs), not only the image quality is maintained. Also the attenuation correction stays the same. Therefore it should be advised to lower tube voltages for the Biograph mCT flow PET-CT scanner. In figure 4-7, reconstructed PET images based on the standard CT scan and the suggested CT-scan are shown.

Figure 4-7: Image of PET phantom corrected by the standard CT protocol (left) and the suggested low dose protocol (right)

In the introduction of this project, it was mentioned that the usage of SUV should be discouraged due to its inaccuracy due to variable parameters that influence its value. Some attempts have been made to 'improve' this parameter, but a correction of PVE has not been shown yet until a study of Srinivas [73]. Since there is still no quantitative alternative to the SUV, a correction look-up table is constructed to correct for the PVE for spherical lesions. The correction is based on measurements of the recovery coefficients for different lesion sizes. If these recovery coefficients are known for a typical scanner, a more accurate measurement of SUV can be achieved. In this project, it has been proven that recovery coefficients are not influenced by tube voltage or tube current, the same recovery coefficients can be used when a lower dose CT protocol is used for PVE correction of the SUV.

Currently every intervention done by a PET-CT scanner is performed by the same scan parameters. Meaning a rather high dose is each time given to the patient for diagnosis, follow-up scans, therapy evaluation, etc. It is logical that for diagnosis, image quality and anatomical localization are important, hence for diagnosis the normal low dose protocol should be used. But for follow-up scans and therapy evaluation, this CT image quality and anatomical localization is not necessary. Therefore very low dose CT scans should be advised only for attenuation correction of the PET image.

4.5.Limitations

A first important limitation is the use of the NEMA PET phantom. In this project, this phantom was used to evaluate and calculate the recovery coefficients. Since in this set-up only homogenous soft tissue was accounted for, since the PET phantom is made out of soft tissue equivalent material. But no high density material is available, for example bone. Bone is important due to its high density, hence high attenuation in CT and PET. In oncology, bone tissue is also important as is it a common site of metastasis. Out of the experiment of the variability of the Hounsfield units, it can be seen that the RMSE is highest for these high density materials. In a study of Abella et al[74], it is shown that the per cent error in PET SUV for bone imaging is roughly proportional to the per cent error in the linear attenuation coefficients estimated from the CT scan. Smaller errors are expected for higher kV scans. In the experiment of Abella, a GE scanner is used. Combining the information about interscanner variation of HU and the experiment of Abella, this should be re-evaluated on the Biograph mCT PET-CT scanner. A follow-up experiment could be to add bone or bone equivalent material to the PET phantom.

A second limitation is that each time rather small phantoms were used if compared to actual patient sizes. The catphan phantom is smaller than the average size of a patient. The PET phantom has the same size as a normal patient. It can be stated that mostly cancer patients will have a normal to low BMI inside a population, but there are still patients who are larger than average. This is not accounted for in this project. The dose reduction proposition is performed on these normal phantoms and in clinical practice the standard protocol of 120 kV is each time used. There is a possibility that by lowering the tube voltage to 100 kV, this could have important consequences on the image quality for very heavy patients (where 120 kV is good). Therefore a threshold based on BMI could be used to use these low dose protocols.

A third limitation in this study is that the IQFinverse was calculated in a subjective way, by reading the images by individuals. To lower the influence of this, three readers were used and taking the mean over these results.

At last Kuwert et al [75] has shown that an increase of the ROI of a factor of 2, results in a loss of 24% in apparent activity. Therefore it is advised by Hoffmann et al [76] to use maximum pixel values within an ROI, which will be the truest measure of the actual activity within the region. In the project, mean values were used instead of maximum values to calculate the recovery coefficient. Maximum measurements were performed and results are added in appendix E. It can be seen that these recovery coefficients are too high (> 1). The reason for these high recovery coefficients is due to outliers inside the ROI used. Therefore mean values are used and not maximum values.

5. Conclusion

The conclusion in the project is twofold. First of all for a normal diagnostic scan it should be advised to lower the tube voltage from the standard 120 kV, which is used for every patient, to 100 kV which will reduce the dose delivered to the patient drastically while maintaining the image quality by increasing the tube current if needed. In this project, it has been shown by using this method that a dose reduction of 30% can be achieved while maintaining the image quality and maintaining the quantitative measurements needed for the diagnosis in the PET image.

Secondly, it should be noted that in the present, there is no change of parameters of the CT component for different investigations. For diagnosis, follow-up or therapy evaluation, the same parameters are used, hence the same radiation exposure is delivered to the patient. In this project it has been proven that if only attenuation correction is needed, a very low dose protocol can be used. For example, lowering the tube voltage to 80 kV and lowering the tube current to 50 mAs. Image quality and anatomical localization will be significantly decreased but this is not necessary in follow-up scans to evaluate the effect of a therapy.

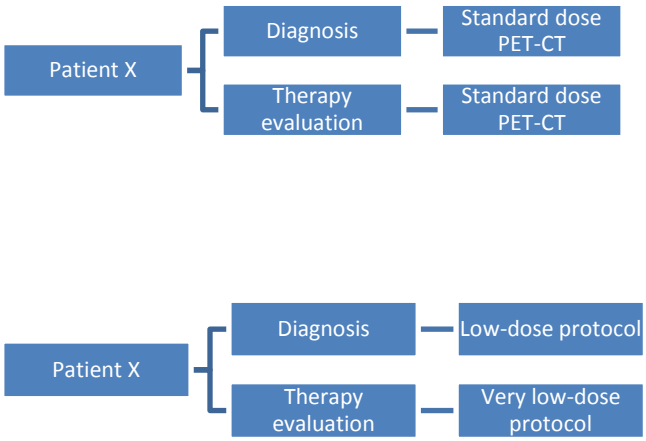

Figure 5-1: Current and future schematic of protocols used for diagnosis and therapy evaluation

To proof the amount of dose reduction that can be achieved that is suggested in this project, a fictional example of a standard person suffering from cancer is used, who undergoes diagnosis PET-CT scan and follow-up PET-CT scans to evaluate the therapy he receives. One diagnosis PET-CT scan is used and four follow up PET-CT scans are made in this fictional example.

In the present, this leads to five standard dose protocols. If the patient had a size similar to the NEMA phantom, this would result in a DLP of 1156.32 mGy*cm, resulting in an effective dose of 19.7 mSv per CT- scan.

In this example, effective dose is used purely for comparison reasons as this is an individual dose risk calculation (whereas effective dose is for populations). The accumulated dose over all scans for this patient will be 98.3 mSv. If we add the dose delivered by five PET scans (31.15 mSv), this results in a total accumulated effective dose of 129.45 mSv over five PET/CT exams.

If the suggested dose protocol for diagnosis would be used on this standard patient, a DLP of 809.4 mGy*cm would be achieved, resulting in an effective dose of 13.76 mSv for this diagnosis exam. More importantly, for the follow-up exams, a very low dose CT protocol can be used, for example a tube voltage of 80 kV and a tube current of 54 mAs would result in a DLP of 116.16 mGy*cm, resulting in an effective dose of 1.97 mSv per exam. In total, the CT component of these five examinations would lead to an effective dose of 21.64 mSv. Adding up the dose delivered by the PET component, this would lead to an effective dose of 52.83 mSv over five exams.

This is visualized in table 5-1. By using the proposed protocol for diagnosis and follow up exams, this leads to an overall reduction of dose delivered to the patient of approximately 60% for a standard patient.

Pseudo - effective dose		**Standard protocol**	**Proposed protocol**
CT – dose (mSv)	diagnose	19.7	13.8
	Follow up	78.6	7.88
PET-dose (mSv)	Diagnose	6.23	6.23
	Follow up	24.92	24.92
		129.45	52.83

Tabel5-1Effective dose for comparison of the standard protocol and the proposed protocol

Reference list

1. *Course 'Contrast agents and biomarkers for imaging and therapy'. Prof Vanhove (2014)*
2. *Imagingcenteratcarlstadt.com*
3. *Who.int*
4. *Bracke,M(2011), Kanker biomedisch bekeken, first edition, Standaard uitgeverij, Antwerpen*
5. *Whs.wsd.wednet.edu*
6. *Course 'Radiological techniques'. Prof Bacher (2012)*
7. *Tavernier, S (2009), Experimental techniques in nuclear and particle physics, VUB*
8. *Quora.com*
9. *Course 'Medical imaging', Prof Vandenberghe (2013)*
10. *Kinahan P, Hasegawa B, Beyer T (2003) X-ray-based attenuation correction for positron emission tomography/computed tomography scanners. Seminars in Nuclear Medicine 33:166-179*
11. *Seeram, E (2009), Computed tomography: Physical principles, clinical applications and quality control, third edition, Saunders, Canada*
12. *Soderberg M, Gunnarsson M (2010) Automatic exposure control in computed tomography – an evaluation of systems from different manufacturers. ActaRadiol 51:625-634*
13. *McCollough C, Primak A, Braun N, Kofler J (2009) Strategies for reducing radiation dose in CT. RadiolClin North Am 49:27-40*
14. *Usa.healthcare.siemens.com*
15. *Schindera S, Winklehner A, Alkadhi H, Goetti R, Fischer M, Gnannt R, Szucs- Farkas Z. (2012) Effect of automatic tube voltage selection on image quality and radiation dose in abdominal CT angiography of various body sizes: A phantom study. Clinical radiology e79-e86.*
16. *Owlnet.rice.edu*
17. *Franck C. (2011) Evaluatie van dosis reductivetechnieken op een dual source CT. Master's thesis. University Gent*
18. *Grant K, SAFIRE: sinogram affirmed iterative reconstruction*
19. *Krueger WR, Fletcher JG, Hough DM (2011) Multi-Reader Study: Sinogram Affirmed Iterative Reconstruction for Noise and Dose Reduction in Contrast-Enhanced Abdominal CT. Abdominal radiology course 30*
20. *Course 'Nuclear physics'. Prof. Sonck (2014)*
21. *Reich-chemistry.wikispaces.com*
22. *Med.harvard.edu*
23. *Wikipedia.org*
24. *Izuishi K, Yamamoto Y, Mori H, Kameyama R (2014) Molecular mechanisms of 18F fluorodeoxyglucose accumulation in liver cancer. Oncol rep;31:701-706*
25. *Macheda M, Rogers S, Best J (2005) Molecular and cellular regulation of glucose transporter (GLUT) proteins in cancer. J Cell Physiol;202:654-662*
26. *Tyler J, Diksic M, Villemure J (1987) Metabolic and hemodynamic evaluation of gliomas using positron emission tomography. J Nucl Med;28:1123-1133*
27. *Franquet E, Palmer M, Gifford E (2014) Rifaximin suppresses background intestinal 18F-FDG uptake on PET/CT scans. Nucl Med Commun;35:1026-1031*
28. *Depths.washington.edu*
29. *Brasse D, Kinahan P, Lartizien C (2005) Correction methods for random coincidences in fully 3D whole-body PET: impact on data and image quality. J Nucl Med; 46:859-867*

30. *Surti S (2015) Update on time-of-flight PET imaging. J Nucl Med;56:98-105*

31. *Karp J, Surti S, Daube-Witherspoon M (2008) Benefit of time-of-flight in PET: experimental and clinical results. J Nucl Med;49:462-470*

32. *Di Chiro G, DeLaPaz R, Rodney M (1982) Glucose utilization of cerebral gliomas measured by 18F fluorodeoxyglucose and positron emission tomography. Neurology;32*

33. *Kim C, Gupta N, Chandramouli B (1994) Standardized uptake values of FDG: body surface area correction is preferable to body weight correction. J Nucl Med;35:164-167*

34. *Hamberg L, Hunter G, Alpert N (1994) The dose uptake ratio as an index of glucose metabolism: useful parameter or oversimplification? J Nucl Med;35:1308-1312*

35. *Keyes J (1995) SUV: Standard uptake or silly useless value? J Nucl Med;36:1836-1839*

36. *Kinahan P, Fletcher J (2010) PET/CT standardized uptake values in clinical practice and assessing response to therapy. Semin Ultrasound CT MR;31:496-505*

37. *Robinson P, Kreel L (1979) Pulmonary tissue attenuation with computed tomography: comparison of inspiration and expiration scans. J Comput Assist Tomogr;3:740-748*

38. *Lacroix K, Tsui B, Hasegawa B (1994) Investigation of the use of X-ray CT images for attenuation compensation in SPECT. IEEE trans Nucl Sci;41:2793-2799*

39. *Beyer T (1999) Construction and validation of a combined PET/CT tomograph for clinical oncology. Doctoral thesis, University of Surrey*

40. *Burger C, Goerres G, Schoenes S (2002) PET attenuation coefficients from CT images: experimental evaluation of the transformation of CT into PET 511-keV attenuation coefficents. Eur J Nucl Med Mol Imaging; 29:922-927*

41. *Charron M, Beyer T, Bohnen N (2000) Image analysis in patients with cancer studies with a combined PET and CT scanner. ClinNucl Med;25:905-910*

42. *Radiologyinfo.org*

43. *Course 'Radiobiology'. Prof Vral (2011)*

44. *Picano E, Vano E, Rehani M, Cuocolo A (2013) The appropriate and justified use of medical radiation in cardiovascular imaging: a position document of the ESC Associations of Cardiovascular Imaging, Percutaneous Cardiovascular Interventions and Electrophysiology. European Heart Journal*

45. *Recommendations of the International Commission on Radiological Protection. Ann ICRP. 1991;21(1-3):1-201*

46. *Huang B, Law M, Khong P (2009) Whole body PET/CT scanning: estimation of radiation dose and cancer risk. Radiology;251:1-2*

47. *Siemens Biography mCT flow manual*

48. *Oral agreement Prof D'Asseler*

49. *Phantomlab.com*

50. *Catphan 500 and 600 manual*

51. *Biodex.com/nuclear-medecine*

52. *Huda W, Rowlett W, Schoepf U (2010) Radiation dose at cardiac computed tomography: facts and fiction. J Thorac imaging;25:204-212*

53. *ICRP Publication 106 – Radiation dose to patients from Radiopharmaceuticals – Addendum 3 to ICRP Publication 53*

54. *McCollough CH (2005) Automatic exposure control in CT: are we done yet? Acta Radiology; 237:755-6*

55. *Fanc.fgov.be*

56. *McCollough C, Primak A, Braun N (2009) Strategies for reducing radiation dose in CT. RadiolClin North Am;47:27-40*

57. *Graser A, Wintersperger B, Suess C (2004) Dose reduction and image quality in MDCT colonography using tube current modulation. AJR Am J Roentgenol;187:695-701*

58. *Greess H, Wolf H, Baum U (2000) Dose reduction in computed tomography by attenuation-based, online modulation of tube current: evaluation of six anatomical regions. Eur Radiol;10:391-394*

59. *Mulkens T, Bellinck P, Baeyaert M (2005) Use of an automatic tube exposure control mechanism for dose optimization in multi-detector row CT examinations: clinical evaluation. Radiology;237:213-223*

60. *Kim J, Lee K (2015) The effect of automatic exposure control with inappropriate scout image on radiation dose: a chest phantom experiment with three different CT machines. EurSoc of Radiology C-0891*

61. *Rego S, Yu L, Bruesewith M. Poster: CARE Dose4D CT automatic exposure control system: physics principle and practical hints. CT clinical innovation center, Department of radiology, Mayo Clinic, Rochester, MN*

62. *Green M, Ostrow H, Seidel J (2010) Experimental evaluation of depth-of-interaction correction in a small animal positron emission tomography scanner. Mol Imaging;9:311-318*

63. *Blankstein R, Bolen M, Pale R (2011) Use of 100 kV versus 120 kV in cardiac dual source computed tomography: effect on radiation dose and image quality. Int J Cardiovasc Imaging;27:579-586*

64. *Auchebach S, Marwan M, Ropers D (2010) Coronary computed tomography angiography with a consistent dose below 1 mSv using prospectively electrocardiogram-triggered high-pitch spiral acquisition. Eur Heart J;31:340-346*

65. *Goetti R, Leschka S, Boschung M (2012) Radiation doses from phantom measurements at high-pitch dual-source computed tomography coronary angiography. Eur J Radiol;8:733-739*

66. *Patientdosimetrie bij toepassing van cardio-CT met behulp van een dual-source CT scanner. (2012) Thesis Mattias Verhelst. UGent*

67. *May M, Kramer M, Eller A, Wuest W (2014) Automated tube voltage adaptation in head and neck computed tomography between 120 and 100 kV: effects on image quality and radiation dose. Neuroradiology;56:797-803*

68. *Zurl B, Tiefling R, Winkler P, Kindl P, Kapp K (2013) Hounsfield units variations: impact on CT-density based conversion tables and their effects on dose distribution, StrahlentherOnkol : 190:88-93*

69. *Skrynski W, Zielinska-dabrowska S, Wachowics M (2010) Computed tomography as a source of electron density information for radiation planning. StrahlentherOnkol 186:327-333*

70. *Zurl B, Tiefling R, Winkler P (2014) Hounsfield units variations: impact on CT-density based conversion tables and their effects on dose distribution. Stahlenter Onkol;190:88-93*

71. *Sande E, Martinsen A, Hole E (2010) Interphantom and interscanner variations for Hounsfield units – establishment of reference values for HU in a commercial QA phantom. PhysMol Biol;55:5123-5135*

72. *Soret M, Bacharach S, Buvat I (2007) Partial-volume effect in PET tumor imaging. J Nucl Med;48:932-945*

73. *Srinivas S, Dhurairaj T, Basu G (2009) A recovery coefficient method for partial volume correction of PET images. Ann Nucl Med;23:341-348*

74. *Abella M, Alessio A, Mankoff D (2012) Accuracy of CT-based attenuation correction in PET/CT bone imaging. Phys.Med.biol;57:2477-2490*

75. *Kuwert T, Ganslandt T, Jansen P (1992) Influence of size of regions of interest on PET evaluation of caudate glucose consumption. J Comput Assist Tomogr;16:789-794*

76. *Hoffman E, Huang S, Phelphs M (1979) Quantitation in positron emission computed tomography: effect of object size. J Comput Assist Tomogr;3:299-308*

Appendix A

T QCC: 09/264 66 46
T Secr: 09/264 65 19
F Secr: 09/264 66 96
E-mail: qcc-gent@UGent.be
Adres: Proeftuinstraat 86, 9000 Gent

FACULTEIT **GENEESKUNDE EN GEZONDHEIDSWETENSCHAPPEN**
Dienst **Medische Fysica**
QCC-GENT
Centrum voor Medische Stralingsfysica in de Radiologie en Nucleaire Geneeskunde

▶ Jaarlijkse kwaliteitscontrole apparaat voor radiodiagnostiek

Dienst: UZ Gent
De Pintelaan 185
9000 Gent

Datum: 9/12/2014

Afdeling: Nucleaire geneeskunde
Zaal:
Toesteltype: PET/CT
Fabrikant: Siemens
Model: Biograph mCT Flow

Gegevens: UZ 101815

▶ Conclusie

Conform de vigerende wetgeving werd het apparaat gecontroleerd op basis van het besluit van het FANC d.d. 14/2/2014 houdende de minnimale aanvaardbaarheidscriteria voor computertomografietoestellen.

Al de gemeten parameters voldoen aan de normen hierin gespecificeerd, met uitzondering van de weergave van de CTDI voor pediatrische protocollen.

De berekening van de CTDI dient bij alle pediatrische protocollen te gebeuren in het 16 cm fantoom. Voor oa pediatrie abdomen en thorax is de CTDI aanduiding gebaseerd op het 32 cm fantoom.

Gelieve ook op te merken dat bij het Abdomen sequentieel programma, de CTDI aanduiding beïnvloed wordt door het aantal coupes. Per definitie is de CTDI de dosis per snede, dus zou deze onafhankelijk moeten zijn van het aantal snedes. Tijdens het overlopen van de andere protocols werd deze opmerking niet vastgesteld.

▶ Meetmateriaal

kV meter/ dosimeter:	Unfors Xi R/F & MAM Detector Platinum
	S/N: 144759 Kalibratie datum: 29/07/2014
	Unfors Xi CT detector
	S/N: 146358 Kalibratie datum: 29/07/2014
Beeldkwaliteit:	Catphan 440 (The Phantom Laboratory)
Zelfontwikkelende film:	Gafchromic XR-CT

▶ Samenvatting

	Basis- / ingestelde waarde	Gemeten	Afwijking	Limiet	Voldaan
Buisspanning					
nauwkeurigheid			9.0%	<10.0%	JA
reproduceerbaarheid			0.8%	<5.0%	JA
variatie met buisstroom			1.9%	<10.0%	JA
CTDI- en dosismetingen					
CTDI: reproduceerbaarheid					
PMMA "head" fantoom			0.3%	<5.0%	JA
PMMA "body" fantoom			0.5%	<5.0%	JA
CTDI: evolutie in de tijd					
PMMA "head" fantoom	17.29	0.00	-	<20.0%	-
PMMA "body" fantoom	9.78	0.00	-	<20.0%	-
CTDI: lineariteit met mA					
gemeten dosis:					
PMMA "head" fantoom		1.000		>0.90	JA
PMMA "body" fantoom		1.000		>0.90	JA
aangeduide dosis:					
PMMA "head" fantoom	-	1.000	-	>0.90	JA
PMMA "body" fantoom	-	1.000	-	>0.90	JA
CTDI: variatie met de tijd					
gemeten dosis:					
PMMA "head" fantoom		1.000		>0.90	JA
PMMA "body" fantoom		1.000		>0.90	JA
aangeduide dosis:					
PMMA "head" fantoom		1.000		>0.90	JA
PMMA "body" fantoom		1.000		>0.90	JA
CTDI: i.f.v. buisspanning					
PMMA "head" fantoom					
70 kV	3.62	3.33	-8.1%	<20%	JA
80 kV	5.77	5.35	-7.2%	<20%	JA
100 kV	11.46	10.44	-8.9%	<20%	JA
120 kV	18.68	17.29	-7.4%	<20%	JA
140 kV	27.26	25.03	-8.2%	<20%	JA
monotoon stijgende functie?					JA
PMMA "body" fantoom					
70 kV	1.50	1.54	3.0%	<20%	JA
80 kV	2.46	2.56	4.2%	<20%	JA
100 kV	5.16	5.43	5.3%	<20%	JA
120 kV	8.75	9.78	11.7%	<20%	JA
140 kV	13.15	13.48	2.5%	<20%	JA
monotoon stijgende functie?					JA
CTDI: i.f.v. collimatie					
PMMA "head" fantoom					
12 (20 x 0.6)	18.68	17.29	-7.4%	<20%	JA
correctiefactor voor CTDIw console		-			
19.20 mm	16.94	15.73	-7.1%	<20%	JA
correctiefactor voor CTDIw console		-			
tov referentie			-9.0%	<25%	JA
PMMA "body" fantoom					
12 (20 x 0.6)	8.75	9.78	11.7%	<20%	JA
correctiefactor voor CTDIw console		-			
19.20 mm	7.94	8.17	2.8%	<20%	JA
correctiefactor voor CTDIw console		-			
tov referentie			-16.5%	<25%	JA
CTDI: bij mAs-modulatie					
PMMA "body" fantoom	12.84	12.74	-0.8%	<20%	JA
Dosis bij voorgeprogrammeerde sequenties					
Volwassenen					
CT Schedel (hersenen)	-	165.43	-		
CT Sinussen	-	27.72	-		
CT Cervicale wervelkolom	-	32.99	-		
CT Lumbale wervelkolom	-	30.98	-		
CT Hart (CCTA)	-	-	-		
CT Thorax	-	8.00	-		
CT Colon	-	12.95	-		
angio-CT Thorax	-	4.87	-		

Kinderen					
CT Schedel (hersenen)	-	165.64	-		
CT Sinussen	-	24.28	-		
CT Thorax	-	6.41	-		
CT Abdomen	-	10.36	-		
Geometrische efficiëntie					
19.20 mm		0.82 mm		> 0.70	JA
12.00 mm		0.76 mm		> 0.70	JA
Nauwkeurigheid positioneringslicht			0.5 mm	≤ 5.0	JA
Afgelegde weg van de tafel					
in gantry			0.0 mm	≤ 2.0	JA
uit gantry			0.0 mm	≤ 2.0	JA
Snededikte (gevoeligheidsprofiel)					
≤ 2 mm: *smooth kernel*			40%	< 50%	JA
sharp kernel			19%	< 50%	JA
> 2 mm: *smooth kernel*			-0.2 mm	<±1.0 mm	JA
sharp kernel			0.9 mm	<±1.0 mm	JA
Beeldkwaliteit (performantie)					
Laag-contrast resolutie					
smooth kernel					
70 kV	5	-			
80 kV	5	-			
100 kV	4	-			
120 kV	3	-			
140 kV	3	-			
sharp kernel					
70 kV	12	-			
80 kV	7	-			
100 kV	5	-			
120 kV	5	-			
140 kV	3	-			
Hoog-contrast resolutie					
smooth kernel					
MTF 2%	7.4	-	-	< 15%	-
MTF 50%	3.3	-	-	< 15%	-
sharp kernel					
MTF 2%	14.39(*)	-	-	< 15%	-
MTF 50%	7.8	-	-	< 15%	-
Beeldruis					
smooth kernel					
70 kV	12.9 HU	-	-	< 50.0 %	-
80 kV	9.5 HU	-	-	< 50.0 %	-
100 kV	7.9 HU	-	-	< 50.0 %	-
120 kV	5.5 HU	-	-	< 50.0 %	-
140 kV	4.9 HU	-			
sharp kernel					
70 kV	88.3 HU	-	-	< 50.0 %	-
80 kV	68.8 HU	-	-	< 50.0 %	-
100 kV	40.4 HU	-	-	< 50.0 %	-
120 kV	36.9 HU	-	-	< 50.0 %	-
140 kV	30.5 HU	-			
Beelduniformiteit					
smooth kernel					
70 kV			4.47 HU	< ±8.00 HU	JA
80 kV			3.93 HU	< ±8.00 HU	JA
100 kV			4.07 HU	< ±8.00 HU	JA
120 kV			1.76 HU	< ±8.00 HU	JA
140 kV			0.77 HU	< ±8.00 HU	JA
sharp kernel					
70 kV			7.31 HU	< ±8.00 HU	JA
80 kV			3.59 HU	< ±8.00 HU	JA
100 kV			3.44 HU	< ±8.00 HU	JA
120 kV			3.05 HU	< ±8.00 HU	JA
140 kV			1.81 HU	< ±8.00 HU	JA

CT-getal						
smooth kernel						
70 kV						
	Lucht	-1000 HU	-1017 HU	-17 HU	< ±50 HU	JA
	Water	0 HU	-1 HU	-1 HU	< ±10 HU	JA
80 kV						
	Lucht	-1000 HU	-1015 HU	-15 HU	< ±50 HU	JA
	Water	0 HU	1 HU	1 HU	< ±10 HU	JA
100 kV						
	Lucht	-1000 HU	-1016 HU	-16 HU	≤ 50 HU	JA
	Water	0 HU	1 HU	1 HU	≤ 10 HU	JA
120 kV						
	Lucht	-1000 HU	-1013 HU	-13 HU	< ±50 HU	JA
	Water	0 HU	1 HU	1 HU	< ±10 HU	JA
140 kV						
	Lucht	-1000 HU	-1016 HU	-16 HU	< ±50 HU	JA
	Water	0 HU	1 HU	1 HU	< ±10 HU	JA
sharp kernel						
70 kV						
	Lucht	-1000 HU	-968 HU	32 HU	< ±50 HU	JA
	Water	0 HU	-1 HU	-1 HU	< ±10 HU	JA
80 kV						
	Lucht	-1000 HU	-974 HU	-26 HU	< ±50 HU	JA
	Water	0 HU	0 HU	0 HU	< ±10 HU	JA
100 kV						
	Lucht	-1000 HU	-983 HU	17 HU	< ±50 HU	JA
	Water	0 HU	1 HU	1 HU	< ±10 HU	JA
120 kV						
	Lucht	-1000 HU	-983 HU	17 HU	< ±50 HU	JA
	Water	0 HU	1 HU	1 HU	< ±10 HU	JA
140 kV						
	Lucht	-1000 HU	-986 HU	14 HU	< ±50 HU	JA
	Water	0 HU	1 HU	1 HU	< ±10 HU	JA
Lineariteit						
smooth kernel						
100 kV			0.994		>0.990	JA
140 kV			0.997		>0.990	JA
70 kV			0.998		>0.990	JA
120 kV			0.992		>0.990	JA
80 kV						
sharp kernel						
100 kV			0.994		>0.990	JA
140 kV			0.990		>0.990	JA
70 kV			0.999		>0.990	JA
120 kV			0.992		>0.990	JA
Buisstroommodulatie						
Z-as modulatie	110%		109.7%	-	< 20%	-
overzichtsscan < fantoom					melding?	JA
X-Y *modulatie*			18%			JA
Overscannen				107 mm	119 mm	JA
Beeldartefacten						OK

▶ Referentie-opname

PMMA "body" fantoom

spanning (kV)	buisstroom (mA)	rotatietijd (s)	collimatie (mm)	FOV (mm)	buisstroom-modulatie	CTDIvol console (mGy)
120	109	1	12 (20 x 0.6)	204	nee	8.75

reconstructie-kernel	reconstructiedikte (mm)	scan modus	pitch	aantal rotaties
B30	5	axiaal	nvt	nvt

▶ Buisspanning

▷ *Nauwkeurigheid*

buisstroom (mA)
100

ingestelde spanning (kV)	gemeten spanning (kV)	afwijking (%)
70	71.6	2.3%
100	103.6	3.6%
120	128.9	7.4%
140	152.6	9.0%
|max. afw.|:		9.0%
typisch:		<10.0%
voldaan:		**JA**

▷ *Reproduceerbaarheid*

ingestelde spanning (kV)	gemeten spanning (kV)
120	100

meting:	gemeten spanning (kV)	afwijking (%)
1	128.9	0.6%
2	127.1	-0.8%
3	128.5	0.3%
4	128.0	-0.1%
gemiddelde:	128.1	
|max. afw.|:		0.8%
limiet:		<5.0%
voldaan:		**JA**

▷ *Variatie met de buisstroom*

ingestelde spanning (kV)
120

buisstroom (mA)	gemeten spanning (kV)
100	128.9
50	126.4
200	127.5
300	127.2
gemiddelde:	127.5
max:	128.9
min:	126.4
max. variatie:	1.9%
typisch:	<10.0%
voldaan:	**JA**

▶ CTDI- en dosismetingen

▷ *CTDI $_{100,c}$: reproduceerbaarheid*

PMMA "head" fantoom

ingestelde spanning (kV)	buisstroom (mA)	rotatietijd (s)	detector (mm)	collimatie (mm)
120	109	1	12 (20 x 0.6)	12

	$CTDI_{100,c}$ (mGy)	**afwijking (%)**
1	17.03	0.0%
2	17.05	0.1%
3	17.07	0.2%
4	16.99	-0.3%
gemiddelde:	17.03	
|max. afw.|:		0.3%
limiet:		<5.0%
voldaan:		**JA**

PMMA "body" fantoom

ingestelde spanning (kV)	buisstroom (mA)	rotatietijd (s)	detector (mm)	collimatie (mm)
120	109	1	12 (20 x 0.6)	12

	$CTDI_{100,c}$ (mGy)	**afwijking (%)**
1	5.97	0.2%
2	5.98	0.4%
3	5.93	-0.5%
4	5.95	-0.1%
gemiddelde:	5.96	
|max. afw.|:		0.5%
limiet:		<5.0%
voldaan:		**JA**

▷ *CTDI $_{w}$ opvolging in de tijd*

PMMA "head" fantoom

ingestelde spanning (kV)	buisstroom (mA)	rotatietijd (s)	detector (mm)	collimatie (mm)
120	109	1	12 (20 x 0.6)	12

$CTDI_w$ per serie (mGy)	basiswaarde* (mGy)	afwijking (%)	**limiet**	voldaan:
	17.29	**-**	< 20 %	**-**

* datum acceptatietest 09/12/2014

PMMA "body" fantoom

ingestelde spanning (kV)	buisstroom (mA)	rotatietijd (s)	detector (mm)	collimatie (mm)
120	109	1	12 (20 x 0.6)	12

$CTDI_w$ per serie (mGy)	basiswaarde* (mGy)	afwijking (%)	**limiet**	voldaan:
	9.78	**-**	< 20 %	**-**

* datum acceptatietest 09/12/2014

▷ *CTDI: lineariteit met mA*

PMMA "head" fantoom

spanning (kV)	rotatietijd (s)	detector (mm)	collimatie (mm)
120	1	12 (20 x 0.6)	12

buisstroom (mA)	$CTDI_{100,c}$ (mGy)	$CTDI_{vol}$ console (mGy)
50	7.76	8.57
109	17.03	18.68
200	31.24	34.27
400	62.36	68.54
r^2	1.00	1.00
limiet:	> 0.90	> 0.90
voldaan:	**JA**	**JA**

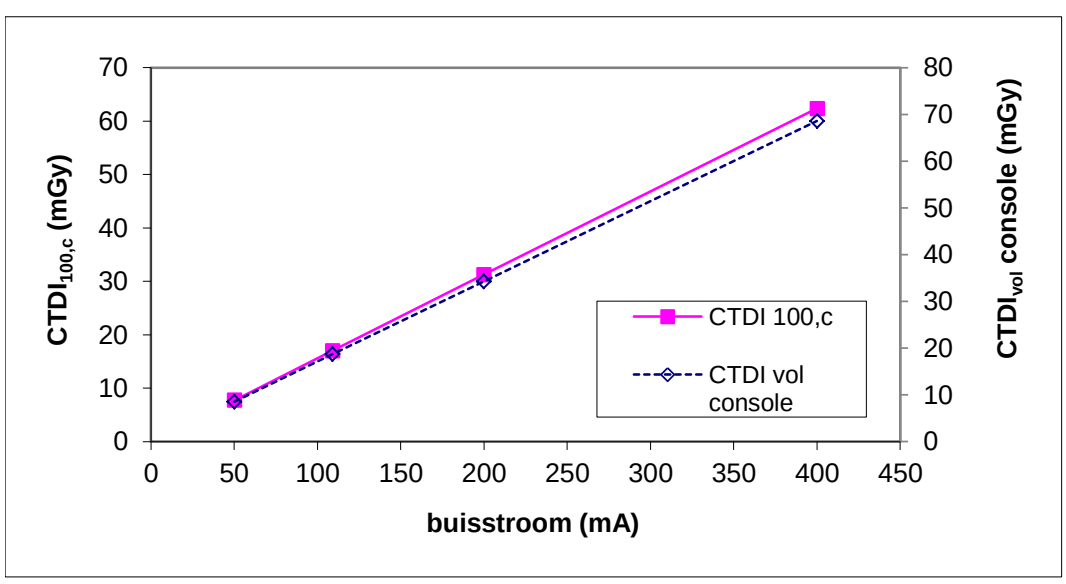

PMMA "body" fantoom

spanning (kV)	rotatietijd (s)	detector (mm)	collimatie (mm)
120	1	12 (20 x 0.6)	12

buisstroom (mA)	$CTDI_{100,c}$ (mGy)	$CTDI_{vol}$ console (mGy)
50	2.71	4.01
109	5.97	8.75
200	10.90	16.06
400	21.63	32.11
r^2	1.00	1.00
limiet:	> 0.90	> 0.90
voldaan:	**JA**	**JA**

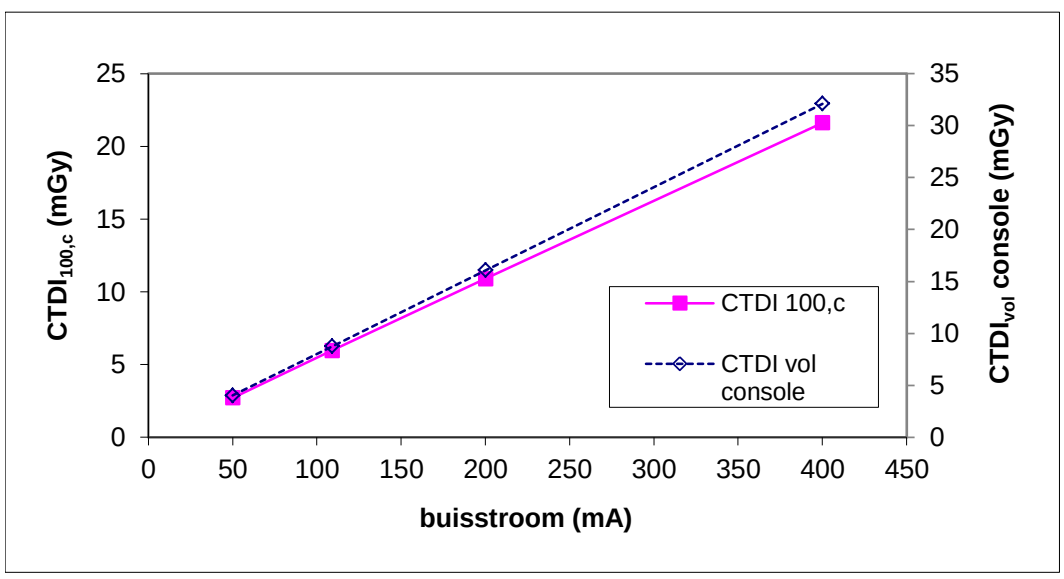

▷ *CTDI: variatie met de tijd*

PMMA "head" fantoom

spanning (kV)	buisstroom (mA)	detector (mm)	collimatie (mm)
120	109	12 (20 x 0.6)	12

rotatietijd (s)	$CTDI_{100,c}$ (mGy)	$CTDI_{vol}$ console (mGy)
0.5	8.68	9.25
1	17.03	18.68
r^2	1.00	1.00
limiet:	> 0.90	> 0.90
voldaan:	**JA**	**JA**

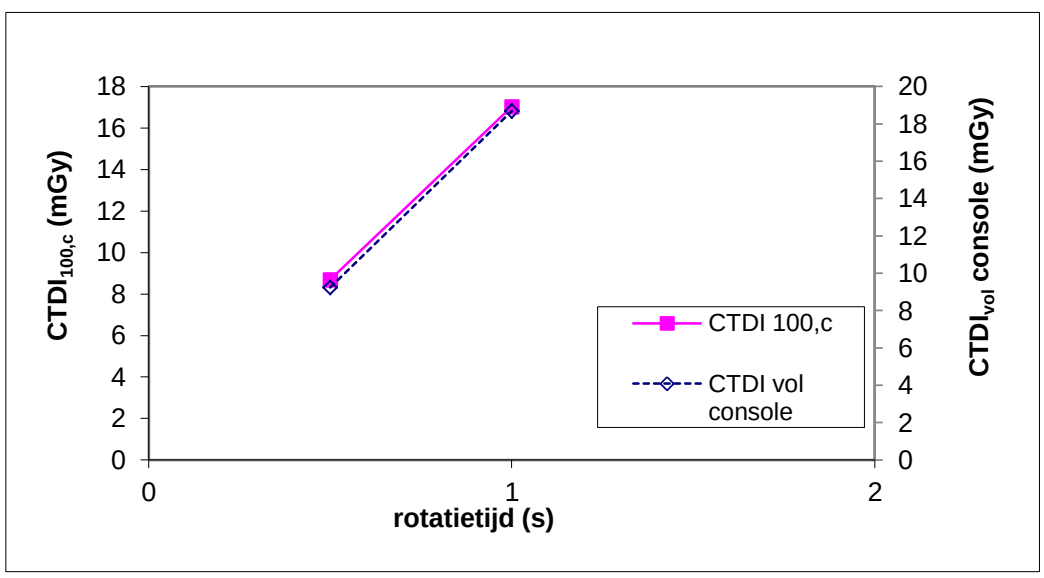

PMMA "body" fantoom

spanning (kV)	buisstroom (mA)	detector (mm)	collimatie (mm)
120	109	12 (20 x 0.6)	12

rotatietijd (s)	$CTDI_{100,c}$ (mGy)	$CTDI_{vol}$ console (mGy)
0.5	3.05	4.34
1	5.97	8.75
r^2	1.00	1.00
limiet:	> 0.90	> 0.90
voldaan:	**JA**	**JA**

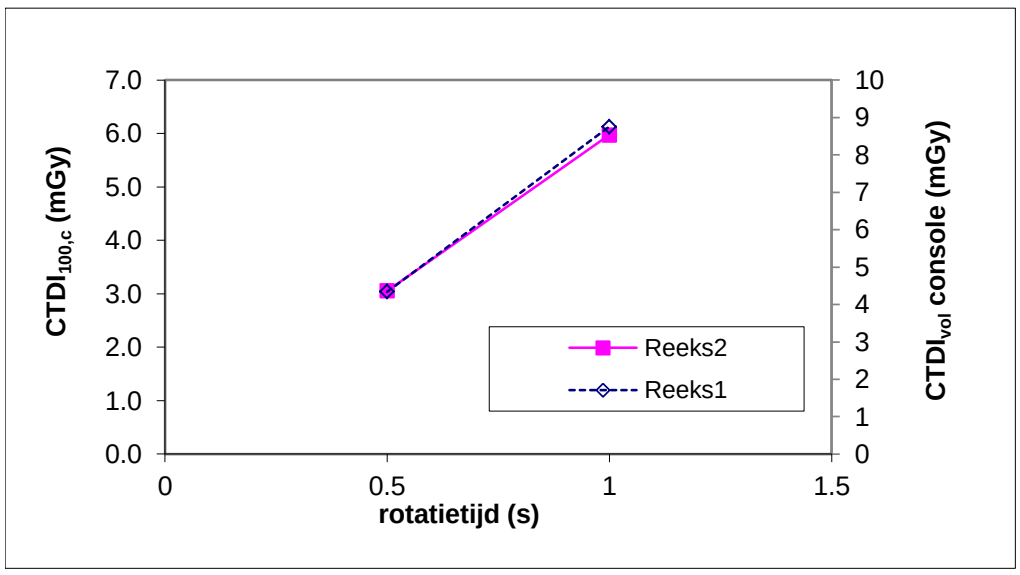

▷ *CTDI: in functie van de buisspanning*

PMMA "head" fantoom

buisstroom (mA)	detector (mm)	collimatie (mm)	rotatietijd (s)
109	12 (20 x 0.6)	12	1

	70 kV	**80**	**100 kV**	**120 kV**	**140 kV**
	mGycm	mGycm	mGycm	mGycm	mGycm
centraal	3.82	6.21	12.43	20.44	29.93
perifeer 1	4.70	7.45	14.43	23.19	34.05
perifeer 2	3.23	5.22	10.62	17.71	26.29
perifeer 3	4.19	6.72	12.62	21.36	30.01
perifeer 4	4.19	6.72	12.62	21.36	30.01
$CTDI_w$ (mGy) per serie	3.33	5.35	10.44	17.29	25.03
$CTDI_w$ (mGy) console	3.62	5.77	11.46	18.68	27.26
afwijking console tov gemeten waarde	-8.1%	-7.2%	-8.9%	-7.4%	-8.2%
limiet:	< 20 %	< 20 %	< 20 %	< 20 %	< 20 %
voldaan:	**JA**	**JA**	**JA**	**JA**	**JA**

rendement (mGy/mAs)	0.03	0.05	0.10	0.16	0.23

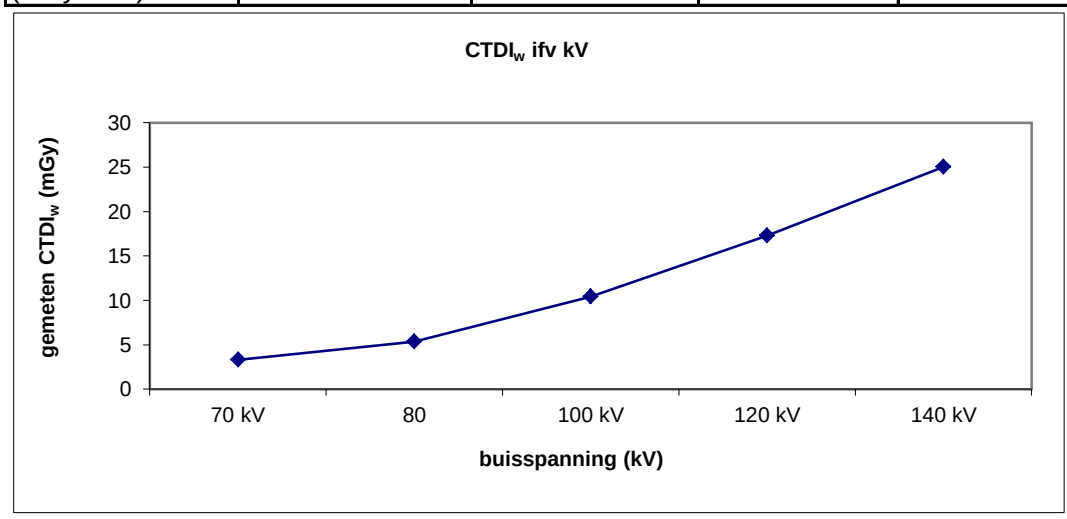

monotoon stijgend? **JA**

PMMA "body" fantoom

buisstroom (mA)	detector (mm)	collimatie (mm)	rotatietijd (s)
109	12 (20 x 0.6)	12	1

	70 kV	**80**	**100 kV**	**120 kV**	**140 kV**
	mGycm	mGycm	mGycm	mGycm	mGycm
centraal	1.03	1.87	4.14	7.16	10.93
perifeer 1	2.55	4.20	8.52	13.10	20.91
perifeer 2	2.12	3.22	7.38	17.95	17.07
perifeer 3	2.20	3.66	7.46	12.51	18.59
perifeer 4	2.20	3.66	7.46	12.51	18.59
$CTDI_w$ (mGy) per serie	1.54	2.56	5.43	9.78	13.48
$CTDI_w$ (mGy) console	1.50	2.46	5.16	8.75	13.15
afwijking console tov gemeten waarde	3.0%	4.2%	5.3%	11.7%	2.5%
limiet:	< 20 %	< 20 %	< 20 %	< 20 %	< 20 %
voldaan:	**JA**	**JA**	**JA**	**JA**	**JA**

rendement (mGy/mAs)	0.01	0.02	0.05	0.09	0.12

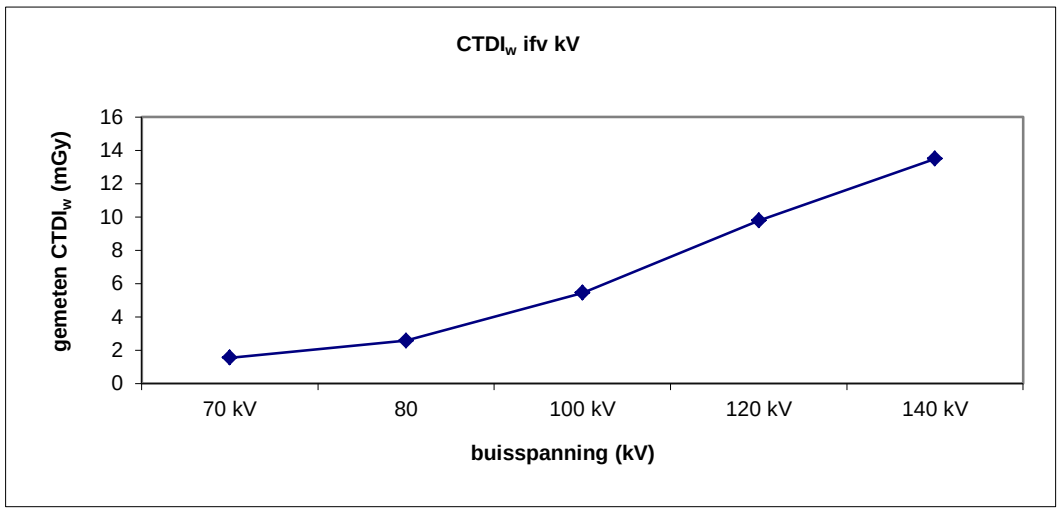

monotoon stijgend? **JA**

▷ *CTDI: in functie van de collimatie*

PMMA "head" fantoom

ingestelde spanning (kV)	buisstroom (mA)	rotatietijd (s)
120	109	1

collimatie (mm)	**12 (20 x 0.6)**	**19.2**
	mGycm	mGycm
centraal	20.44	29.68
perifeer 1	23.19	33.95
perifeer 2	17.71	25.62
perifeer 3	21.36	31.14
perifeer 4	21.36	31.14
berekende CTDIw (mGy)	17.29	15.73
CTDIw (mGy) console	18.68	16.94
afwijking console tov gemeten waarde	-7.4%	-7.1%
limiet:	< 20 %	< 20 %
voldaan:	**JA**	**JA**
correctiefactor voor CTDIw console	**-**	**-**

afwijking CTDIw t.o.v. CTDIw van ref.setting	**-**	-9.03%
limiet:	**-**	<25.0%
voldaan:		**JA**

PMMA "body" fantoom

ingestelde spanning (kV)	buisstroom (mA)	rotatietijd (s)
120	109	1

collimatie (mm)	**12 (20 x 0.6)**	**19.2**
	mGycm	mGycm
centraal	7.16	10.33
perifeer 1	13.10	19.13
perifeer 2	17.95	17.89
perifeer 3	12.51	18.19
perifeer 4	12.51	18.19
berekende CTDIw (mGy)	9.78	8.17
CTDIw (mGy) console	8.75	7.94
afwijking console tov gemeten waarde	11.7%	2.8%
limiet:	< 20 %	< 20 %
voldaan:	**JA**	**JA**
correctiefactor voor CTDIw console	**-**	**-**

afwijking CTDIw t.o.v. CTDIw van ref.setting	**-**	-16.47%
limiet:	**-**	<25.0%
voldaan:		**JA**

▷ *CTDI: verificatie bij modulatie van de exposie*

PMMA "body" fantoom

spanning (kV)	aangegeven buisstroom (mA)	rotatietijd (s)	pitch	detector (mm)	aantal rotaties
120	271	1	1	12 (20 x 0.6)	1.00

	mGycm	$CTDI_{vol}$ (mGy) per serie	$CTDI_{vol}$ (mGy) console	afwijking console tov gemeten waarde
centraal	9.90	12.74	12.84	-0.80%
perifeer 1	20.58		typisch:	< 20 %
perifeer 2	16.33		**limiet:**	**JA**
perifeer 3	16.96			
perifeer 4	18.03			

▷ *Verificatie van de dosis bij de voorgeprogrammeerde sequenties*

Volwassenen

Protocol	Lokale naam	mAs-modulatie?	CTDI-fantoom	Huidige $CTDI_{vol}$ (mGy)	Voorgaande $CTDI_{vol}$ (mGy)	Afwijking (%)
CT Schedel (hersenen)	Head routine	JA	16cm	165.43	-	-
CT Sinussen	Sinus	JA	16cm	27.72	-	-
CT Cervicale wervelkolom	C-spine	JA	32cm	32.99	-	-
CT Lumbale wervelkolom	Spine routine	JA	32cm	30.98	-	-
CT Hart (CCTA)	-	-	-	-	-	-
CT Thorax	thorax routine	JA	32cm	8	-	-
CT Abdomen	Abdomen routine	JA	32cm	12.95	-	-
CT Thorax-Abdomen	ThorAbd	JA	32cm	4.87	-	-
CT Colon	Colonografie	JA	32cm	4.59	-	-
angio-CT Thorax	-	-	-	-	-	-

Kinderen

Protocollen leeftijds- of gewichtsgebaseerd? NEE

Protocol	Lokale naam	mAs-modulatie?	CTDI-fantoom	Huidige $CTDI_{vol}$ (mGy)	Voorgaande $CTDI_{vol}$ (mGy)	Afwijking (%)
CT Schedel (hersenen)	Head routine	JA	16cm	165.64	-	-
CT Sinussen	Sinus	JA	16cm	24.28	-	-
CT Thorax	thorax routine	JA	32cm	6.41	-	-
CT Abdomen	Abdomen routine	JA	32cm	10.36	-	-
CT Thorax-Abdomen	-	-	-	-	-	-

▶ Geometrische efficiëntie

Detector
Gafchromic film

isocentrum

Ingestelde bundelbreedte (mm)	Gemeten FWHM dosisprofiel (mm)	Geometrische efficiëntie	**limiet:**	voldaan:	melding "beperkte Z-efficiëntie" ?
19.20	23.53	0.82	> 0.70	**JA**	
12.00	15.86	0.76	> 0.70	**JA**	

▶ Nauwkeurigheid van het positioneringslicht

afwijking centrum RX-veld t.o.v. positioneringslicht (mm)	**limiet:**	voldaan:
0.5	≤ 5.0	**JA**

▶ Afgelegde weg van de tafel

richting	afwijking nominale afstand t.o.v. werkelijk afgelegde weg (mm)*	limiet:	voldaan:
in gantry	0.0	≤ 2.0	**JA**
uit gantry	0.0	≤ 2.0	**JA**

* gantry verschoven over 100cm

▶ Snededikte (gevoeligheidsprofiel)

Snededikte ≤ 2 mm

ingestelde spanning (kV)	buisstroom (mA)	rotatietijd (s)	Collimatie (mm)	Reconstructie-dikte (mm)	Reconstructie-kernel
120	109	1	12 (20 x 0.6)	1	B30s

Berekende snededikte (mm)	Afwijking t.o.v. aangegeven snededikte (%)	**limiet:**	voldaan:
1.4	40%	< 50 %	**JA**

ingestelde spanning (kV)	buisstroom (mA)	rotatietijd (s)	Collimatie (mm)	Reconstructie-dikte (mm)	Reconstructie-kernel
120	109	1	12 (20 x 0.6)	1	B70s

Berekende snededikte (mm)	Afwijking t.o.v. aangegeven snededikte (%)	**limiet:**	voldaan:
1.19	19%	< 50 %	**JA**

Snededikte > 2 mm

ingestelde spanning (kV)	buisstroom (mA)	rotatietijd (s)	Collimatie (mm)	Reconstructie-dikte (mm)	Reconstructie-kernel
120	109	1	12 (20 x 0.6)	5	B30s

Berekende snededikte (mm)	Afwijking t.o.v. aangegeven snededikte	**limiet:**	voldaan:
5.2	-0.2	<±1.0	**JA**

ingestelde spanning (kV)	buisstroom (mA)	rotatietijd (s)	Collimatie (mm)	Reconstructie-dikte (mm)	Reconstructie-kernel
120	109	1	12 (20 x 0.6)	5	B70s

Berekende snededikte (mm)	Afwijking t.o.v. aangegeven snededikte	**limiet:**	voldaan:
4.1	0.9	<±1.0	**JA**

▶ Beeldkwaliteit (performantie)

▷ *Laag-contrast resolutie*

buisstroom (mA)	rotatietijd (s)	Collimatie (mm)	Reconstructie-dikte (mm)	Reconstructie-kernel
109	1	12 (20 x 0.6)	5	B30s

	Buisspanning (kV)				
	70	80	100	120	140
Diameter kleinst zichtbare 0,5% laag-contrast nodule (mm)					
Basiswaarde*	5.0	5	4	3	3

buisstroom (mA)	rotatietijd (s)	Collimatie (mm)	Reconstructie-dikte (mm)	Reconstructie-kernel
109	1	12 (20 x 0.6)	5	B70s

	Buisspanning (kV)				
	70	80	100	120	140
Diameter kleinst zichtbare 0,5% laag-contrast nodule (mm)					
Basiswaarde*	12.0	7	5	5	3

acceptatietest: 09/12/2014

▷ *Hoog-contrast resolutie*

spanning (kV)	buisstroom (mA)	rotatietijd (s)	Collimatie (mm)	Reconstructie-dikte (mm)	Reconstructie-kernel
120	109	1	12 (20 x 0.6)	5	B30s

Berekende MTF 2% (cy/cm)	Basiswaarde MTF*	Afwijking	Limiet	Voldaan
	7.35	-	< 15.0%	-

Berekende MTF 50% (cy/cm)	Basiswaarde MTF*	Afwijking	Limiet	Voldaan
	3.32	-	< 15.0%	-

spanning (kV)	buisstroom (mA)	rotatietijd (s)	Collimatie (mm)	Reconstructie-dikte (mm)	Reconstructie-kernel
120	109	1	12 (20 x 0.6)	5	B70s

Berekende MTF 2% (cy/cm)	Basiswaarde MTF*	Afwijking	Limiet	Voldaan
	14.39(*)	-	< 15.0%	-

(*)boven Nyquist

Berekende MTF 50% (cy/cm)	Basiswaarde MTF*	Afwijking	Limiet	Voldaan
	7.82	-	< 15.0%	-

* datum acceptatietest 09/12/2014

▷ *Beeldruis*

Centrale ROI (500mm²)

buisstroom (mA)	rotatietijd (s)	Collimatie (mm)	Reconstructie-dikte (mm)	protocol	convolutie kernel
109	1	12 (20 x 0.6)	5	AbdomenSeq	B30s

	Buisspanning (kV)				
	70	80	100	120	140
	stdev (HU)	stdev (HU)	stdev (HU)	stdev (HU)	stdev (HU)
gemeten					
basiswaarde*	12.85	9.49	7.85	5.51	4.90
Afwijking	-	-	-	-	-
Limiet	< 50.0%	< 50.0%	< 50.0%	< 50.0%	< 50.0%
Voldaan:	**-**	**-**	**-**	**-**	**-**

* datum acceptatietest 09/12/2014

buisstroom (mA)	rotatietijd (s)	Collimatie (mm)	Reconstructie-dikte (mm)	protocol	convolutie kernel
109	1	12 (20 x 0.6)	5	AbdomenSeq	B70s

	Buisspanning (kV)				
	70	80	100	120	140
	stdev (HU)	stdev (HU)	stdev (HU)	stdev (HU)	stdev (HU)
gemeten					
basiswaarde*	88.28	68.82	40.37	36.85	30.45
Afwijking	-	-	-	-	-
Limiet	< 50.0%	< 50.0%	< 50.0%	< 50.0%	< 50.0%
Voldaan:	**-**	**-**	**-**	**-**	**-**

* datum acceptatietest 09/12/2014

▷ *Beelduniformiteit*

buisstroom (mA)	rotatietijd (s)	Collimatie (mm)	Reconstructie-dikte (mm)	Reconstructie-kernel
109	1	12 (20 x 0.6)	5	B30s

	Buisspanning (kV)				
	70	80	100	120	140
ROI	CT-getal (HU)	CT-getal (HU)	CT-getal (HU)	CT-getal (HU)	CT-getal (HU)
centraal	-24.87	-11.61	6.59	14.07	19.94
perifeer 1	-25.22	-11.69	4.64	13.67	19.68
perifeer 2	-24.5	-11.26	4.88	13.95	19.87
perifeer 3	-28.45	-11	5.82	14.16	19.34
perifeer 4	-29.34	-15.54	2.52	12.31	19.17
max verschil perifeer en centraal	4.47	3.93	4.07	1.76	0.77
Limiet	< ±8.00 HU	< ±8.00 HU	< ±8.00 HU	< ±8.00 HU	< ±8.00 HU
Voldaan	**JA**	**JA**	**JA**	**JA**	**JA**

buisstroom (mA)	rotatietijd (s)	Collimatie (mm)	Reconstructie-dikte (mm)	Reconstructie-kernel
109	1	12 (20 x 0.6)	5	B70s

	Buisspanning (kV)				
	70	80	100	120	140
ROI	CT-getal (HU)	CT-getal (HU)	CT-getal (HU)	CT-getal (HU)	CT-getal (HU)
centraal	-24.49	-11	4.88	13.65	19.84
perifeer 1	-29.02	-9.84	6.58	14.11	20.78
perifeer 2	-23.72	-13.89	5.31	11.73	21.18
perifeer 3	-27.3	-7.41	2.62	15.66	19.37
perifeer 4	-31.8	-9.08	8.32	10.6	18.03
max verschil perifeer en centraal	7.31	3.59	3.44	3.05	1.81
Limiet	< ±8.00 HU	< ±8.00 HU	< ±8.00 HU	< ±8.00 HU	< ±8.00 HU
Voldaan	**JA**	**JA**	**JA**	**JA**	**JA**

▷ *CT-getal*

spanning (kV)	buisstroom (mA)	rotatietijd (s)	Collimatie (mm)	Reconstructie-dikte (mm)	Reconstructie-kernel
70	109	1	12 (20 x 0.6)	5	B30s

	standaard-waarde	gemiddelde HU	Afwijking (HU)	**Limiet**	Voldaan:
Lucht	-1000	-1017	-17	< ±50 HU	**JA**
Teflon	990	921	-69		
LDPE	-100	-146	-46		
Acryl	120	85	-35		
Water	0	-1	-1	< ±10 HU	**JA**

spanning (kV)	buisstroom (mA)	rotatietijd (s)	Collimatie (mm)	Reconstructie-dikte (mm)	Reconstructie-kernel
80	109	1	Collimatie(mm)	5	B30s

	standaard-waarde	gemiddelde HU	Afwijking (HU)	**Limiet**	Voldaan:
Lucht	-1000	-1015	-15	< ±50 HU	**JA**
Teflon	990	904	-86		
LDPE	-100	-124	-24		
Acryl	120	101	-20		
Water	0	1	1	< ±10 HU	**JA**

spanning (kV)	buisstroom (mA)	rotatietijd (s)	Collimatie (mm)	Reconstructie-dikte (mm)	Reconstructie-kernel
100	109	1	12 (20 x 0.6)	5	B30s

	standaard-waarde	gemiddelde HU	Afwijking (HU)	**Limiet**	Voldaan:
Lucht	-1000	-1016	-16	≤ 50 HU	**JA**
Teflon	990	871	-119		
LDPE	-100	-106	-6		
Acryl	120	112	-8		
Water	0	1	1	≤ 10 HU	**JA**

spanning (kV)	buisstroom (mA)	rotatietijd (s)	Collimatie (mm)	Reconstructie-dikte (mm)	Reconstructie-kernel

120	109	1	12 (20 x 0.6)	5	B30s

	standaard-waarde	gemiddelde HU	Afwijking (HU)	**Limiet**	Voldaan:
Lucht	-1000	-1013	-13	< ±50 HU	**JA**
Teflon	990	856	-134		
LDPE	-100	-94	6		
Acryl	120	122	2		
Water	0	1	1	< ±10 HU	**JA**

spanning (kV)	buisstroom (mA)	rotatietijd (s)	Collimatie (mm)	Reconstructie-dikte (mm)	Reconstructie-kernel
140	109	1	12 (20 x 0.6)	5	B30s

	standaard-waarde	gemiddelde HU	Afwijking (HU)	**Limiet**	Voldaan:
Lucht	-1000	-1016	-16	< ±50 HU	**JA**
Teflon	990	945	-45		
LDPE	-100	-91	9		
Acryl	120	127	7		
Water	0	1	1	< ±10 HU	**JA**

spanning (kV)	buisstroom (mA)	rotatietijd (s)	Collimatie (mm)	Reconstructie-dikte (mm)	Reconstructie-kernel
70	109	1	12 (20 x 0.6)	5	B70s

	standaard-waarde	gemiddelde HU	Afwijking (HU)	**Limiet**	Voldaan:
Lucht	-1000	-968	32	< ±50 HU	**JA**
Teflon	990	906	-84		
LDPE	-100	-143	-43		
Acryl	120	85	-35		
Water	0	-1	-1	< ±10 HU	**JA**

spanning (kV)	buisstroom (mA)	rotatietijd (s)	Collimatie (mm)	Reconstructie-dikte (mm)	Reconstructie-kernel
80	109	1	12 (20 x 0.6)	5	B70s

	standaard-waarde	gemiddelde HU	Afwijking (HU)	**Limiet**	Voldaan:
Lucht	-1000	-974	26	< ±50 HU	**JA**
Teflon	990	982	-9		
LDPE	-100	-124	-24		
Acryl	120	101	-19		
Water	0	0	0	< ±10 HU	**JA**

spanning (kV)	buisstroom (mA)	rotatietijd (s)	Collimatie (mm)	Reconstructie-dikte (mm)	Reconstructie-kernel
100	109	1	12 (20 x 0.6)	5	B70s

	standaard-waarde	gemiddelde HU	Afwijking (HU)	**Limiet**	Voldaan:
Lucht	-1000	-983	17	< ±50 HU	**JA**
Teflon	990	850	-140		
LDPE	-100	-102	-2		
Acryl	120	108	-12		
Water	0	1	1	< ±10 HU	**JA**

spanning (kV)	buisstroom (mA)	rotatietijd (s)	Collimatie (mm)	Reconstructie-dikte (mm)	Reconstructie-kernel
120	109	0	12 (20 x 0.6)	5	B70s

	standaard-waarde	gemiddelde HU	Afwijking (HU)	**Limiet**	Voldaan:
Lucht	-1000	-983	17	< ±50 HU	**JA**
Teflon	990	840	-150		
LDPE	-100	-91	9		
Acryl	120	122	2		
Water	0	1	1	< ±10 HU	**JA**

spanning (kV)	buisstroom (mA)	rotatietijd (s)	Collimatie (mm)	Reconstructie-dikte (mm)	Reconstructie-kernel
140	109	1	12 (20 x 0.6)	5	B70s

	standaard-waarde	gemiddelde HU	Afwijking (HU)	**Limiet**	Voldaan:
Lucht	-1000	-986	14	< ±50 HU	**JA**
Teflon	990	826	-165		
LDPE	-100	-86	14		
Acryl	120	126	6		
Water	0	1	1	< ±10 HU	**JA**

▷ *Lineariteit*

Smooth kernel	Buisspanning			
	100 kV	140 kV	70 kV	120 kV
Correlatiecoëfficiënt	0.994	0.997	0.998	0.992
limiet	>0.990	>0.990	>0.990	>0.990
voldaan?	**JA**	**JA**	**JA**	**JA**
functie door 0 ± 10 HU ?	JA	JA	JA	JA
functie door -1000 ± 50 HU ?	JA	JA	JA	NEE

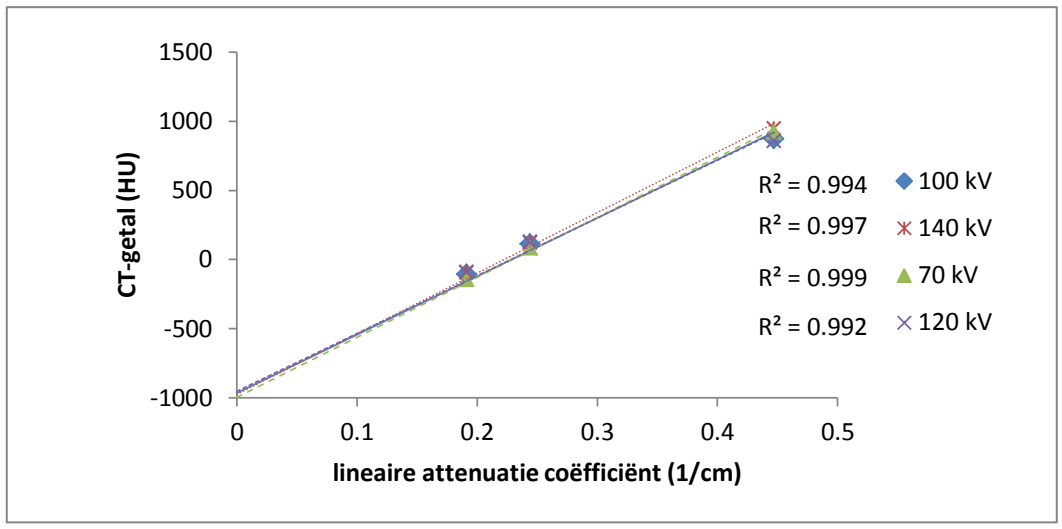

Sharp kernel	Buisspanning			
	100 kV	140 kV	70 kV	120 kV
Correlatiecoëfficiënt	0.994	0.990	0.999	0.992
limiet	>0.990	>0.990	>0.990	>0.990
voldaan?	**JA**	**JA**	**JA**	**JA**
functie door 0 ± 10 HU ?	JA	JA	JA	JA
functie door -1000 ± 50 HU ?	NEE	NEE	NEE	NEE

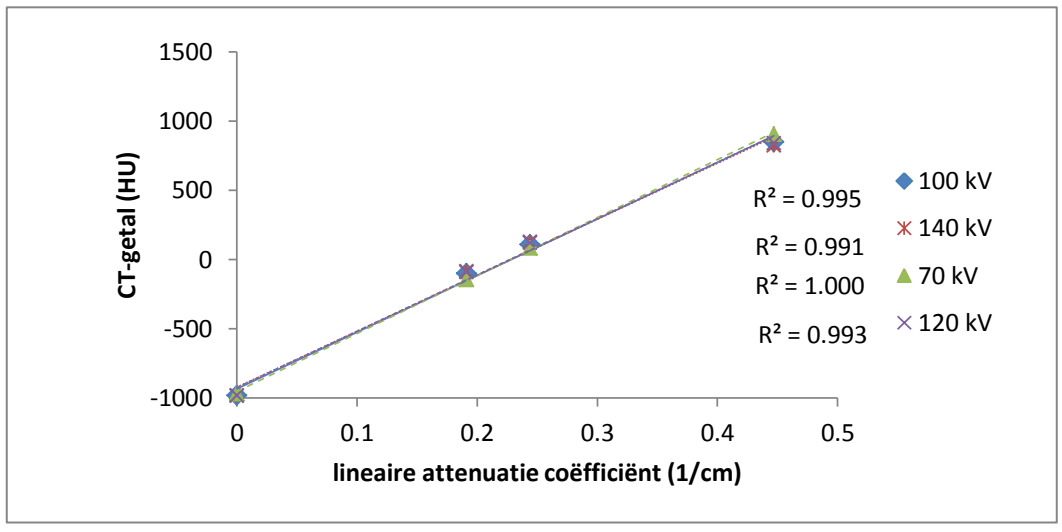

▶ Buisstroommodulatie

▷ *Z-as modulatie*

	mAs				ruis	
	$CTDI_{16}$	$CTDI_{32}$	stijging	bassiwaarde*	$CTDI_{16}$	$CTDI_{32}$
vaste mAs	190	190			3.504	19.672
mAs-modulatie	93	195	110%	110%	4.814	18.027

Afwijking: -
Limiet: < 20%
* datum acceptatietest 09/12/2014 Voldaan: **-**

Melding wanneer scan buiten buiten gebied van scout view? **JA**

▷ X-Y *modulatie*

mA-range: 229
noise level:

Positie dosimeter	Gecumuleerde dosis (mGycm)	reductie (%)		
90°	7.49			
180°	6.18	18%	**Voldaan:**	**JA**

▶ Overscannen

spanning (kV)	buisstroom (mA)	rotatietijd (s)	ingestelde afstand (mm)	collimatie (mm)	pitch
80	470	0.5	96	19.2	0.6

Effectief bestraalde lengte	107	mm
Limiet	< 119	mm
Voldaan?	**JA**	

▶ Beeldartefacten

Er werden geen beeldartefacten waargenomen.

Appendix B

Table: Tube currents in mA for the different protocols in the automatic exposure control experiment

Z-direction (mm)	Standard PA		Lat		AP	PA 99	PA 253
	Cranio-caudal	Caudo-cranial	Cranio-caudal	Caudo-cranial	Cranio-caudal	Cranio-caudal	Cranio-caudal
0	119	80	84	65	91	107	150
3	126	84	88	66	96	113	167
6	139	86	93	66	101	120	181
9	150	88	101	66	109	132	200
12	162	93	108	68	118	141	239
15	180	100	114	69	125	152	254
18	195	100	126	72	138	167	284
21	210	112	134	75	148	179	336
24	230	118	142	79	156	189	356
27	240	123	154	84	168	204	388
30	254	139	156	86	179	214	415
33	271	151	156	95	182	218	441
36	271	162	160	100	197	235	447
39	279	188	157	105	198	237	456
42	294	196	152	119	195	235	476
45	288	206	151	126	201	247	482
48	295	227	149	131	198	241	486
51	298	243	147	137	192	231	496
54	293	257	151	141	197	234	499
57	288	271	152	143	196	228	499
60	282	281	154	140	195	222	499
63	275	290	159	140	200	225	500
66	274	304	158	143	199	219	497
69	273	305	159	146	200	217	493
72	269	300	156	148	200	222	498
75	270	302	155	149	201	218	494
78	279	306	150	155	201	220	489
81	286	299	147	156	201	218	484
84	274	280	147	157	205	220	481
87	274	275	141	155	206	218	479
90	276	281	142	153	207	218	477
93	278	274	144	153	207	223	480
96	274	268	144	151	207	225	475
99	260	270	146	152	207	230	476
102	260	278	149	145	209	235	473
105	264	285	152	145	203	236	473
108	264	277	155	145	203	240	470
111	251	285	158	140	206	243	468
114	251	294	162	139	206	240	474

Z-direction (mm)	Standard PA		Lat		AP	PA 99	PA 253
	Cranio-caudal	Caudo-cranial	Cranio-caudal	Caudo-cranial	Cranio-caudal	Cranio-caudal	Cranio-caudal
117	266	303	162	142	209	250	474
120	267	295	161	148	213	251	473
123	266	288	158	151	215	247	472
126	260	289	158	154	214	247	471
129	270	293	154	160	215	245	470
132	278	290	152	163	212	235	463
135	264	282	151	163	210	228	461
138	259	291	152	160	207	223	456
141	257	302	153	158	215	224	461
144	260	305	153	156	210	218	452
147	252	301	150	153	201	206	431
150	239	299	148	153	195	209	421
153	231	298	146	151	192	214	395
156	232	295	140	153	186	209	375
159	225	272	138	154	172	205	341
162	208	268	136	152	174	205	330
165	204	272	135	150	173	205	324
168	207	273	134	151	169	206	306
171	208	268	133	144	163	200	296
174	205	255	135	141	156	195	277
177	193	252	137	139	154	192	276
180	199	252	139	136	152	188	271
183	198	239	141	136	148	177	254
186	189	214	144	134	146	172	254
189	186	209	146	133	147	170	252
192	186	214	146	132	149	170	251
195	190	212	145	136	146	165	247
198	184	202	144	138	147	161	243
201	184	194	142	140	145	162	244
204	182	197	140	143	145	164	247
207	183	198	137	146	144	165	252
210	183	186	136	148	140	155	239
213	184	178	136	145	141	159	236
216	185	181	135	143	145	159	244
219	193	188	136	141	150	162	257
222	193	193	135	139	148	155	253
225	194	188	135	138	143	148	235
228	193	189	135	136	143	153	242
231	193	193	135	136	143	155	247
234	191	190	135	137	138	152	239
237	183	182	136	136	133	150	223
240	178	180	139	134	136	155	226
243	179	190	142	132	144	166	242
246	185	195	140	134	147	168	247

Z-direction (mm)	Standard PA		Lat		AP	PA 99	PA 253
	Cranio-caudal	Caudo-cranial	Cranio-caudal	Caudo-cranial	Cranio-caudal	Cranio-caudal	Cranio-caudal
249	185	188	136	135	143	164	243
252	183	183	135	135	138	162	238
255	179	186	133	136	138	164	239
258	179	189	131	139	137	162	240
261	171	183	127	140	127	152	234
264	166	179	128	139	127	148	229
267	167	183	130	137	134	151	235
270	175	187	132	134	141	152	249
273	178	186	131	133	140	147	246
276	178	186	130	131	135	140	237
279	179	185	129	129	137	143	234
282	178	185	128	129	137	145	235
285	177	185	126	130	134	144	232
288	170	185	125	131	130	141	219
291	170	183	125	131	133	143	223
294	170	183	126	130	135	152	234
297	178	188	126	129	143	156	242
300	181	186	125	128	141	156	238
303	182	183	125	127	139	156	234
306	182	184	125	126	139	159	239
309	187	185	125	125	140	162	239
312	186	183	124	124	138	156	240
315	180	180	125	124	134	155	236
318	179	180	127	124	138	159	240
321	179	183	128	124	139	163	246
324	179	185	127	125	139	159	246
327	180	184	126	125	138	157	242
330	178	183	125	125	140	159	236
333	179	183	124	127	140	156	236
336	179	183	122	128	140	155	236
339	178	179	121	127	136	152	229
342	178	175	121	126	135	152	225
345	177	172	122	125	135	155	225
348	177	176	122	125	134	153	228
351	177	175	122	124	131	151	227
354	176	173	120	123	126	148	221
357	173	174	120	122	129	148	226
360	173	176	119	122	131	148	229
363	173	177	117	126	129	145	228
366	172	170	116	128	129	147	223
369	171	176	116	128	131	149	224
372	171	174	116	131	134	152	227
375	171	169	116	132	133	150	225
378	171	175	115	131	130	147	219

Appendix C

Table: Parameters for CT-acquistion 3 and 4 (lateral topogram)

Parameters	CT-acquisition 3	CT-acquisition 4
Scan direction	Cranial-caudal	Caudal-cranial
Topogram direction	Lateral	Lateral
Tube voltage (kV)	120	120
mAs/reference (mAs)	74/110	72/110
CAREdose	YES	YES
CAREkV	NO	NO
CTDIvol	5.45	5.28
DLP	214	207
Slice thickness (mm)	3	3
Table height	150	150

Figure: tube current as a function of z-direction length for the lateral topograms with a cranial-caudal and caudal-cranial scan direction

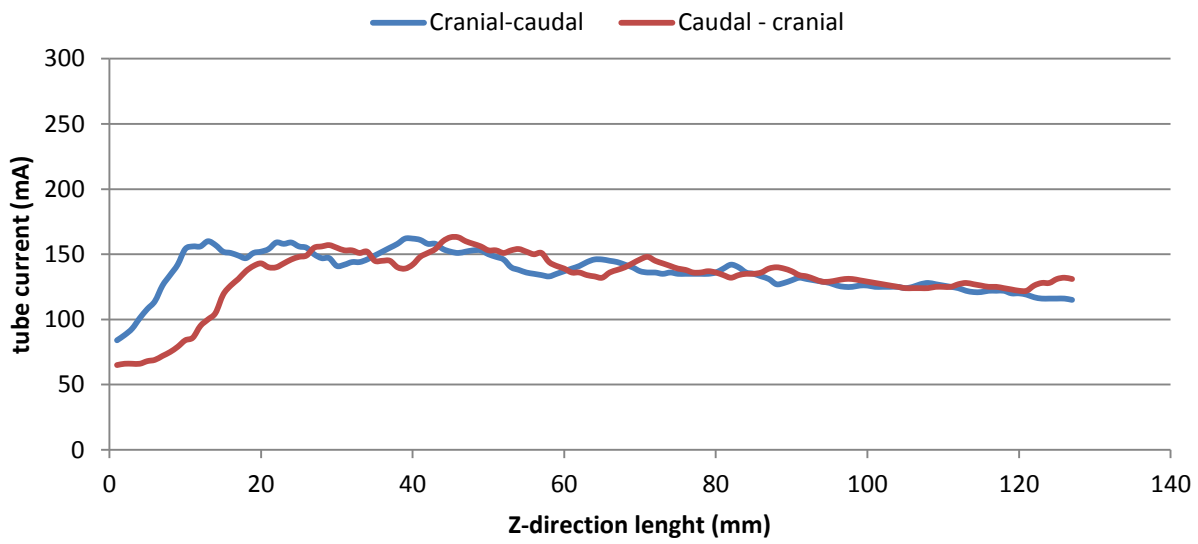

Appendix D

Figure 1: Recovery coefficient as a function of tube current for a constant tube voltage (up: 120 kV; down 100 kV)

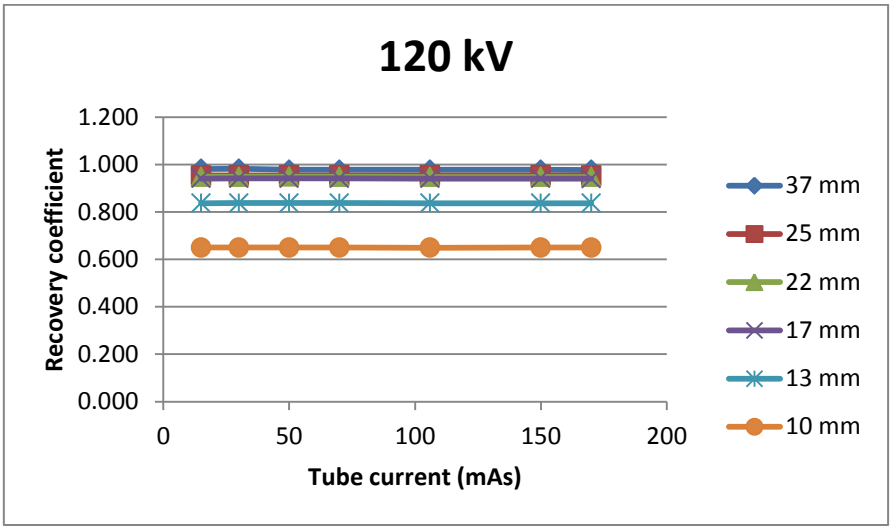

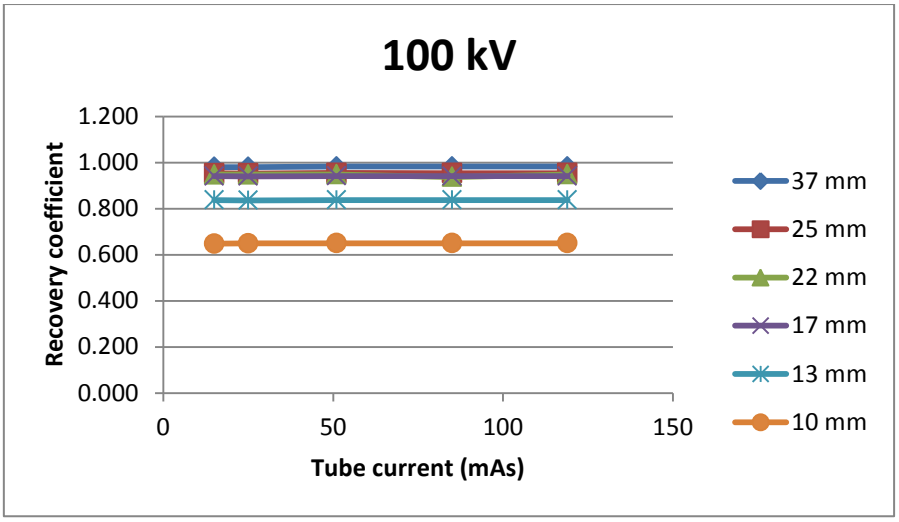

Figure 2: Recovery coefficients as a function of tube voltage for a constant tube current of 50 mAs

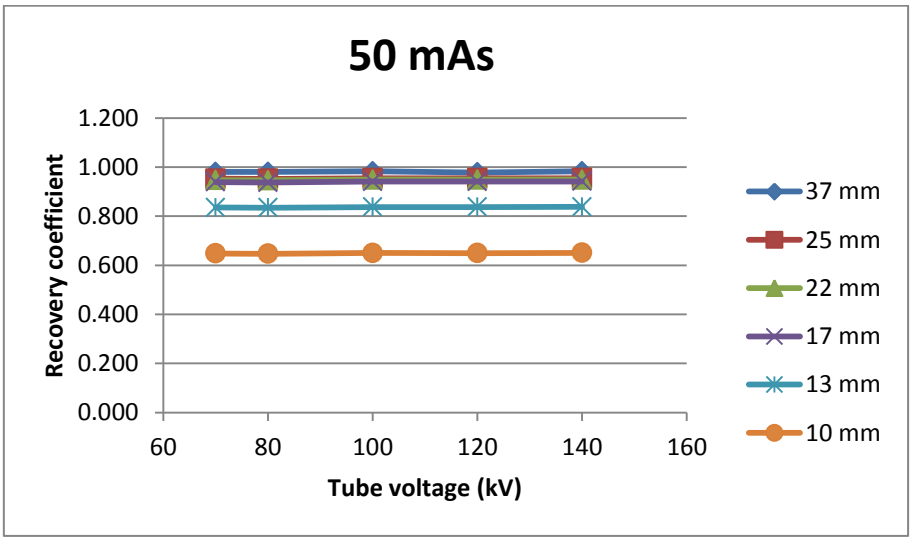

Appendix E

Figure: Recovery coefficients calculated on the maximum values as a function of sphere diameter